Journal of Neurocytology **30**, 593–654 (2002)

A molecular phenotype atlas of the zebrafish retina

ROBERT E. MARC[1,*] and DAVID CAMERON[2]

[1] *John Moran Eye Center, Department of Ophthalmology, University of Utah School of Medicine, Salt Lake City, UT 84132, USA;*
[2] *Department of Neuroscience and Physiology, SUNY Upstate Medical University, Syracuse NY 13210, USA*
robert.marc@hsc.utah.edu

Received 14 December 2001; revised and accepted 25 February 2002

Abstract

The rasborine cyprinid *Danio rerio* (the zebrafish) has become a popular model of retinal function and development. Its value depends, in part, on validation of homologies with retinal cell populations of cyprinine cyprinids. This atlas provides raw and interpreted molecular phenotype data derived from computationally classified sets of small molecule signals from different cell types in the zebrafish retina: L-alanine, L-aspartate, L-glutamine, L-glutamate, glutathione, glycine, taurine and γ-aminobutyrate. This *basis set* yields an 8-dimensional signature for every retinal cell and formally establishes molecular signature homologies with retinal neurons, glia, epithelia and endothelia of other cyprinids. Zebrafish photoreceptor classes have been characterized previously: we now show their metabolic profiles to be identical to those of the corresponding photoreceptors in goldfish. The inner nuclear layer is partitioned into precise horizontal, bipolar and amacrine cell layers. The horizontal cell layer contains at least three and perhaps all four known classes of cyprinine horizontal cells. Homologues of cyprinid glutamatergic ON-center and OFF-center mixed rod-cone bipolar cells are present and it appears likely that all five classes are present in zebrafish. The cone bipolar cells defy simple analysis but comprise the largest fraction of bipolar cells, as in all cyprinids. Signature analysis reveals six molecular phenotypes in the bipolar cell cohort: most are superclasses. The amacrine cell layer is composed of $\approx$64% GABA+ and 35% glycine+ amacrine cells, with the remainder being sparse dopaminergic interplexiform cells and other rare unidentified neurons. These different amacrine cell types are completely distinct in the dark adapted retina, but light adapted retinas display weak leakage of GABA signals into many glycinergic amacrine cells, suggesting widespread heterocellular coupling. The composition of the zebrafish ganglion cell layer is metabolically indistinguishable from that in other cyprinids, and the signatures of glial and non-neuronal cells display strong homologies with those in mammals. As in most vertebrates, zebrafish Müller cells possess a high glutamine, low glutamate signature and contain the dominant pool of glutathione in the neural retina. The retinal pigmented epithelium shows a general mammalian signature but also has exceptional glutathione content (5–10 mM), perhaps required by the unusually high oxygen tensions of teleost retinas. The optic nerve and the marginal zone of the retina reveal characteristic metabolic specializations. The marginal zone is strongly laminated and its nascent neurons display their characteristic signatures before taking their place in the retina proper.

Introduction

This atlas surveys the comparative molecular neuroanatomy of the zebrafish using computational molecular phenotyping methods. The description of the structural neurochemistry of the retina of the teleost cyprinid (*Danio rerio*) primarily focuses on cellular and chemical homologies with other cyprinid fishes and, where possible, with other vertebrates including mammals. Though the cyprinid classification might seem taxonomically narrow, alas, it is not. Over 2000 extant cyprinid species are split into >200 genera, with successful invasions of virtually every freshwater niche. New species are described yearly. Within this complex, zebrafish are the only members of the small subfamily Rasborinae to come into common scientific use as a model. Various members of the more diverse and cosmopolitan subfamily Cyprininae have served as physiological models, but are poor genetic tools. The need for a decisive comparison seems clear. Formal cellular homology has been a knotty problem in neuroscience, and the task has largely depended on *ad hoc* comparisons of structure. We here employ comprehensive molecular phenotyping based on signature groupings of small molecules invariant across taxa (Marc *et al.*, 1995).

The diverse photic histories of vertebrates impact our abilities to establish vertebrate homologies among extant taxa. Teleost fishes are of relatively modern emergence, expanding first in the early Cenozoic and leaving their legacy in the teeming Eocene fossil beds of Italy and the western United States. A last common ancestor with the tetrapoda predated the

*To whom correspondence should be addressed.

Osteichthyan-Sarcopterygian divergence and teleosteans are now the most diverse extant vertebrate group and evince the most extensive displays of retinal specializations known, many of which may be apomorphies. Teleosts have undergone ≈400 million years of uninterrupted selection, while mammals experienced a cataclysmic reduction in retinal complexity during their emergence, most likely in the early Jurassic. Early mammals collapsed in size from their large mammal-like reptilian predecessors to tiny insectivores resembling modern shrews and voles (Carroll, 1988). Along with this new body plan, early mammals were nocturnal, fossorial and cryptic: environments biased for myopic, achromatic and largely scotopic vision. The chromatic vision of modern teleosts is highly evolved and supported by over 110 classes of retinal neurons, while that of primates is barely 20 million years in the making, with likely no more than 60 classes of retinal neurons in hand. The zebrafish retina undoubtedly contains cell types, specializations and processes alien to mammalian vision.

This atlas is not a review of zebrafish literature. It is a molecular survey of the zebrafish retina with the goal of defining retinal cell types and establishing their homologies in other vertebrates. It provides a comprehensive mapping of the zebrafish retina in different areas, orientations, scales and adaptive states. The figures are available on CD at screen resolution so data may be viewed scales higher than print permits. Our emphasis is cell classification and retinal lamination, for from these structural data we find links to physiological attributes. The retinas of cyprinines (goldfish, *Carassius auratus*; koi, *Cyprinus carpio*; common carp, *Carassius carassius*; Japanese dace, *Tribolodon hakio*; rudd, *Scardinius erythrophthlamus*; roach, *Rutilis rutilis*; tench, *Tinca tinca*) have provided the broad physiological outlines of the vision of fishes, with strong homologies to and functional analogies with the retinas of anurans, reptiles and avians (Marc, 1992). Cyprinine retinas are complex, with up to seven cone cone classes showing distinct morphologies, four horizontal cell classes, eighteen bipolar cell classes, perhaps seventy amacrine cell classes and no less than fifteen ganglion cell classes: >110 classes of neurons (Marc, 1999b). The retina of the goldfish has been extensively mapped, structurally and neurochemically (Marc *et al.*, 1978; Marc & Lam, 1981; Yazulla, 1981; Marshak *et al.*, 1982; Yazulla *et al.*, 1984; Mosinger & Yazulla, 1985; Yazulla *et al.*, 1985; Mosinger *et al.*, 1986; Yazulla *et al.*, 1986; Yazulla *et al.*, 1987; Studholme & Yazulla, 1988; Yazulla & Zucker, 1988; Kalloniatis & Marc, 1990; Marc *et al.*, 1990; Yazulla & Studholme, 1990; Yazulla, 1991; Marc, 1992; Marc *et al.*, 1995) with predominant emphasis on fast glutamatergic, GABAergic and glycinergic pathways. Is the zebrafish a goldfish? Can we circumnavigate cumbersome and challenging physiological and structural analyses in zebrafish by structural/ chemical homologies that are known surrogate markers for function? We will show here that the zebrafish follows the known cyprinid *bauplan*: it is accurately patterned, strongly metabolically differentiated, and laminated at both the cellular and synaptic levels in the same manner as in other vertebrates.

The second theme of this atlas is the use of computational molecular phenotyping as a tool to differentiate cell types. Based on small molecule signatures at the single cell level, molecular phenotyping provides a compact biochemical description of cells, regardless of size, distribution, tissue or species. Though conceived and developed for the nervous system, the technology is applicable to all cells in all tissues, in all kingdoms. The most striking discovery emerging from computational molecular phenotyping is that virtually all cells, not just neurons, have metabolic specializations and useful class signatures. Of all neural complexes, the vertebrate retina is the most strongly specialized in cell types and metabolic differentiation. Computational molecular phenotyping extracts quantitative small molecule signals from every cell in a sample tissue array (Marc *et al.*, 1995).

We here use eight key molecules—a well-tested *basis set*—for retinal comparisons across taxa: L-alanine (A, ala); γ-aminobutyrate (γ, GABA); L-aspartate (D, asp); L-glutamine (Q, gln); L-glutamate (E, glu); glutathione (J, GTH); and taurine (τ, tau). The intracellular contents of these molecules reflect stoichiometric demands on source pools for (1) group transfer, (2) direct synthesis of other molecules, (3) osmoregulation, (4) redox regulation and (5) intercellular communication. There is a finite carbon skeleton budget for all cells and a fraction is dedicated to amines. The scale of this budget is millimolar, ≈10–100× greater than the levels of individual amino acids required to charge aminoacyl tRNA for protein synthesis. This makes a great variety of mixtures possible and these mixtures are characteristic signatures for neuronal classification.

Four technologies drive computational molecular phenotyping: (1) generation of serial thin section tissue arrays; (2) quantitative, reproducible immunochemistry; (3) quantitative computational signal capture and image registration; and (4) computational classification. With these tools, it becomes possible to extract a multidimensional signature from each cell in a tissue; the signature is the key to molecular phenotyping. Variations in small molecule content across cells permit statistical differentiation of classes (Marc *et al.*, 1995; Kalloniatis *et al.*, 1996; Kalloniatis & Tomisich, 1999; Marc & Jones, 2002) and provide snapshots of the metabolic functioning of each cell. While it is traditional to focus on the three amino acids glutamate, glycine and GABA as the fast neurotransmitter triumvirate of the brain and retina, we must stress that the relationships between

these molecules and neurotransmitter function are not binary... not a question of presence or absence... but rather quantitative questions of sufficiency and source. How much glutamate does a photoreceptor need? How much is required for synaptic transmission? Do some signals arise due to coupling or uptake rather than synthesis? Molecular phenotyping can answer many such questions directly and set boundary conditions for others.

Computational molecular phenotyping of the zebrafish retina reveals signatures that differentiate diverse cell cohorts: the retinal pigmented epithelium (RPE), the pigmented and non-pigmented ciliary epithelium (PCE and NPCE), choroidal melanocytes and vascular cells; glial cells; and, of course, many retinal neurons. The signatures of virtually all cell types strongly match those established for mammalian counterparts, including the epithelial variants. This provides an strong argument for using the zebrafish as a model of general ocular processes such as fluid transport, intraocular pressure regulation, and uveal tract functions. The general similarity of zebrafish and primate Müller cell signatures suggests that zebrafish-based models of glutamate regulation should be valid for all vertebrates. New neurons are continually added to the margin of the zebrafish retina during growth in the adult, and it can regenerate retinal neurons after retinal damage or ablation (Cameron, 2000; Cameron & Carney, 2000; Cameron & Powers, 2000; Stenkamp *et al.*, 2001). The molecular signatures of cells in the marginal zone are already laminated, prefiguring the emergence of photoreceptors, inner nuclear layer neurons and ganglion cell layer neurons.

Materials and methods

CLASS TERMINOLOGY

Retinas are built from six formal cell *types*, distinguished by position and shape: photoreceptor, bipolar, horizontal, amacrine, ganglion and glial cells. But each type admits division based on morphology, connectivity and neurochemistry. In computational analysis, we define classes and superclasses as subsets of a type extracted by some quantitative method such as molecular phenotyping. A statistical class is defined by its position and dispersion in N-dimensional signal space and if it is well separated from its fellows and cannot be separated further in additional dimensions of any nature, it may be a *natural class*: a true homogeneous, biological cell class. That conclusion is strengthened if the statistical class possesses additional features associated with the natural classes. Alternatively, groups of natural classes may share so many molecular features that they can be grouped as a statistical *superclass*. In this atlas we will describe subsets of cell types that are likely to represent natural classes (statistical classes) and subsets that are clearly assemblies of several natural classes (statistical superclasses). Further details are given in Marc and Jones (2002). For conciseness, we sometimes denote the small molecule signals and their enrichment or depletion as single letter codes. Thus glutathione-rich, glutamate-poor cells can be termed J+ E−.

STRUCTURAL TERMINOLOGY

The cell types and classes that comprise the known cyprinid retinas have been formally named and we apply those conventions to the zebrafish in detail. Cyprinid cones fall into morphologically distinct classes (Marc, 1982, 1999b), which each contain a specific dominant pigment and engage in cone-specific synaptic connectivity patterns (Scholes & Morris, 1973; Scholes, 1975; Stell & Harosi, 1975; Marc & Sperling, 1976, 1977). Zebrafish cones are similar to those of other cyprinids (Raymond *et al.*, 1993; Robinson *et al.*, 1993), although other nomenclatures have emerged. We revert to the standard cyprinid nomenclature to stress class homologies. The zebrafish retinal mosaic is patterned with unequal double cones: Red VP570 opsin in the long double (LD) and green VP480 opsin in the short double (SD) members. Zebrafishes do not possess long single (LS) cones homologous to those of the goldfish, carp, roach or rudd. The blue VP415 opsin cones of zebrafish are structurally and, as will be shown, metabolically homologous to the short single (SS) cones of other cyprinids. Further, the UV VP362 opsin cones of zebrafish are structurally and metabolically homologous to the miniature short single cones (MSS) of the goldfish.

Cyprinids display pure rod and pure cone horizontal cells (Stell, 1975; Stell & Lightfoot, 1975) and the latter possess large axon terminal extensions (see review by Djamgoz *et al.* (1995)). The red cone dominated, monophasic H1 horizontal cells have a distinctive $\gamma+$ signature; spectrally opponent H2 and H3 (collectively termed Hx) horizontal cells have a $\gamma-$ signature; rod horizontal cells have a $\gamma-$/ E+ (glutamate-positive) signature (Marc *et al.*, 1995; Watt *et al.*, 2000).

Cyprinid bipolar cells have mixed rod-cone or pure cone inputs (Scholes & Morris, 1973; Famiglietti *et al.*, 1975; Scholes, 1975; Ishida *et al.*, 1980a; Sherry & Yazulla, 1992). ON-center mixed rod-cone bipolar cells form a superclass separable into three classes (Bb1, 2, 3) in sublamina b (the proximal half) of the inner plexiform layer. OFF-center mixed rod-cone bipolar cells form a superclass separable into two classes (Ba1, 2) that terminate in the distal half of the inner plexiform layer, sublamina a. Homologues of the Ba and Bb superclasses are clearly present in the zebrafish retina. The remaining large cohorts of pure cone Ca, Cb, and Cab bipolar cells are complex and more difficult to compare, but evidence of C bipolar cell superclasses is strong. No satisfactory terminology has emerged for the complex amacrine cell and ganglion cell populations. Finally, the inner plexiform layer is highly structured and we use the *level* terminology (Ammermuller & Weiler, 1981; Marc, 1986) to specify position: the amacrine cell layer proximal border is level 0, and the ganglion cell layer distal border is level 100, with all other loci linearly scaled between.

RETINAL PREPARATIONS

These methods follow those described previously (Marc *et al.*, 1995). Light-and dark-adapted laboratory raised adult unsexed *Danio rerio* were deeply anesthetized in MS-222 aquarium water and cervically transected. Both eyes were rapidly removed, the corneoscleral junction immediately pierced

with a 27 ga needle tip and flushed with room temperature fixative: 2% glutaraldehyde, 1% paraformaldehyde, 0.08 M phosphate buffer, 3% sucrose, 1 mm $MgSO_4$, pH 7.4. The anterior segment was removed and the eyecups fixed overnight. Speed of dissection was important for retention of GABA in horizontal cells and glycine in amacrine cells. All tissue was processed for resin embedding as previously described (Marc *et al.*, 1990).

SPECIMEN PREPARATION AND IMMUNOCYTOCHEMICAL VISUALIZATION

Each sample was sectioned serially at 250 nm onto 12-spot Teflon-coated slides (Cel-Line, Fisher Scientific). The immunocytochemical and IgG production procedures were as described previously (Marc *et al.*, 1995). The samples were serially probed with IgGs targeting alanine, aspartate, glutamate, glutathione, glutamine, glycine, GABA, and taurine obtained from Signature Immunologics Inc[1] (Salt Lake City, Utah). The selectivities of these probes have been extensively tested against their naturally occurring fee amino acid targets, as well as against a spectrum of other amines (Marc *et al.*, 1995; Marc & Jones, 2002). In practice, their selectivities for their target haptens is >3 log units in most cases. The relevant exceptions are as follows. (1) Anti-L-glutamate is only 8-fold selective for L-glu versus the metabolite N-acetyl-aspartyl-glutamate. However, N-acetly-aspartyl-glutamate is N-blocked and not captured by aldehyde fixation. (2) Anti-GABA is only 80-fold selective for GABA versus β-alanine. This poses no significant cross-contamination, as discussed in Marc and Jones (2002)). (3) Anti-glutathione does not discriminate between reduced and oxidized forms; it reports only total glutathione content. Primary IgG signals were detected with goat-anti-rabbit IgGs adsorbed to 1nm gold particles (Pharmacia-Amersham Intl plc) and visualized with silver intensification using the silver-intensification protocol of Kalloniatis and Fletcher (1993). The silvering process was run at 30°C for 240 sec before quenching. All preparations received identical probing and visualization treatments, yielding 2 orders of magnitude of detection range with differential concentration sensitivity as low as 40 μM based on artificial standards. Standard and augmented single letter amino acid codes are sometimes used to denote alanine (A), aspartate (D), glutamate (E), glutathione (J), glycine (G), glutamine (Q), and taurine (τ) and GABA (γ).

IMAGE CAPTURE

All images of immunoreactivity were captured as 8-bit frames under fixed CCD camera gain and gamma as previously described (Marc, 1999a). The objective lenses were either 20× apochromats or 40× oil planapochromats, yielding resolutions ranging from 485 nm/ pixel to an over-sampled maximum of 126 nm/ pixel; most images were captured at 243 nm/ pixel, as this provides the maximum practical resolution and optimal pixel density for optical microscopy. Silver-intensified immunogold labelling produces *density-scaled* images, and linear image inversion produces *intensity-scaled* images that are linear with $\log_{10}$(concentration) of the target molecule over a range of 0.05–10 mM.

IMAGE ARCHIVE CREATION

The central step in molecular phenotyping is the creation of permanent data archives from registered image sets. Registration is a highly demanding operation and cannot be achieved by simply shifting images manually. Computational classification demands optimized data quality, which is a function of alignment precision. Even simple linear alignment at unit scaling requires both translations and rotations calculated from good control points. These are often difficult to identify in images that have complex or weak correlations in signature space. If there is any small shear due to section stretch, it cannot be managed by manual adjustment. Large sections often possess visually undetectable distortions that can corrupt linear alignments. A section 1 mm in extent with a mechanical stretch distortion of only 1%, embeds a propagating misalignment reaching 10 μm (two bipolar cell widths) in a linearly scaled image. This means that, starting from one "good" region of alignment, the data will be misaligned by a full cell halfway across the image and, in practice, over 90% of the image data will be useless. As we require <200 nm (<1 pixel) alignment precision, nonlinear spatial transform algorithms are essential. For similar reasons, automatic image alignment algorithms have never been successfully implemented. The most effective tool, in our hands, has long been remote sensing registration code from PCI Geomatica® (Richmond, Hill, Ontario, Canada).

Registered image archives were generated in two steps: registration of arrays of image tiles into mosaic channels (Fig. 1a) and registration between mosaic channels (Fig. 1b). Most of our data images subtend 187 μm × 140 μm, so a patch of tissue scaled at >40 tiles/ mm^2 assembles into a single channel image of >17 megabytes (Mb)/ mm^2. Thus 10 registered mosaics form a single ≈170 Mb/ mm^2 file of aligned image channels at optimal resolution. Alignment was initiated by manual selection of small set of corresponding control points in master and slave images. These need not be at final precision, as the registration algorithms predict the best next slave image coordinate point based on Nth-order geometric models or local spline methods. Even with such predictive algorithms, it is extremely difficult to register images that lack strong signal differentiation or clear landmarks and the creation of datasets can take many weeks of work. Registered files are then exported from the proprietary file structure of the PCI Geomatica® code into a standard TIFF 6.0 format as a list of alpha channels.

Image classification based on small molecules has been detailed previously but follows this general scheme: (1) Isodata clustering of N registered channels, (2) theme map generation, (3) histogram exploration and, if necessary, (4) deconvolution and theme map correction. After theme map generation, univariate and bivariate signal histograms were explored for each emergent class. In cases where a signal was clearly multimodal, the histogram was deconvolved and each cell recoded. Classes resolved by clustering were formally *statistically separable* and those resolved by deconvolution were formally *statistically significant* (see below). Classifications were performed using the isodata algorithm (PCI Geomatica®) and data explored with applications written in IDL® (Research Systems Inc., Boulder, CO). An overview of and reference lists for pattern recognition methods are provided in Marc *et al.* (1995). The isodata algorithm resembles simpler K-means

clustering methods but adds heuristic splitting of high variance classes and merging of highly overlapping classes (Ball & Hall, 1967). When the means and covariances for a set of N-dimensional data allow classifying a sample of those data into distinct classes, we call them *statistically separable*. The probability of error (p_e), estimated from the transformed divergences of the classes assuming equal *a priori* probability densities, is ≤ 0.01 for classes deemed *separable*. Separable classes are also inherently *statistically significant* classes. Natural classes need not be inherently separable by clustering and could have signature overlaps greater than required for separability yet still be statistically significant classes. Exploration of datasets with histogramming tools and deconvolution methods increases the sensitivity of analysis and permits detection of classes hidden in the complex array of N-dimensional data. Strongly separable cells can be removed first, simplifying analysis of the remaining data.

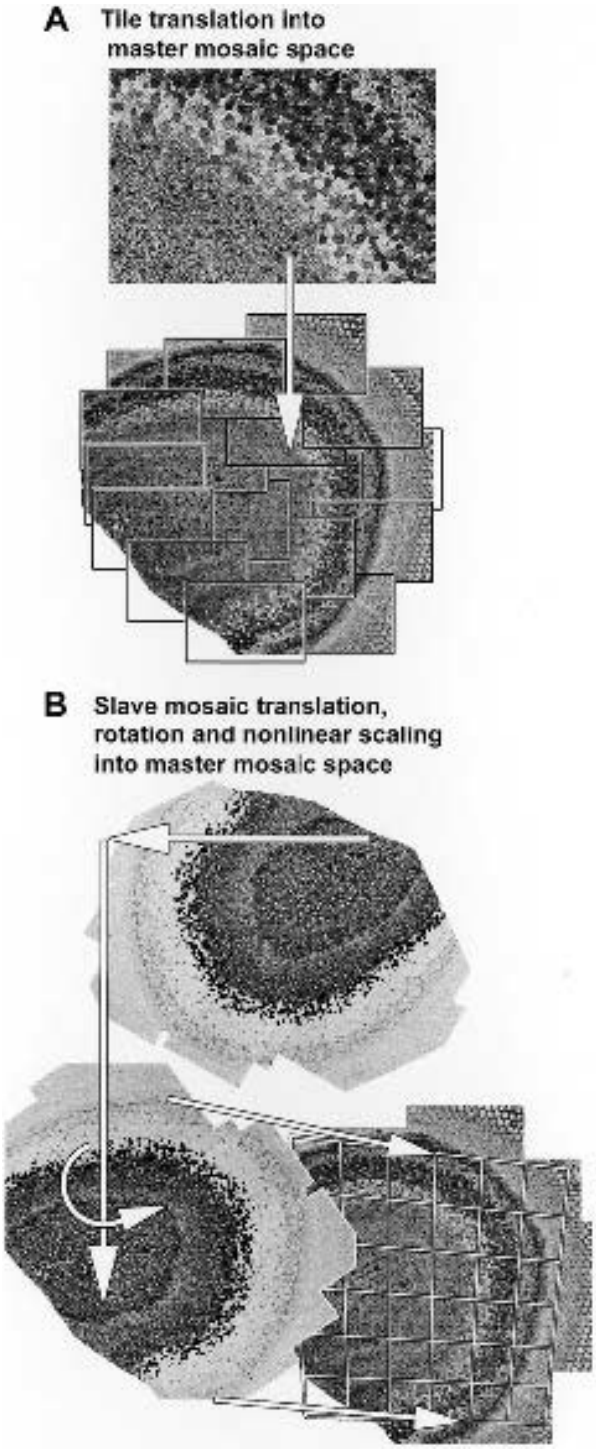

Fig. 1. Assembly of mosaics and registered channel sets. A. Single image tiles are spliced together with <200 nm error to form a large mosaic at optimal light microscope resolution (<250 nm). Each mosaic ranges from 5–20 Mb in size. This example illustrates the embedment of a single glutamate signal tile into an oblique section glutamate signal mosaic. B. Each mosaic in a series is precision-registered with all other mosaics, including corrections for shear and local warping. This example illustrates the translation, rotation and nonlinear scaling of a slave GABA signal mosaic to register it with a master glutamate signal mosaic. The grid represents the kind of distortion encountered with some large sections.

No set of monochrome images can visualize molecular mixtures or partial signatures. Selected 3-dimensional class signatures were visualized as follows: (1) *rgb* maps encoding molecular signal triplets as additive red, green and blue signals (see appendix in Marc *et al.* (1995)); (2) **cmy** maps encoding signals as subtractive cyan, magenta, and yellow triplets; and (3) *rgb*/ **cmy** mixtures when visualization of classes is facilitated by a complex color space (*e.g.*, *r*-**m**-*b*, additive red, subtractive magenta, additive blue). The discriminations made by triplet mapping can be powerful, as quantitative colocalizations can be displayed, but no single triplet can capture the characteristic signatures of all cells. Sets of triplets are required and the particular triplets must be chosen carefully. After all, there are 56 unique triplets possible in 8-space, and four possible display conditions (pure *rgb*, pure **cmy**, and two mixtures) yielding over 200 "looks" at the same data, ignoring color permutations. Visually searching all these displays for correlations is ineffective and non-quantitative, but the right ones can reveal populations and relationships visible no other way.

Classification, as described above, is one proper solution to acquiring real numbers that characterize cell classes. *Classifications* were visualized as formal theme maps, where each color or other code represents a statistically significant group (class or superclass). The actual N-dimensional signatures were displayed as stacked bivariate *2N-plots* (Marc & Jones, 2002). Classical single bivariate plots display the area occupied by a class in a two dimensional chemical space. 2N-plots superimpose bivariate plots, capturing pairwise most of the features discriminating cell groupings in an N-space (Fig. 2). This method was inspired by the parallel coordinate space described by Inselberg and Dimsdale (1990). Pairs of signals were displayed as class means bounded by 1 SD margins. The XY axes spanned 0.1–10 mM with logarithmic scaling and the XY pairs were color-coded: grey AJ, gold Eγ, cyan DQ, and magenta Gτ. The class means were acquired after first transforming the raster-based image sets to *object* sets of

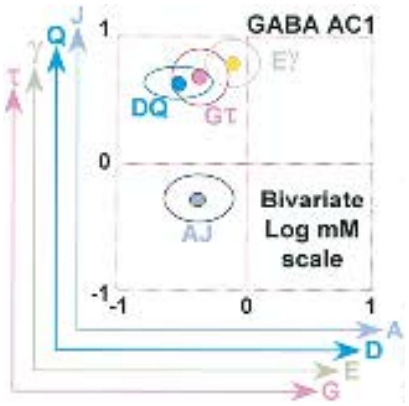

Fig. 2. N-plot for the ADEGJQ$\tau\gamma$ basis set. This N-plot was derived from the molecular phenotype data of class 1 GABA amacrine cells (GABA AC1). Each dot encodes a bivariate mean on a logarithmic mM scale (*i.e.* $-1 = 0.1$ mM, $0 = 1$ mM, $1 = 10$ mM), and is bounded by a 1 standard deviation ellipse. Four pairs of points represent a projection of 8-space into 2-space, and distinctions among classes are thus represented by the differing patterns of signals in N-plots (see Marc & Jones (2001)). The XY pairs are arbitrarily formed but constant throughout this manuscript: AJ (grey), DQ (cyan), Eγ (gold), Gτ (magenta). In this plot, it can be quickly determined that the mean A, D, G, E and J values are less than 1 mM in this class, because their coordinates are all below the log 0 mM line. Conversely, the mean Q, γ and τ values are all $\gg 1$ mM.

classified cells and the means and variances calculated from cell numbers rather than pixel numbers.

Average cell sizes and cell spacings were acquired with the object utilities in ImagePro (Media Cybernetics, Silver Spring, MD). All cell sizes in each sample were measured only from individual 250 nm sections, such as the glutamate channel, so cell size estimates contain no registration errors and require no use of dissector or other stereological correction methods. Some classified cells often appeared to form regular arrays, and these were numerically characterized by their *conformity ratios* (also known as regularity indices): the ratio of the class mean nearest-neighbor distance to its standard deviation. The significance of the deviation of a conformity ratio from that predicted for a random pattern was determined from significance charts (Cook, 1996).

FIGURE PREPARATION

All images are digital, assembled from the raw data captured by CCD camera (see *Image Analysis* above). Selected frames of raw Tagged Image Format (*.tif) files were extracted for display and contrasts were adjusted with linear remapping to optimize fidelity of prints to the original microscopic images. All final images were prepared in Adobe PhotoShop® 6.01.

Results

The general metabolic phenotypes of various zebrafish retinal cells are similar to most vertebrates, including mammals, but the specific classes that they fall into of define zebrafish as cyprinid fishes as surely as any taxonomic feature: a row patterned cone mosaic, at least three and likely four horizontal cell classes, bipolar cell classes with characteristic Ba and Bb terminal morphologies, a $\approx$2:1 γ+/ G+ amacrine cell population ratio, the presence of glycinergic interplexiform cells, and simple ganglion cell layer with minimal coupling signals.

THE GENERAL PLAN OF THE RETINA

Both cellular organization and metabolic differentiation are well illustrated by the patterning of glutamate signals in the dark-adapted zebrafish retina shown in Figure 3. This image is essentially a quantitative map of glutamate distribution and clearly distinguishes the cell types of the retina. The adaptation state is an important topic to which we will return. The highest neuronal glutamate levels are expressed by some bipolar cells, their dendrites in the outer plexiform layer and their axon terminals in the inner plexiform layer. The signal strength corresponds to 5–10 mM free glutamate in the cytosol. This high concentration is not unique to neurons, however, as the endothelial cells forming the radially arrayed vitreal blood vessels that line the proximal margin of the retina contain as much or more glutamate. The remaining bipolar cells, most ganglion cells and dark-adapted long (LD) and short (SD) double cones and rods express roughly 2–5 mM glutamate. The next lower range (0.5–1 mM) includes the short (SS) and miniature (MSS) short single cones, the RPE, and the horizontal cells. The lowest retinal glutamate levels (<0.3 mM) are displayed by amacrine and Müller cells.

Two important concepts emerge from the image in Figure 3. First, the cells of the zebrafish retina are exceptionally well laminated in comparison to most other vertebrates, including its cyprinid relatives. The somas of the bipolar cells are displaced some 5 μm from the outer plexiform layer by the interposed somas of the horizontal cells and 10 μm from the inner plexiform layer by the interposed amacrine cells; thus distinct horizontal, bipolar and amacrine cell layers comprise the inner nuclear layer proper. As will be shown, the somas of the Müller cells are less precisely positioned, but preferentially occupy the border between the bipolar and amacrine cell layers. The inner plexiform layer also displays a precise division into sublayers occupied by characteristic cyprinid bipolar cell cohorts. Classically, sublaminas *a* and *b* represent zones dominated by OFF-center and ON-center rod and long-wave cone processing, respectively. This is reflected in the laminar partitioning of characteristic size groupings of bipolar cell terminals: (1) the large 5–7 μm diameter terminals of ON-center Bb bipolar cells at level 80–100; (2) the medium 3–5 μm terminals of OFF-center Ba bipolar cells, which are further divisible in to classes Ba1

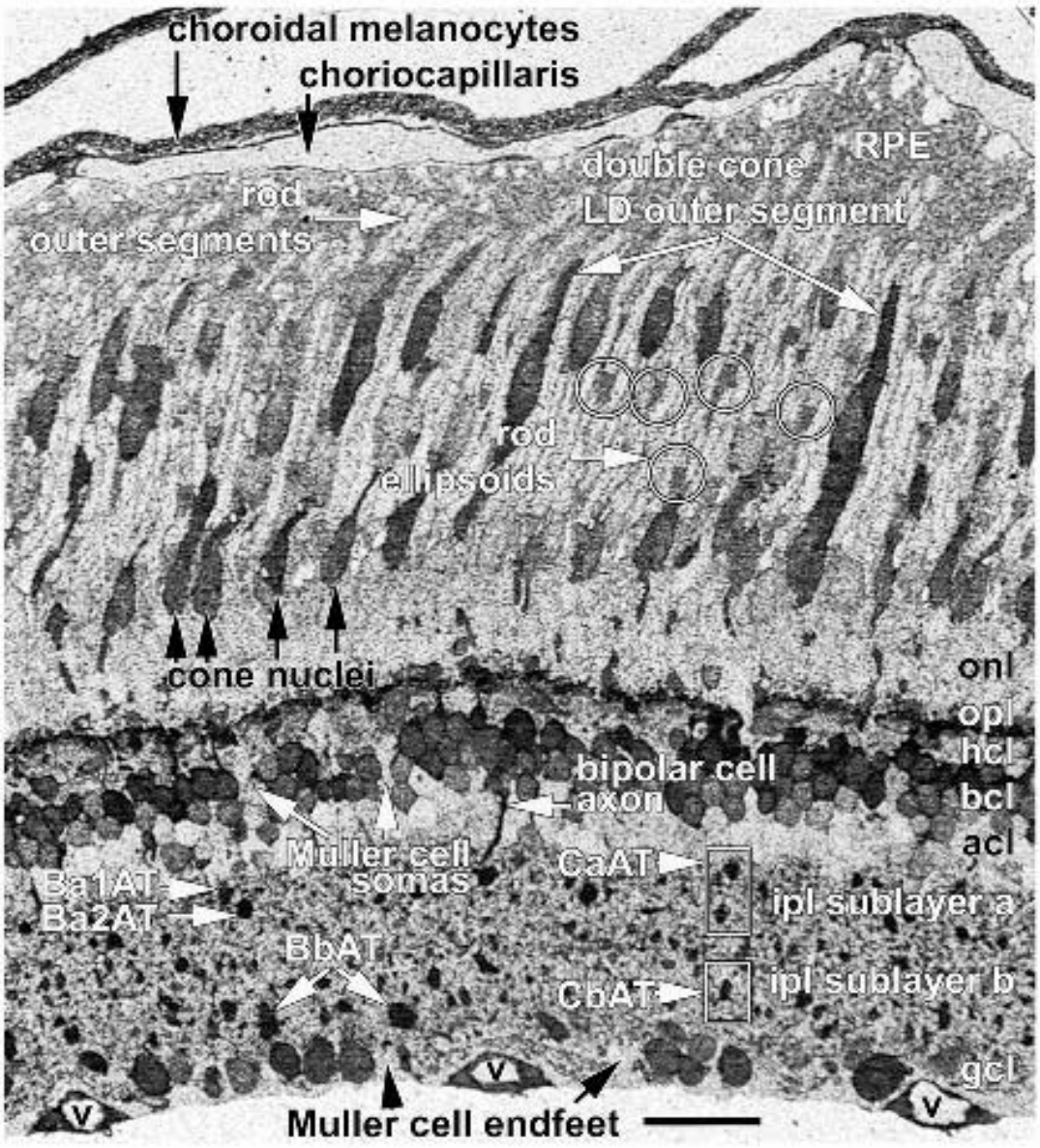

Fig. 3. Glutamate signals in the dark-adapted zebrafish retina. This single image displays virtually all choroidal, RPE and retinal cell types by virtue of their varying contents of free glutamate. Rod ellipsoids are circled and key structures labeled. Section thickness: 250 nm. Scale 20 μm. Abbreviations: acl, amacrine cell layer; Ba1AT, class Ba1 bipolar cell axon terminal; Ba2AT, class Ba2 bipolar cell axon terminal; BbAT, class Bb bipolar cell axon terminal; CaAT, class Ca bipolar cell axon terminal; CbAT, class Cb bipolar cell axon terminal; bcl, bipolar cell layer; gcl, ganglion cell layer; hcl, horizontal cell layer; ipl, inner plexiform layer; LD, long double cone member; onl, outer nuclear layer; opl, outer plexiform layer; RPE, retinal pigmented epithelium; v, radial vitreal blood vessel.

and Ba2; and (3) profuse examples of small pure cone bipolar cell varicosities (Ca, Cb). The separations and precisions of the sublayer borders are actually superior to that of the best-studied cyprinid, the goldfish. Even though the adult zebrafish eye is some 6-fold smaller in area than a 3–4 year old goldfish, the inner plexiform layer is still as thick as the central goldfish retina inner plexiform layer, $\approx$30–35 μm. This suggests that the zebrafish contains as many bipolar/ amacrine/ ganglion cell types *per mosaic unit cell* as the goldfish, despite its small size.

The second concept emerging from Figure 3 is that each retinal cell type shows a distinctive, stable, but *dynamic* metabolic profile: the profile is the consequence

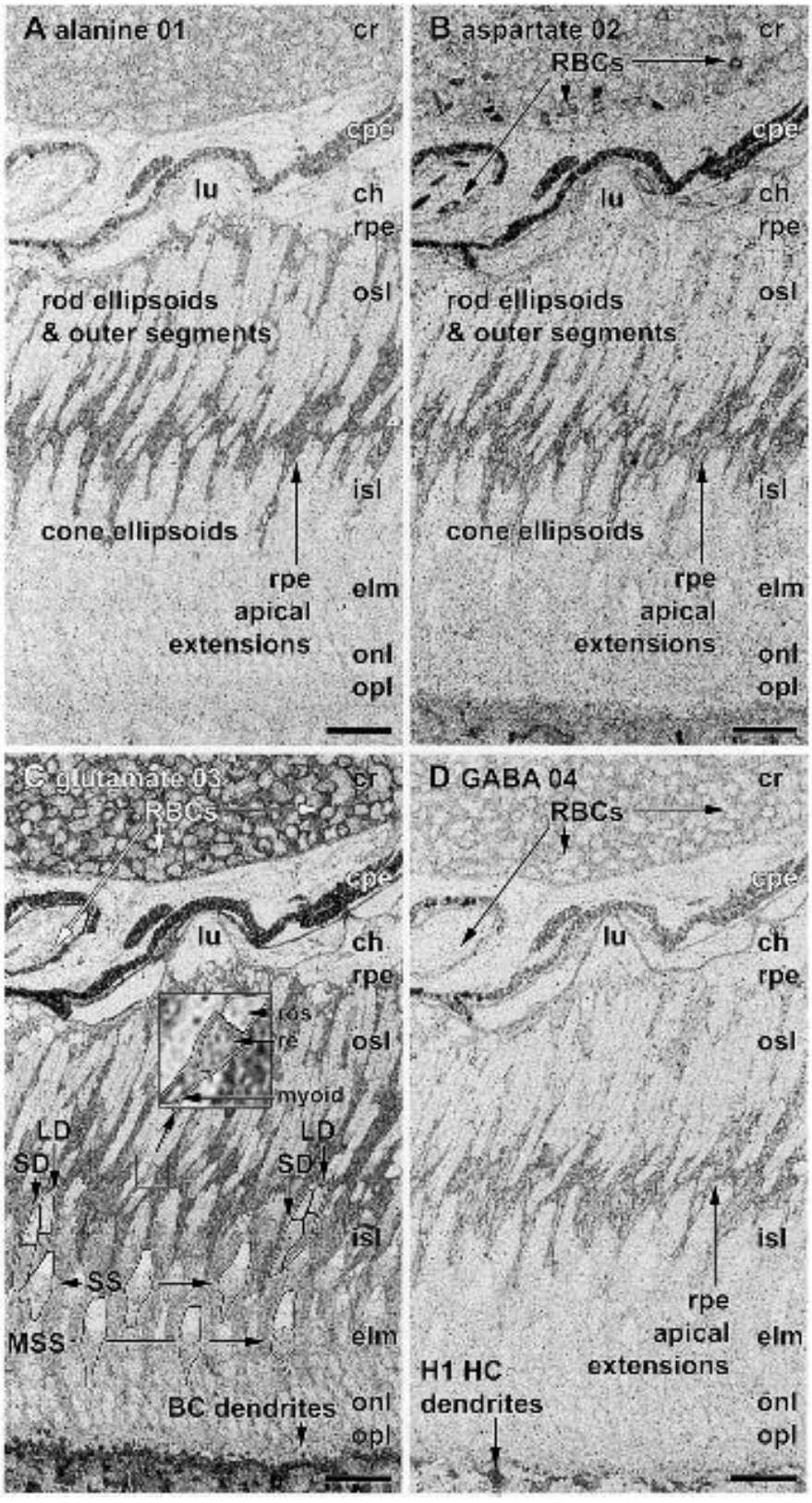
A alanine 01
cr
cpe
lu
ch
rpe
osl
rod ellipsoids
& outer segments
isl
cone ellipsoids
rpe
apical
extensions
elm
onl
opl
B aspartate 02
RBCs
C glutamate 03
ros
re
myoid
LD
SD
SS
MSS
BC dendrites
D GABA 04
H1 HC
dendrites

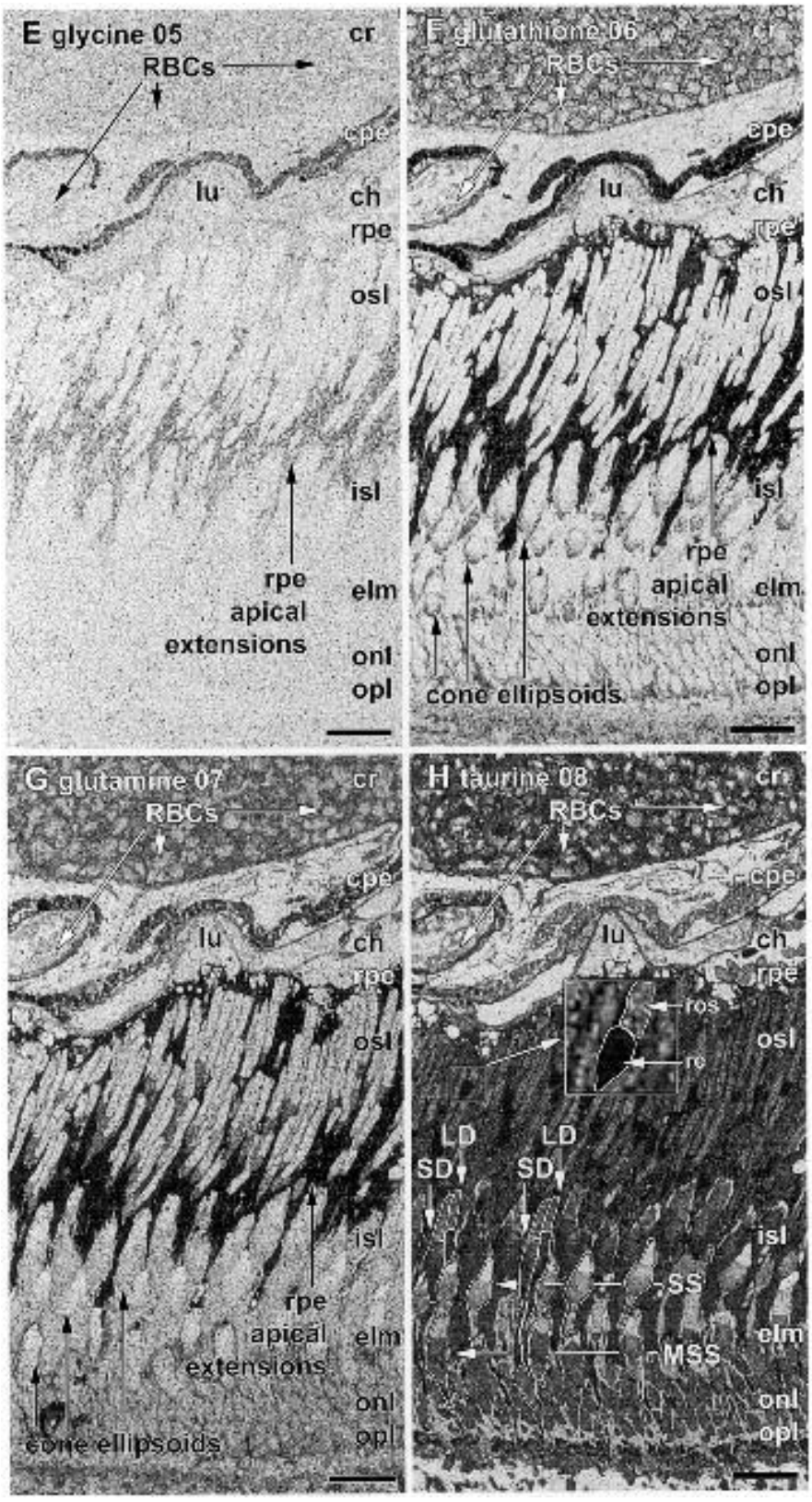
E glycine 05
RBCs
cr
cpe
lu
ch
rpe
osl
isl
rpe
apical
extensions
elm
onl
opl
F glutathione 06
RBCs
cr
cpe
lu
ch
rpe
osl
isl
rpe
apical
extensions
elm
cone ellipsoids
onl
opl
G glutamine 07
RBCs
cr
cpe
lu
ch
rpe
osl
isl
rpe
apical
extensions
elm
cone ellipsoids
onl
opl
H taurine 08
RBCs
cr
cpe
lu
ch
rpe
ros
osl
rc
LD
LD
SD
SD
isl
SS
elm
MSS
onl
opl

of multiple fluxes. For example, it is well-known that the most potent glutamate transport in the retina is displayed by the Müller cells, both due to their high expression of transporters and their massive surface area, which includes both the proximal and distal diffusive seals of the neural retina. Even so, the Müller cells display the lowest steady-state glutamate content, due to their expression of very high levels of glutamine synthetase. Either chemical inhibition of glutamine synthetase (Pow & Robinson, 1994) or pathologic loss of glutamine synthetase expression (Marc *et al.*, 1998a) evokes a rise in intracellular glutamate in Müller cells that reaches the levels of glutamatergic neurons. As we will see, these and other cells exhibit either static or dynamic metabolic phenotypes depending on the linkage of source and sink processes to adaptational or respiratory states. We will now explore the molecular phenotypes of retinal cells in a distal → proximal fashion, using molecular phenotypes (where necessary) to distinguish cell classes.

THE LIGHT-ADAPTED OUTER RETINA

The outer retina, in a metabolic sense, is a compartment sealed between the basolateral tight junctions of the RPE and the microvillar tight junctions of the Müller cells (Fig. 4). The RPE serves as a distal transport monolayer between the extracellular plasma in the lumens of the fenestrated choriocapillaris endothelia and the extracellular subretinal space. The zebrafish, possesses a teleost apomorphic organ, the *choroidal rete*, which mediates counter-current amplification of oxygen tension. By analogy with larger fishes, this structure is expected to generate pO_2 values of >300 mm Hg, 3 to 4 (Fonner *et al.*, 1973) times the saturated arterial values of mammals. The zebrafish retina likely has the same ultrahigh oxygen demands as other teleosts and is thus not a plausible general model for oxygenation in the outer retina of mammalians. The diverse cellular composition of this compartment displays subtly diverse molecular phenotypes when probed with the basis metabolite set of alanine, aspartate, glutamate, glycine, glutathione, glutamine, taurine and GABA (abbreviated ADEGJQ$\tau\gamma$).

Alanine levels are extremely low in the outer retina, reaching their maximum value in the RPE of 0.5–1 mM, and roughly half of that in the endothelia of the choroidal rete (Fig. 4A). To put this minor elevation in perspective, the photoreceptors, with perhaps the highest sustained rates of retinal protein synthesis, maintain less than 50 μM alanine. What, then, is the purpose of a metabolic pathway that maintains such an elevated level of alanine in the RPE? Alanine is not an essential dietary amino acid in fishes, but is a key metabolite in the maintenance of pyruvate pools via general transamination paths and is a source of amino groups (Michal, 1999). As will be considered below, one source of retinal glycine synthesis may involve transamination of alanine and glyoxylate.

Aspartate signals are a little lower than alanine signals in most cells of the outer retina, with the exception of nucleated red blood cells, evident both in the choriocapillaris and the choroidal rete (Fig. 4B). In contrast, *glutamate* signals are actually weaker than aspartate in the red blood cells. The vascular endothelia, the RPE and photoreceptors all express elevated glutamate levels, but with some significant differences (Fig. 4C). The highest glutamate levels in the light-adapted outer retina are maintained by the RPE at ≈1 mM, while all photoreceptors maintain lower levels, especially the SS cones. As in the goldfish (Marc *et al.*, 1995), light-adapted zebrafish photoreceptors maintain glutamate levels in the 100–800 μM range. We are accustomed to the idea that cells must maintain high cytoplasmic levels of their specific neurotransmitters, yet it is evident here that only very low intracellular levels of glutamate

Fig. 4. (Previous 2 pages) Single channel, registered ADEGJQ$\tau\gamma$ signals in the light-adapted photoreceptor layer. The index number following the signal label on each image indicates its position in the series. A, alanine 01. Only the RPE has significant signals. The signal strength in the choroidal pigmented epithelium reveals the basal optical density produced by endogenous melanin. B, aspartate 02. The RPE aspartate content is low, exposing the positioning of melanin in the RPE apical extensions. Conversely, the choroidal pigmented epithelium contains high levels of aspartate, as do RBCs. C, glutamate 03. Glutamate signals are elevated in the RPE, choroidal pigmented epithelium and all choroidal endothelia. Photoreceptor levels are modest and slightly less than the RPE. The two inset boxes are 10 μm square and show the details of glutamate distribution in a rod. D, GABA 04. Only basal signals are present, but for the dendrites of horizontal cells. E, glycine 05. Only low levels of glycine are present. F, glutathione 06; The RPE and choroidal pigmented epithelium display extremely high glutathione content, with lower more complex patterns in other cells. G, glutamine 07. Similar to glutathione, glutamine reaches extremely high concentrations in the RPE and choroidal pigmented epithelium. H, taurine 08. Taurine is the most abundant amino acid in the outer retina and is enriched in all cell types but for the choroidal pigmented epithelium and short single cones. The two inset boxes are 10 μm square and show the details of taurine distribution in a rod. Section thickness: 250 nm. Scale 20 μm. Abbreviations: BC, bipolar cell; ch, choroid; cpe, choroidal pigmented epithelium; cr, choroidal rete; elm, external limiting membrane; H1 HC, class H1 horizontal cells; lu, vascular lumens in the choriocapillaris; isl, inner segment layer; MSS, miniature short single cones; osl, outer segment layer; re, rod ellipsoid; ros, rod outer segment; SD, short double cone members; SS, short single cones; RBCs, nucleated erythrocytes; other abbreviations as in Figure 3.

are needed to support photopic glutamatergic synaptic transmission in the outer plexiform layer. This implies that the efficacy of vesicle loading by glutamate is very high.

The non-protein amino acid *GABA* is best known as a vertebrate inhibitory neurotransmitter and, consistent with this, its signals are extremely low in the outer retina (Fig. 4D). The elevated GABA signal in H1 horizontal cell dendrites gives visual scaling. There is $\approx$100 μM GABA in the endothelia of the rete and the RPE, though these cells do not express detectable levels of glutamic acid decarboxylase (GAD) by qualitative immunocytochemical criteria. But it is critical to recall that GABA is a primary respiratory metabolite in plants and bacteria and that GAD expression directly couples to the maintained level, so low levels of GABA are not necessarily surprising in non-neural cells. Furthermore, GABA is an obligate intermediate in the polyamine degradation pathway (Michal, 1999), and cells with high polyamine synthesis rates might accumulate low levels of GABA. *Glycine* is also best known as an inhibitory neurotransmitter, but is clearly maintained at protein synthesis levels (50–300 μM) in the outer retina (Fig. 4E).

One of the most dramatic signal patterns in the outer retina is the partitioning of *glutathione* (Fig. 4F), which reaches 5–10 mM levels in the somas and apical extensions of the RPE. Glutathione levels are immeasurably low in photoreceptor outer segments, but reach about 0.5 mM in granular zones surrounding the proximal margin of the ellipsoid in all cone types. Moderate levels are expressed in the endothelium of the rete and higher levels in the choroidal pigmented epithelial stroma. The demand for glutathione can arise from three primary processes: (1) the need for thiol reducing equivalents in various metabolic reactions; (2) the need to quench reactive oxygen species formation; (3) the need for glutathione-coupled amino acid transmembrane transport. At the least, the RPE is likely to require the latter two functions to accompany its roles in degrading photoreceptor outer segment membranes rich in oxidizable fatty acids, operating in excessive oxygen tensions and mediating transcellular amine transport. The apical extensions of the RPE reach within 20 μm of the external limiting membrane. Müller cells also contain $\approx$1 mM glutathione, as evidenced by the outlining of the rod nuclei and a distinct band of glutathione-rich punctae at the level of the outer limiting membrane. Thus the subretinal space is bordered by cells that maintain exceptionally high glutathione levels.

The content of the amino acid *glutamine* somewhat resembles that of glutathione, though it is more abundant in rod inner segments than cone inner segments. The RPE contains over 10 mM glutamine: a level rivalled only by ganglion cells. In neurons, glutamine is thought to be a primary source of glutamate via phosphate-activated glutaminase in the inner mitochondrial membrane. The RPE clearly does not need to maintain this pool of glutamine just for glutamate synthesis and it is not clear how the RPE synthesizes or acquires it. Glutamine is, however, one of the major sources of amino equivalents for the generation of amino sugars and pyrimidine interconversions.

Finally, the non-protein acidic amine taurine is widely distributed in the outer retina and every cell contains supramillimolar levels. The highest levels are located in the ellipsoids of rod cells, followed by the RPE, the endothelia of the rete, and the LD and SD cones. The lowest taurine levels are maintained by the SS cones, as in other cyprinid fishes. These images also reveal that the outer segments of photoreceptors are possibly well-equilibrated with the cytosol of the inner segments. The taurine level is always lower in the outer segments but matches that in the inner segments: outer segments of cones with higher inner segment taurine are also taurine-enriched. Outer segments are composed of extremely dense arrays of rod discs or cone lamellae, with little intracellular space. Based on electron microscopic images, the cytosol of rod and cone outer segments likely comprises less than 1/ 3 of the outer segment volume, and apparent taurine signals should be correspondingly reduced even if fully equilibrated with the inner segment due to optical blurring. Taurine has never been found to have a significant metabolic or neurochemical role and is widely thought to be one of several small organic osmolytes involved in volume regulation. In addition to ion channel permeations that may change water distribution, the photoreceptors and the RPE of many aquatic vertebrates undergo large shape changes in light and dark adaptation that may require robust pressure regulation.

Though the outer retina is a relatively simple compartment, it is heterocellular, with 9 resident cell classes: four photoreceptor classes, two endothelial classes, two epithelial classes, and one glial cell class. Qualitative differentiation of these classes is gained by examining color triplet images. Mapping the triplet taurine $\rightarrow$ red, glutamine $\rightarrow$ green, glutamate $\rightarrow$ blue (abbreviated τQE $\rightarrow$ *rgb*), clearly distinguishes most of the cellular elements in a single step, with the yellow (τQ) signal of RPE cells setting them apart from the dark-to-bright red τ signal of photoreceptors and the bright green threads of the Müller cells in the outer nuclear layer (Fig. 5A). The endothelia of the choroids are a pale pink signal, while blood elements are only poorly visible. Changing the triplet mixture to DJE $\rightarrow$ *rgb* (Fig. 5B) reveals the high aspartate levels in red blood cells and contrasts the RPE against the darkened photoreceptors. Only glutathione-rich necklaces proximal to the cone ellipsoids identify them. The most complete separation of the RPE signature from all others cells is achieved with a τJQ $\rightarrow$ *rgb* mapping (Fig. 5C), which renders it virtually white by summing the high signals of each metabolite. The triplet values indicate that the free amine content of the RPE is around 25 mM, considering these three

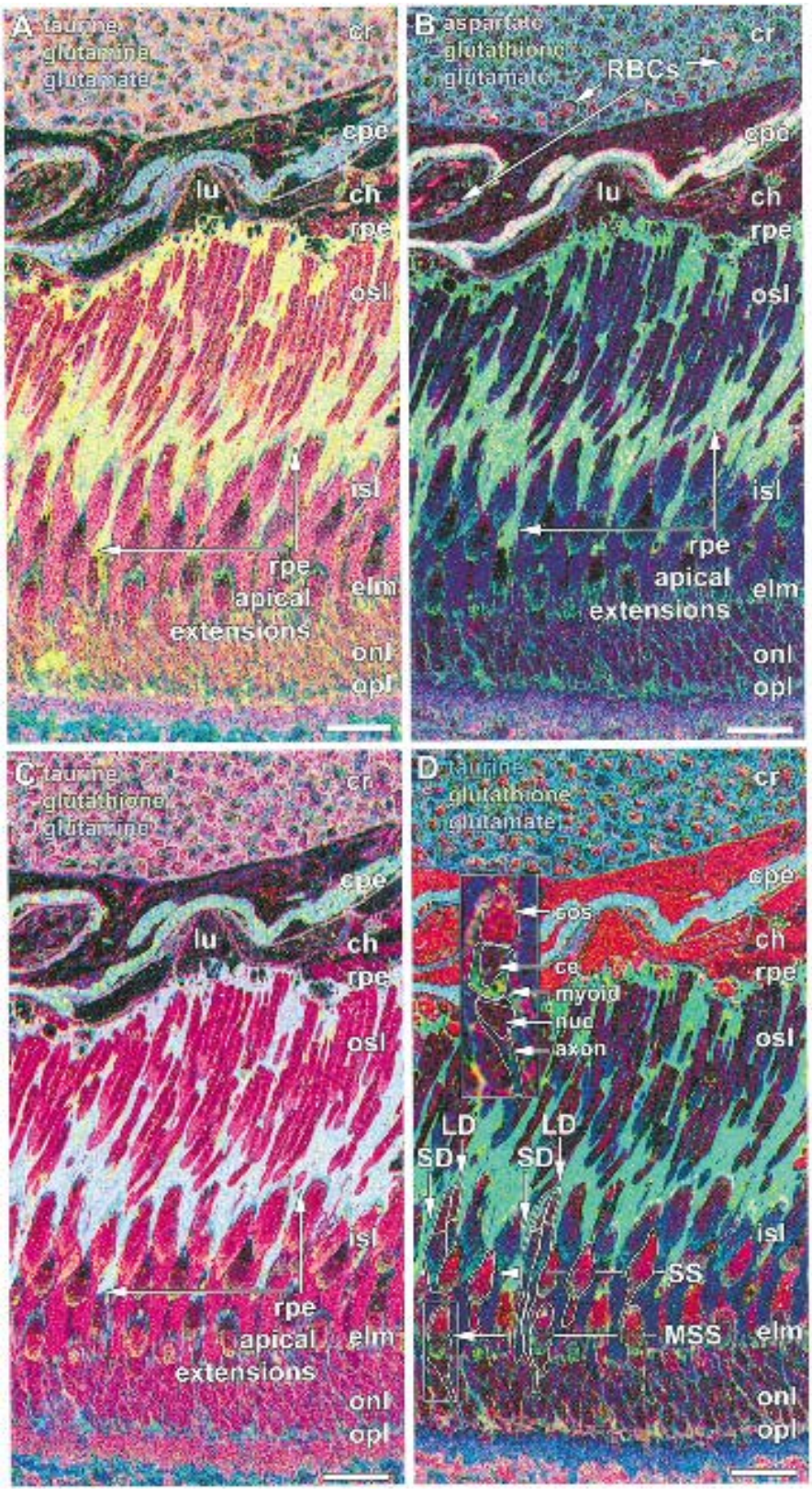
A
taurine
glutamine
glutamate
cr
cpe
lu
ch
rpe
osl
isl
rpe
apical
extensions
elm
onl
opl
B
aspartate
glutathione
glutamate
RBCs
cr
cpe
lu
ch
rpe
osl
isl
rpe
apical
extensions
elm
onl
opl
C
taurine
glutathione
glutamine
cr
cpe
lu
ch
rpe
osl
isl
rpe
apical
extensions
elm
onl
opl
D
taurine
glutathione
glutamate
cr
cpe
cos
ch
ce
rpe
myoid
nuc
axon
osl
LD
LD
SD
SD
isl
SS
MSS
elm
onl
opl

metabolites alone. We have measured most of the other free amino acids (*e.g.*, cysteine, lysine, leucine, arginine, serine, threonine, tryptophan and tyrosine) and found them to range from below 50 up to 250 μM. If all the remaining amino acids are of similar concentrations, they will total less than an additional 2–4 mM. Since the intracellular osmolarity of freshwater fish retinas is between 260–300 mOsm, one can reasonably assume that about 10% of that is derived from the total free amine pool. Free sugars, carboxylates, nucleotides, etc., likely represent at least another 10%, but the exact measurements remain to be made.

Finally, remapping into a complex space by τJQ → **c***gb* (subtractive cyan, additive green and blue) strongly delineates the metabolic compartments surrounding and within the cones, as illustrated by the inset in Figure 5D. A MSS cone has distinct metabolic mixtures in its outer segment, ellipsoid, myoid and axonal regions. Part of this is due to the specialized accumulation of glutathione (probably in vesicular compartments), the accumulation of taurine in the cytosol and mitochondria and the small cytosolic volume of the outer segment.

THE DARK-ADAPTED OUTER RETINA

One might consider this depth of metabolic profiling an academic exercise were it not for the facts (1) that there are no proven norms for neuronal metabolism *at the cellular level*... we are discovering them... and (2) that some signatures change upon adaptation, indicating rapid coupling between the cellular and system states. By revisiting the zebrafish retina following dark adaptation, we discovered that the glutamate contents of rods and some cones increase several-fold (Fig. 6A). The glutamate content of the RPE, however, remains unchanged. Conversely, the glutamine levels of the photoreceptors drop (Fig. 6B).

A comprehensive summary of these changes, based on monochrome and color triplet images, would be qualitative and tedious. But we can summarize all the quantitative data for various cell types by exploiting N-plots as described in the Methods. Figure 7 displays N-plots for the RPE, rods, MSS, SS, SD, and LD cones. All 8 basis molecules are plotted in 4 superimposed XY pairs (AJ, DQ, Eγ, Gτ) in both light and dark-adapted states. MSS cones change little, with a 2-fold decrease in glutamine content. The shift in SS cones is a bit more dramatic, with increases in glutamate and decreases in both glutamine and taurine levels. Rods show a large glutamate increase and a glutamine decrease but no evidence of taurine redistribution. The LD and SD cones show by far the most dramatic changes, with 6-fold increases in glutamate content up to 2–4 mM and concomitant drops in glutamine and taurine. The RPE serves as an internal control, with no change in glutamate content and minor (statistically insignificant) shifts in other signals. This is a more quantitative description of the process first described for the goldfish retina (Marc *et al.*, 1995). The meaning of these changes is unknown, but they

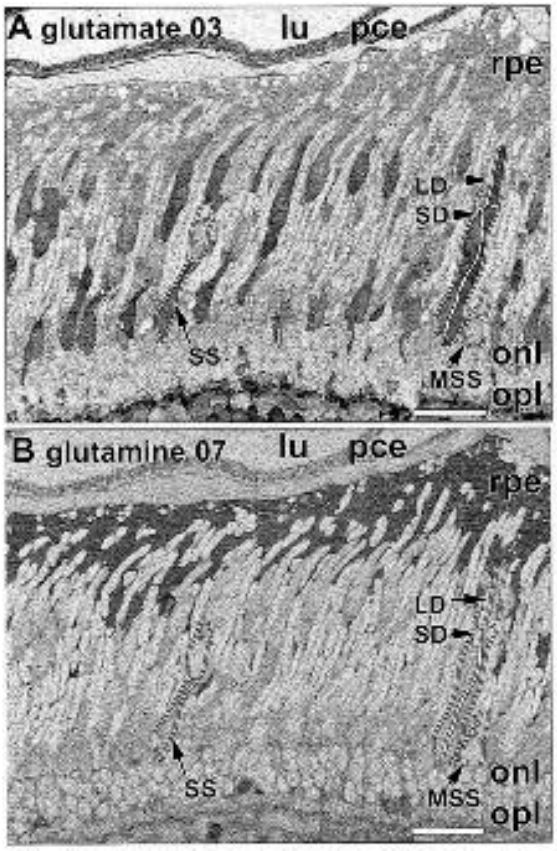

Fig. 6. Registered EQ signals in the dark-adapted photoreceptor layer. A, glutamate 03. The ellipsoids and myoids of LD and SD cones display large increases in glutamate content as they undergo photomechanical extension towards the RPE. B, glutamine 07. The same cones display decreases in glutamine content, while the RPE signals remain unchanged. Section thickness: 250 nm. Scale 20 μm.

Fig. 5. Triplet mapped basis set signals in the light-adapted photoreceptor layer. A, τQE → *rgb*. B, DJE → *rgb*. C, τJQ → *rgb*. D, τQE → **c***gb*, *i.e.* a complex mapping of subtractive cyan, additive green and blue. The two inset boxes are 10 μm × 30 μm and show the varied signal mixtures in MSS cone subcellular compartments. Scale 20 μm. Abbreviations: ce, cone ellipsoid; cos, cone outer segment; nuc, nucleus; other abbreviations as in Figures 3 and 4.

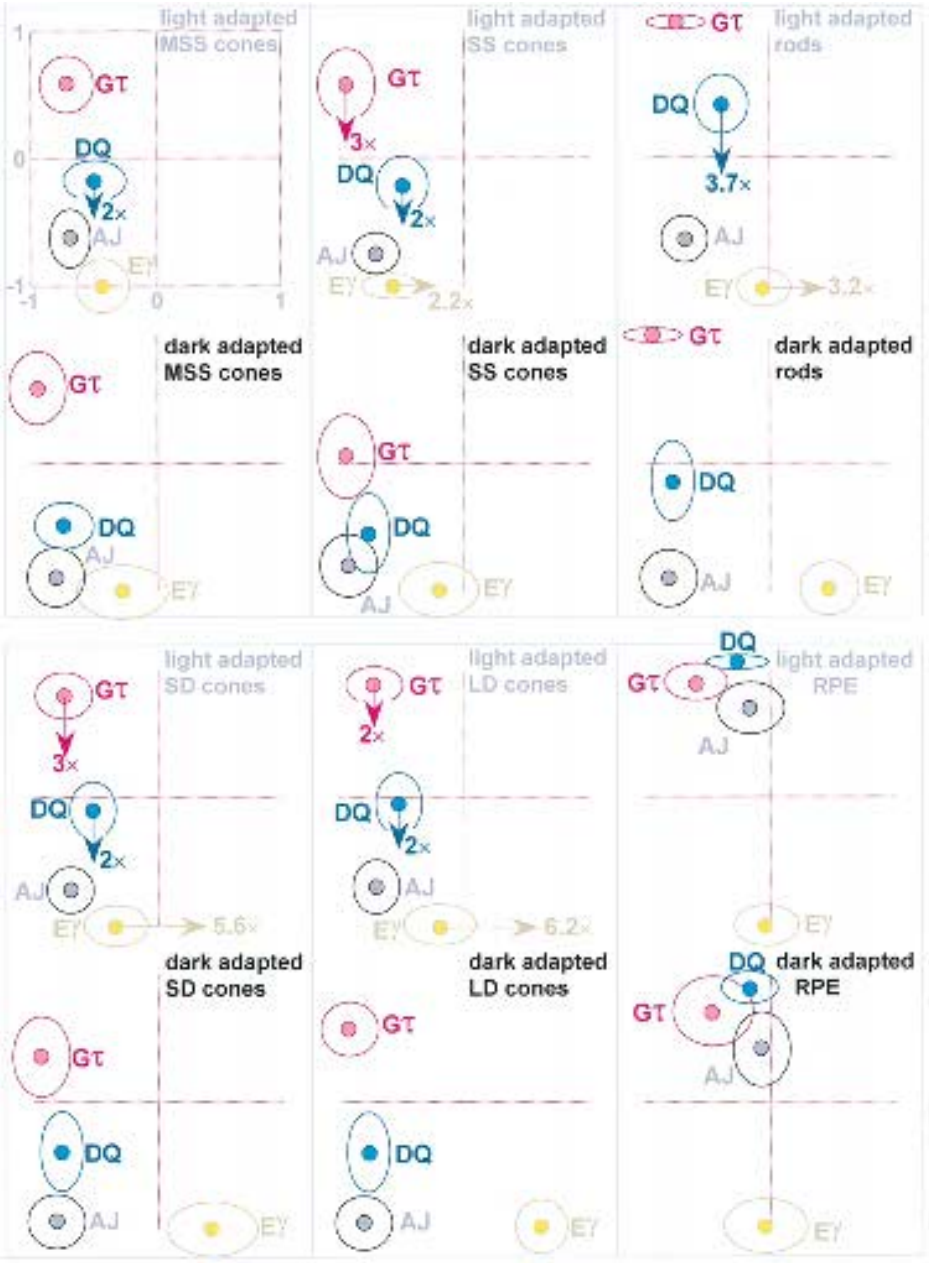

Fig. 7. Photoreceptor/ RPE molecular phenotyping N-plots. All details as in Figure 2. Each cell class is plotted as a pair of N-plots, light-adapted above and dark-adapted below. The RPE shows no significant changes in signature upon adaptation, while rods, SD and LD cones show extensive increases in glutamate content and decreases in both glutamine and taurine levels.

parallel the dramatic adaptation-driven change in cell morphology displayed by LD and SD cones in teleost retinas. Dark-adaptation activates a tremendous increase in the surface area of the myoid and may involve volume changes large enough to demand compensatory responses. The smaller changes in SS and MSS cones are in accord with their smaller morphological alterations upon dark adaptation.

CONE ARRAYS

The strong signal differentiation of the dark-adapted cones also permits a unique chemical visualization of the cone mosaic in the zebrafish retina. Sectioned in dorsal retina at the level of the MSS cones, Figures 8 and 9 display the modest glutamate signal of MSS cones ellipsoids and the precisely arrayed high glutamate myoid LD-SD pairs next to one. Sandwiched between MSS

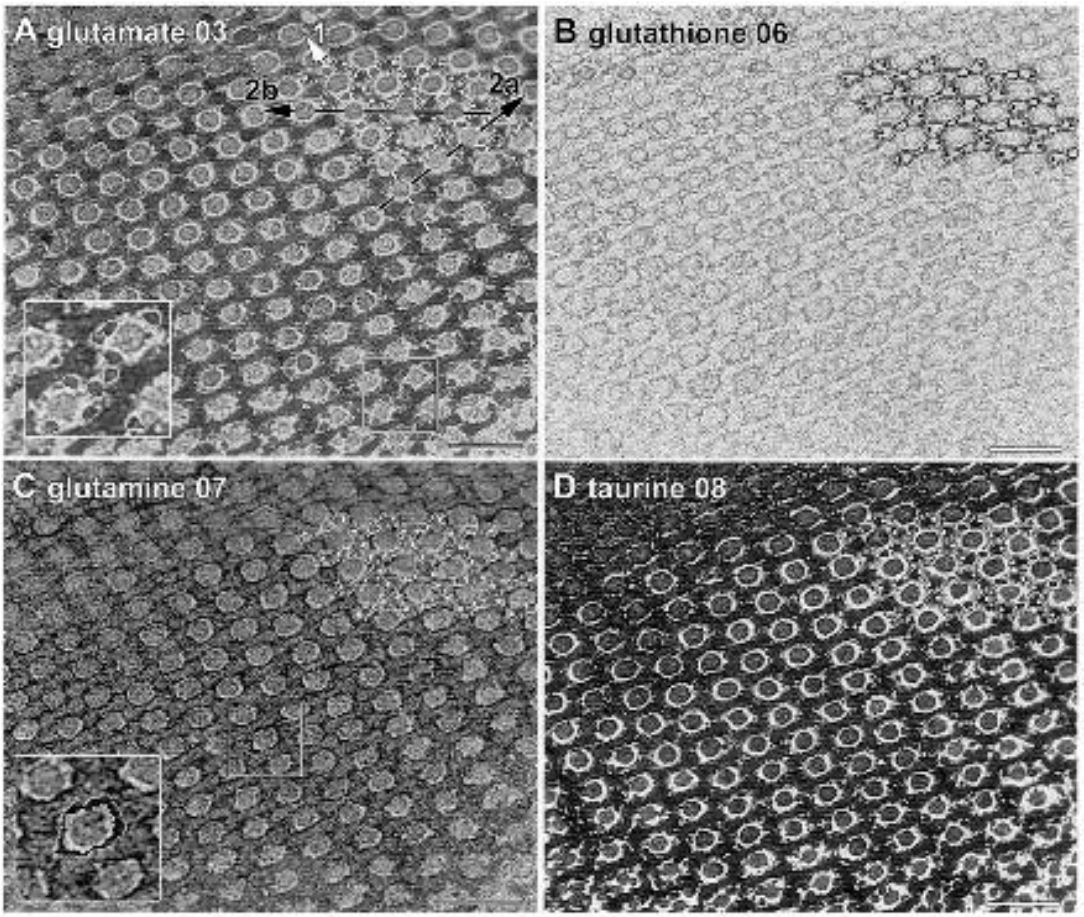

Fig. 8. Single channel, registered EJQτ signals in the dark-adapted cone mosaic. A, glutamate 03. The circular elements are the UV cones and surrounding extracellular matrix and the glutamate-rich bow-tie structures are the myoids of double cones (double outlined) aligned with the myoids of blue cones. According to the scheme of Raymond *et al.* (1993) and Robinson *et al.* (1993), the UV cones are always adjacent to the green SD cones, indicated by white dots. The primary (1) and secondary (2a,b) tiling axes are marked for a patch of the mosaic. The two inset boxes are 20 μm square and show the emergence of rod ellipsoids (outlined) in the distal portion of the dark-adapted cone mosaic. B, glutathione 06. The glutathione signals are precisely positioned within cone ellipsoids and the melanin-free RPE apicial extensions around all cone borders. C, glutamine 07. The highest contents are in the RPE apical extensions. The two inset boxes are 20 μm square and show the high glutamine signals of RPE processes outlining the MSS cone extracellular space. D, taurine 08. All cellular elements express high taurine levels, selectively exposing the extracellular space. Section thickness: 250 nm. Scale 20 μm.

cones are the small myoids of SS cones. Each double cone and SS cone myoid element is completely surrounded by a thin glutamine- and glutathione-enriched rind of RPE processes, while a 500–750 nm thick ring of extracellular matrix resides between the MSS cone ellipsoids and the RPE processes. The precision of the zebrafish cone mosaic appears to be superior to that of the goldfish. Both MSS and SS cones are present at density of 9400 cones/ mm^2 (uncorrected for shrinkage) in this dorsal retinal sample, some 2–4$\times$ higher than the density of SS cones in the adult goldfish retina. Both cone placements have conformity ratios >13, far higher than the precision of cell patterning of any cell class in the mammalian retina. The double cone density = SS cone density $\times \sqrt{2}$, just as in the goldfish retina. Though the mosaic appears as a pure row mosaic, the precise 1/ 2 cycle offset of neighboring rows forces the scaling to be the same as the pure square mosaic found in cyprinine and perciform retinas. The chromatic sampling originally proposed by Scholes (1975) holds as well for the zebrafish as for other cyprinids: when optimally focused on a long-wave target, lens chromatic aberration forces short-wave cone mosaics to be coarser. Any denser SS or MSS cone packing would be empty resolution.

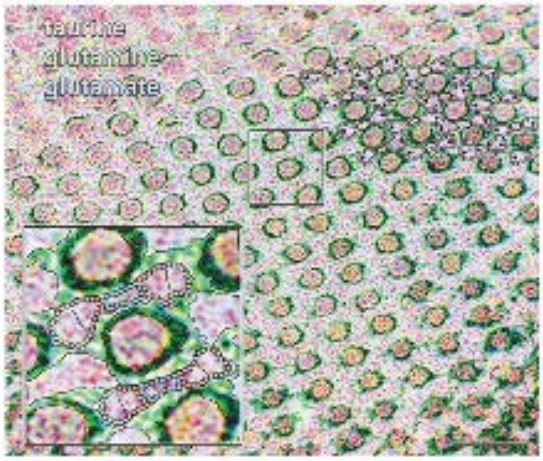

Fig. 9. Triplet mapped τQE → *rgb* signals in the dark-adapted cone mosaic. The separate zones of the mosaic tiling express different signatures. The two inset boxes are 20 μm square and show the continuum of green RPE processes (solid black outlines) around the pink SS and double cone myoids (blue, red and green dotted outlines), and the ≈1 μm dark ring of extracellular matrix around each MSS cone ellipsoid. Scale 20 μm. Tiling axes as in Figure 8.

THE INNER RETINA

The inner retina displays much greater signal differentiation than the outer retina due to its abundance of specialized neurons and their precise lamination. As with the outer retina, we can begin with a general survey of the molecular signals.

As in the outer retina, *alanine* signals are for the most part weak, but are clearly elevated in the inner plexiform layer and in a subset of cells in the amacrine cell layer (Fig. 10A). However, *aspartate* signals (Fig. 10B) are more differentiated in the inner retina, with a clear elevation in the horizontal cell layer and especially in rod horizontal cells (to be discussed below). Strong aspartate signals are also evident in small subsets of the bipolar and amacrine cell populations. Again, very distinctive partitioning of the retina is achieved with *glutamate* signals (Fig. 10C) with nearly all glutamate-rich bipolar cells perfectly sandwiched between the horizontal and amacrine cell layers, their terminals dispersed in patterns through the inner plexiform layer. The ganglion cell layer displays a high and fairly uniform glutamate signal, but gaps appear which will be later shown to be the somas of displaced γ+ amacrine cells. As in the outer retina, *glycine* levels are low in the inner retina, but the ≈0.7–2 mM signals of G+ amacrine cells sets them apart from all other cell types (Fig. 10D). There is a distinctive G+ band at level 50 of the inner plexiform layer, with diffuse punctae throughout the inner plexiform layer. No G+ somas were detected in the ganglion cell layer. *Glutathione* signals set the Müller cells apart from all neurons and reveal that Müller cell somas are predominantly positioned in the distal portion of the amacrine cell layer, next to the bipolar cell layer (Fig. 10E). The end-feet of the Müller cells form a J+ border at the vitreal margin. The strong *GABA* signals of many amacrine cells virtually fill the inner plexiform layer and outline the characteristic bipolar cell terminals (Fig. 10F). GABA+ displaced amacrine cells that correspond to the glutamate-weak neurons of Figure 10C are indicated. The GABA signals in the amacrine cell layer are diverse and, as will be shown, constitute distinct superclasses of amacrine cells. The horizontal cell layer contains weakly γ+ somas that we presume are the homologues of H1 horizontal cells in other cyprinids. But at this scale and orientation, it is difficult to be certain of their identities. *Glutamine* signals are strongly differentiated (Fig. 10G): moderate in Müller cells, low in most bipolar cells, diverse in amacrine cells and uniformly high (≥10 mM) in ganglion cells. This is similar to the pattern observed in the goldfish (Marc *et al.*, 1995) and is roughly replicated in the mammalian retina (Kalloniatis *et al.*, 1996; Marc *et al.*, 1998b; Marc & Jones, 2002).

The *taurine* signals of the inner retina are almost identical to those of the goldfish, but seem better differentiated, perhaps because of the better lamination of the inner plexiform layer (Fig. 10H). Both horizontal cells and ganglion cells are virtually devoid of taurine, while bipolar cells and their terminals possess exceptionally high levels. Amacrine cells display intermediate values. As will be discussed later, this patterning demonstrates that there is no obvious association of taurine with any simple functional property such as glutamatergic transmission (both bipolar cells and ganglion cells are glutamatergic, but have opposite taurine signals) or mode of signal integration (both bipolar cells and horizontal cells are sustained, but have opposite taurine signals).

It is easy to forget that all of the foregoing data represent signals in the very same set of cells. The display of signal triplets more effectively captures these data correlations. A conventional γGE → *rgb* triplet reveals that γ+ and G+ amacrine cells appear to be completely distinct populations in the dark-adapted zebrafish retina (Fig. 11A), though this is not a quantitative demonstration of that likelihood. Similarly, the E+ bipolar and ganglion cells are set apart as dark blue. But this view is incomplete, as the molecular phenotypes displayed by bipolar and ganglion cells are quite distinct. The use of τQE → *rgb* mapping completely segregates the entire E+ cohort of the retina into cyan ganglion cells, pink-magenta bipolar cells, and red photoreceptors (Fig. 11B). Thus each distinct glutamatergic cell type in the zebrafish retina has its own molecular phenotype. The Müller cells display a yellowish-green signal that is characteristic of this glial cell type across all vertebrates (Kalloniatis *et al.*, 1994; Marc *et al.*, 1995; Kalloniatis *et al.*, 1996; Marc *et al.*, 1998b; Kalloniatis & Tomisich, 1999). The taurine signal is significantly

weaker in zebrafish than other cyprinids and this will be discussed later. Müller cell placement is better visualized with *glutathione* signals in a γJE $\rightarrow$ *rgb* mapping (Fig. 11C), especially the enrichment of processes around the horizontal cells in the outer plexiform layer and at the external limiting membrane. Finally, the positioning of horizontal cells is best set off with a τ DE $\rightarrow$ *rgb* mapping (Fig. 11D) that shows a cyan band of cells between the $\tau+$ photoreceptor and bipolar cell layers, and even some fine hue differentiation among horizontal cell classes.

LAYER VIEWS OF THE INNER RETINA

Even large numbers of registered vertical sections are inadequate for better distinction of cell classes simply because of the great diversity of classes. Larger, contiguous samples become essential and it is then important to create databases from horizontal or shallow oblique serial sections. As described in the methods, each image must be acquired at an optimal resolution for light microscopy, *i.e.* <250 nm/ pixel. Resolutions higher than that simply produce empty data bins by replicating blurred neighbors. Lower resolutions limit the precision of registration. Figure 12 displays a full mosaic of registered ADEGJQ$\tau\gamma$ images for serial oblique sections through the layers of the inner retina. These mosaics have three advantages: (1) they document the uniformity of signal quality over the array... quality unequaled by any other immunochemical method; (2) they provide sufficient obliquity to garner large samples of some patterned elements; (3) they retain precise laminar boundaries. Revisiting the basis signals allows clearer differentiation of cell classes associated with each signal and a better appreciation of their patterning. As before each signal is shown in its serial sequence in the data array (Fig. 12A alanine 01; 12B aspartate 02; 12C glutamate 03; 12D GABA 04; 12E glycine 05; 12F glutathione 06; 12G glutamine 07; 12H taurine 08). The cellular segregations of alanine signals can be better visualized in oblique sections, even though they still represent modest concentrations. The patterning suggests a preferential association with a diffuse set of amacrine cells, and a characteristic banding pattern in the inner plexiform layer resembles a hybrid of glycine and GABA banding. The aspartate signals are complex, with patches of high signals in the horizontal, bipolar and amacrine cell layers, multiple laminae in the inner plexiform layer and distinct labeling of ON-center bipolar cell terminals. The glutamate distribution is likewise complex but more interpretable, based on previous data from goldfish: the band in the outer plexiform layer is mostly composed of bipolar cell dendrites, with an interposed wide band of horizontal cells, followed by the strong glutamate signals of the bipolar cell layer proper. The amacrine cell layer displays characteristic mixed, weak glutamate signals that we shall explore in more detail shortly. Showing more clearly than in vertical sections, the highest glycine signals are localized to a poorly laminated set of amacrine cells distributed throughout the amacrine cell layer, slightly biased to the distal half. A band of strong glycine signals, unique to the zebrafish among cyprinids, is positioned at roughly level 50 of the inner plexiform layer.

Selected *rgb* triplets preferentially reveal subsets of the entire retinal cell cohort, even at low magnification. The subsets are overlapping, but this display is not merely an academic exercise as the correct triplets can form a screen for specific cell populations, especially in disease states (Marc *et al.*, 1998a). The γGE triplet (Fig. 13A) is a standard that captures all neurons in the retina and categorizes them as in a single image. A sprinkling of cyan cells in the inner nuclear layer represents the sparse glycinergic interplexiform cell population. A decrease in GABA signal occurs at about level 50 of the inner plexiform layer, where a class of G+ amacrine cell has a dense arborization, but the overall GABA signal is otherwise uniform throughout, as in the goldfish (Marc & Liu, 2000). The τQE triplet (Fig. 13B) is diagnostic of Müller cells due to their extremely high glutamine contents. However, the taurine content of Müller cells in the zebrafish is roughly half that found in the goldfish and other vertebrates, giving the overall image a green cast. The bipolar cell layer is distinctively magenta, as in all vertebrates, while the photoreceptor layer is red-shifted, indicating the much higher taurine content in photoreceptors. Though difficult to see at low magnification, the γJA triplet (Fig. 13C) isolates the extensive Müller cell branching in the outer plexiform layer better than any other and also indicates the partial segregation of alanine-rich cells from the $\gamma+$ amacrine cell cohort in the inner nuclear layer. The array of black dots in the middle of the image, deep in the inner plexiform layer, are the terminal arrays of Bb ON-center bipolar cells. Conversely, a $\gamma\tau$D mapping (Fig. 13D) exposes the ganglion cells as black dots deep in the inner plexiform layer, whereas most bipolar cell terminals become a cyan hue. Mixed blue and red signals in the outer plexiform layer denote multiple horizontal cell types. One of the richest triplets for displaying subsets of cell types is the γDE mapping (Fig. 13E), with distinct cyan rod horizontal cells in the horizontal cell layer, pale blue aspartate-rich ON-center bipolar cells, mixed GABA amacrine cells cohorts of red, orange and yellow. This metabolic diversity serves as a marker for cell classes, even though we have no biochemical model to explain it. The complex banding of the inner plexiform layer is particularly rich, and a discerning trichromat can likely pick out at least eight layers. We will return to this point later, as it is a key issue in the characterization of the zebrafish retina. Finally, the AGJ mapping (Fig. 13F) is subtle, but shows that most of the high alanine contents of cells in the zebrafish retina (and in mammals, as well) are associated with G+ amacrine

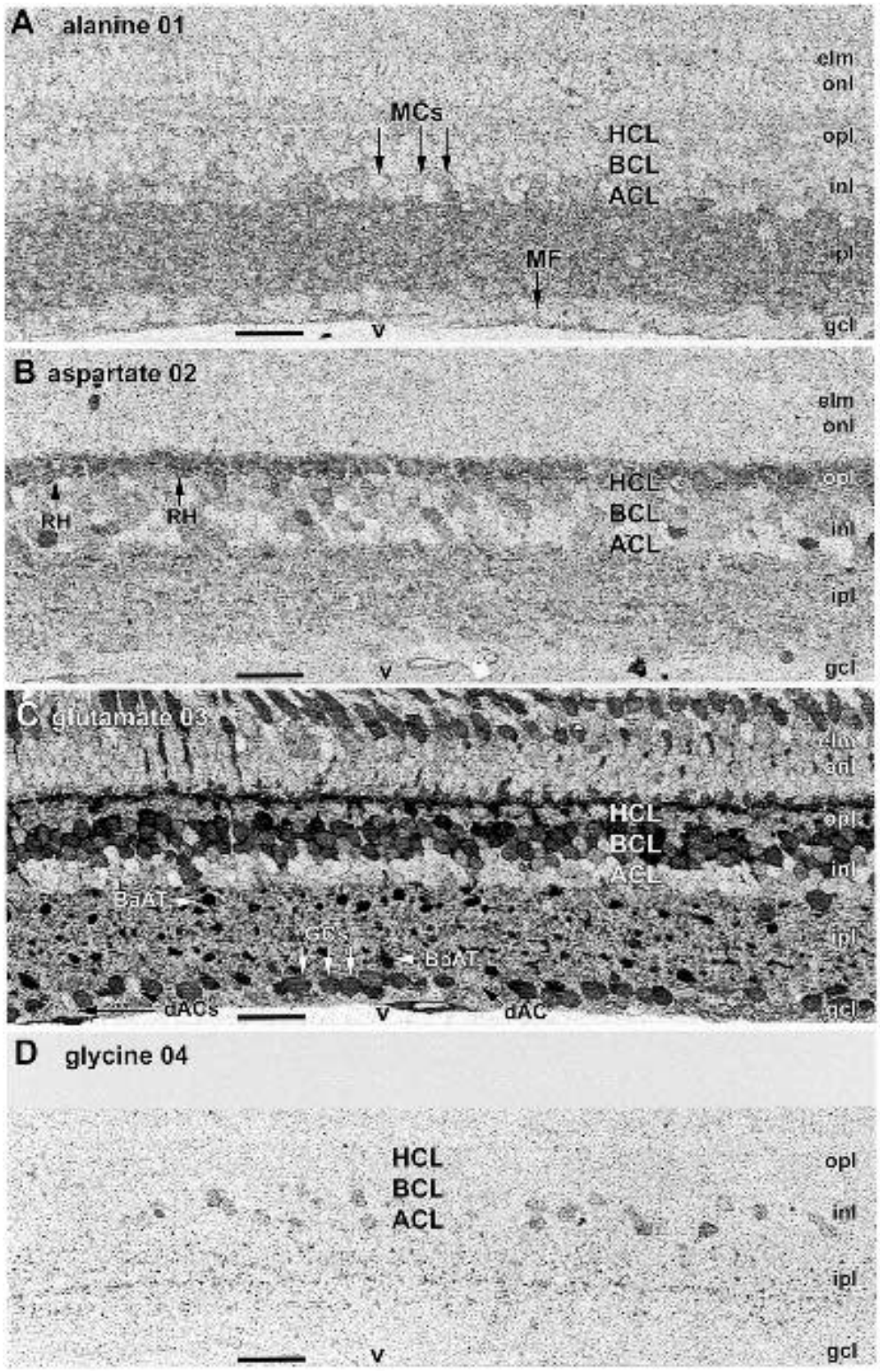
A alanine 01
MCs
HCL
BCL
ACL
MF
v
elm
onl
opl
inl
ipl
gcl
B aspartate 02
RH
RH
HCL
BCL
ACL
v
elm
onl
opl
inl
ipl
gcl
C glutamate 03
HCL
BCL
ACL
BaAT
GC
BaAT
dACs
v
dAC
opl
inl
ipl
gcl
D glycine 04
HCL
BCL
ACL
v
opl
inl
ipl
gcl

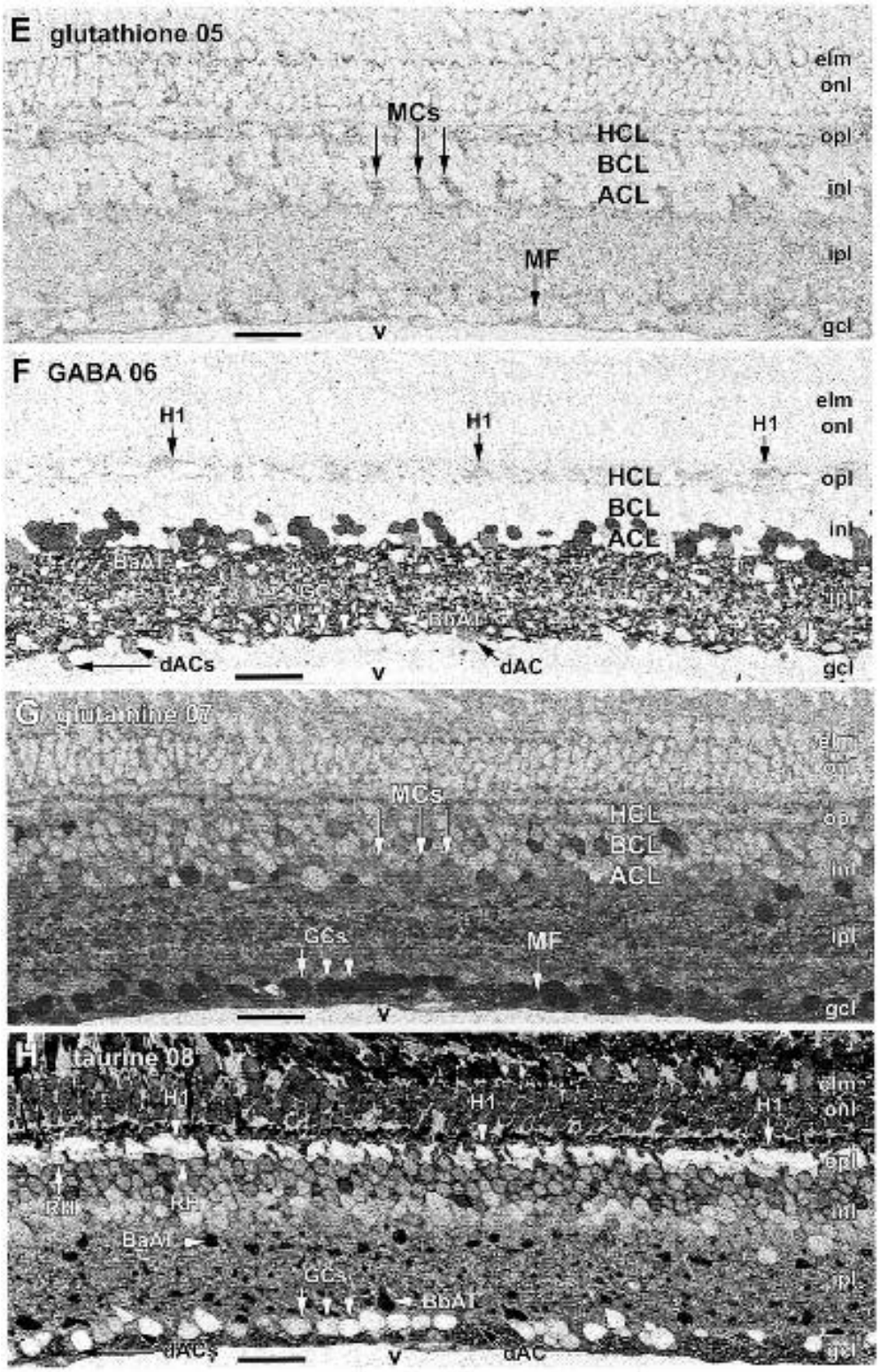

Fig. 10. Single channel, registered ADEGJQ$\tau\gamma$ signals in the dark-adapted inner retina. A, alanine 01. B, aspartate 02. C, glutamate 03. D, glycine 04. E, glutathione 05. F, GABA 06. G, glutamine 07. H, taurine 08. Each channel highlights a different set of cellular compartments. Section thickness: 250 nm. Scale 20 μm. Abbreviations: inl, inner nuclear layer; MC, Müller cells; RH, rod horizontal cells; dAC, displaced amacrine cells; other abbreviations as in Figures 3–5.

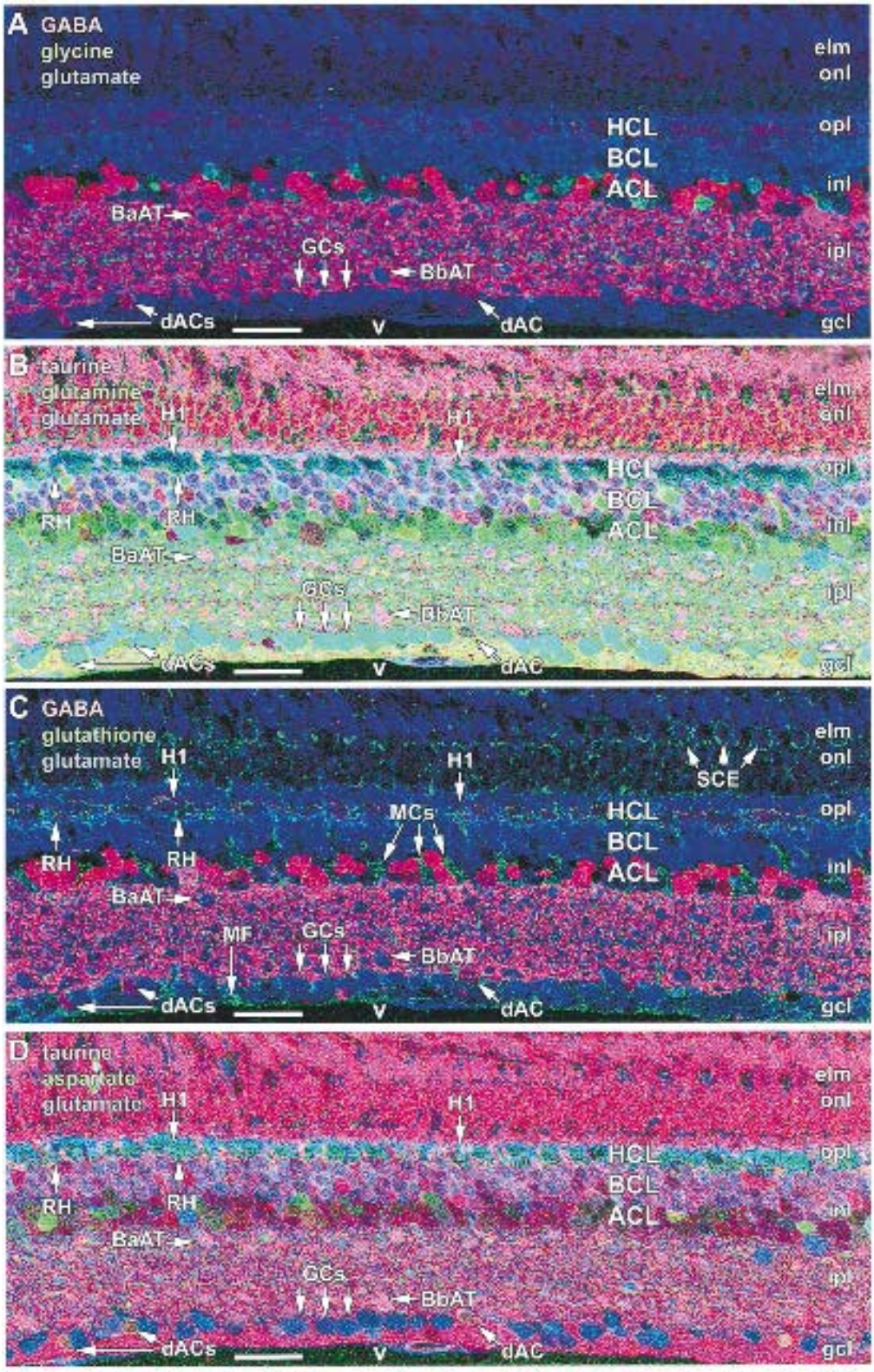

Fig. 11. Triplet mapped basis set signals in the dark-adapted inner retina. A, γGE $\rightarrow$ *rgb*. B, τQE $\rightarrow$ *rgb*. C, γJE $\rightarrow$ *rgb*. D, τDE $\rightarrow$ *rgb*. Each triplet delineates a subset of elements in the retina, but no one triplet uniquely captures all elements.

cells, including the characteristic band at level 50 of the inner plexiform layer.

CLASSIFICATION OF THE INNER NUCLEAR LAYER

The comprehensive dataset, with its rich differentiations of cell cohorts, allows the luxuries of a large sample and high resolution. One can literally zoom into these datasets and browse cell populations at optimum resolution (Fig. 14A–H). This oblique sampling permits high cell numbers and preservation of laminar boundaries. Even casual observation allows numerous distinctions of possible cell classes and metabolic associations. For example, there is a strong albeit incomplete correlation between alanine (Fig. 14A) signals and glycine (Fig. 14E) signals; this is the first metabolic clue regarding the possible mechanism of glycine synthesis in glycinergic amacrine cells (see Discussion). Aspartate (Fig. 14B) signals definitely reveal metabolic subsets of horizontal, bipolar and amacrine cell populations. As in every retina, the glutamate (Fig. 14C) contents of bipolar cells are variable and we might well ask whether this is simply metabolic instability or specific metabolic profiles expressed by bipolar cell classes. The fact that some cones change their glutamate profiles in adaptation suggests that many cells could alter profiles for many physiological reasons, suggesting we should proceed with care; that we perhaps ought not equate metabolic and natural classes without other data. Classification can help this analysis, as we will see later. The diversity in GABA (Fig. 14D) signal strength is similar: some cells have high signals, others low, and it is obvious that some somas in the bipolar cell layer have elevated GABA signals. The origin and significance of these variations, in the weak signals especially, need to be sorted out, but this is not possible by surveying monochrome images alone.

An important feature emerges in these images: the layer of fine, $\gamma+$ processes immediately proximal to the H1 horizontal cell somas. These are the axon terminal expansions of the cone horizontal cells. We will later discuss this point in detail for those unfamiliar with this teleostean neuronal oddity, but for now simply note that these processes are much smaller ($\approx 1\ \mu$m in width, unknown length) than those in the closely related carp and goldfish (5–10 μm in width, up to 400 μm long). In general, only Müller cells show high levels of glutathione (Fig. 14F) signals, so glutathione is a good Müller cell marker in the zebrafish. Glutamine (Fig. 14G) levels help segregate Müller cells to some degree, but oblique sections reveal significant variation in glutamine signals across both amacrine and bipolar cells. Finally, the negative taurine (Fig. 14H) signals of horizontal cells, however inexplicable, are a stroke of good fortune, as they cleanly separate them from all other cell classes in a binary fashion. The rich mesh of horizontal axon terminal expansions is particularly evident, suggesting that there are many more kinds of cone horizontal cells than $\gamma+$ H1 horizontal cells.

Subsets of cell types become even more evident in triplet mappings. The standard γGE mapping (Fig. 15A) displays the complete quantitative segregation of $\gamma+$ and G+ amacrine cells, including glycinergic interplexiform cells. And amidst the deep blue bipolar cell layer array, one can detect the faint red $\gamma+$ bipolar cells. In the horizontal cell layer proper, both H1 horizontal cell somas and their axon terminals evince a weak $\gamma+$ signal. In Figure 15B, we have used a mixed τQE $\rightarrow$ **c***gb* mapping that strongly segregates the Müller cells, horizontal cells and their axon terminals. Most of the Müller cell somas are positioned at the interface between the amacrine and bipolar cell layers. Figure 15C is also a mixed γDE $\rightarrow$ **c***g***y** mapping that simultaneously discriminates rod horizontal cells, two subsets of the bipolar cell cohort, and several subsets of the $\gamma+$ amacrine cell population. Finally, AGJ $\rightarrow$ *rgb* mapping (Fig. 15D) clearly links the highest alanine contents with the highest glycine contents in the amacrine cell layer and the glycinergic interplexiform cells (Marc & Lam, 1981; Marc & Liu, 1984).

Given this complex array of signals, one might reasonably despair of further resolving all the cell types. This is where molecular phenotyping, clustering and deconvolution analyses come into play. Molecular phenotyping effectively covers all cellular space: no cells are left out of the analysis. Figure 16 is the final map produced by assigning the proper molecular phenotype class code to every cell in the image. The $\gamma+$ amacrine cell type was readily divisible into seven molecular phenotype classes. This does not mean that there are only seven natural classes of $\gamma+$ amacrine cells in the zebrafish: only that there are seven stable molecular phenotype groupings, each likely to represent a superclass of many natural classes sharing the same signature. The G+ amacrine type was coded as a single superclass for simplicity, but deconvolution analysis suggests that it is composed of no less than three groups. Unlike other cyprinids analyzed so far, the zebrafish has remarkably strong metabolic differentiation across bipolar cells, and six classes were resolved. Some of these are certainly natural classes, as will be discussed, while most are superclasses of many natural classes. Finally, the horizontal cell layer is composed of islands of proximal cells that we presume to be rod horizontal cells, intermediate islands likely to be Hx cone horizontal cells and distal $\gamma+$ H1 horizontal cells. We will consider the exact signatures underlying each of these cell classes below.

HORIZONTAL CELLS

Knowing that the inner nuclear layer can be formally classified by molecular phenotyping allows a more

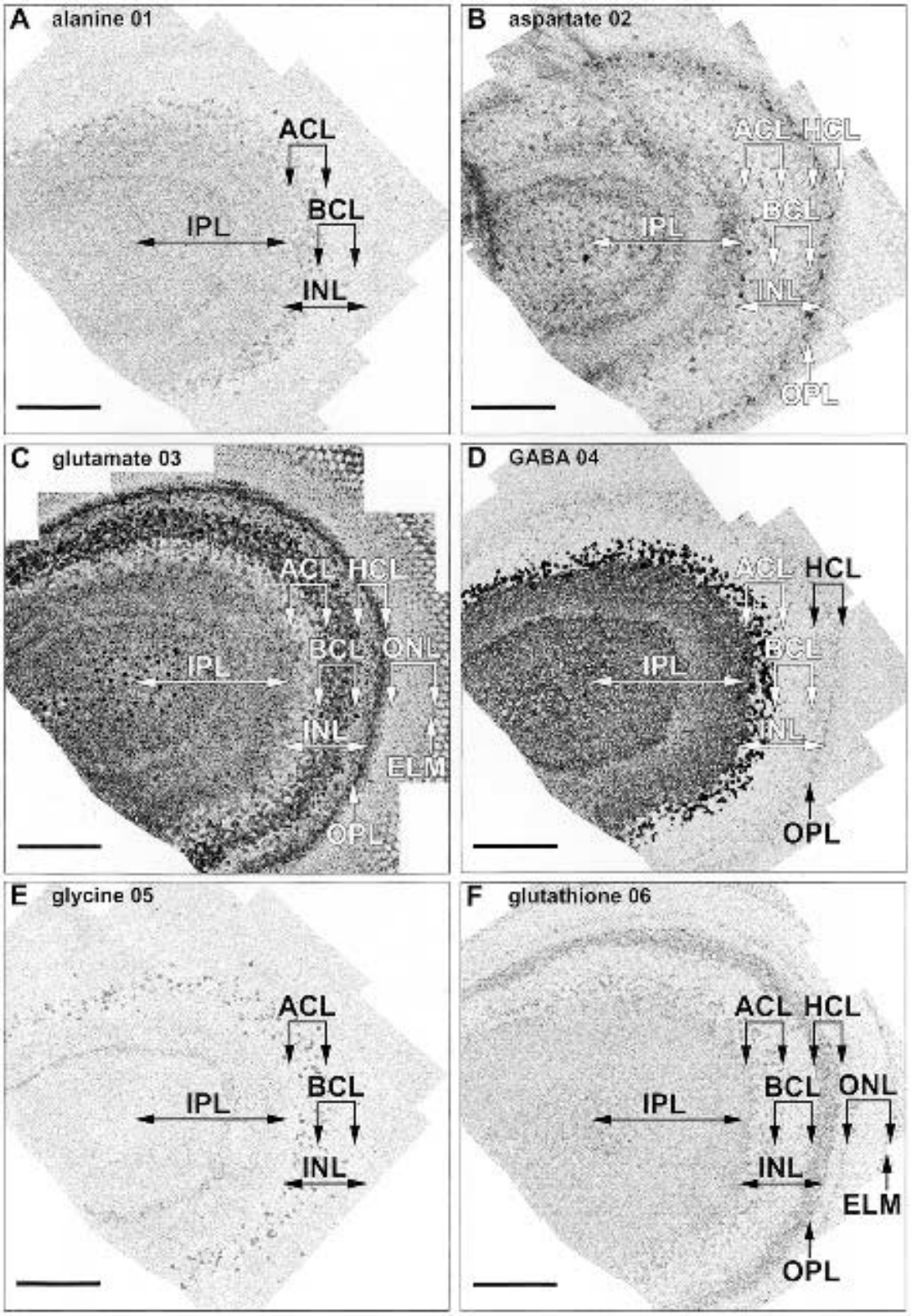
A alanine 01
ACL
BCL
IPL
INL
B aspartate 02
ACL HCL
BCL
IPL
INL
OPL
C glutamate 03
ACL HCL
BCL ONL
IPL
INL
ELM
OPL
D GABA 04
ACL HCL
BCL
IPL
INL
OPL
E glycine 05
ACL
BCL
IPL
INL
F glutathione 06
ACL HCL
BCL ONL
IPL
INL
ELM
OPL

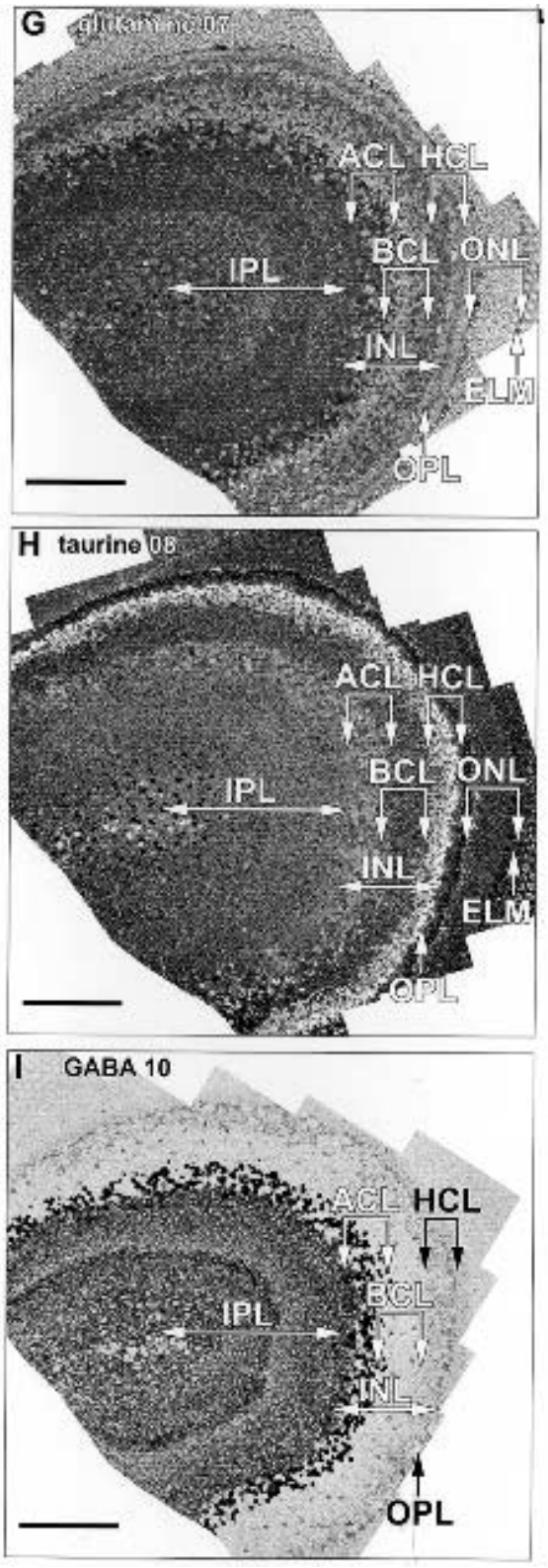

aggressive decomposition of cell classes in each major cell type. How many horizontal cell classes are there? This is not a trivial question since we know that all other cyprinids studied structurally and/ or physiologically display four types: spectrally monophasic, $\gamma+$ H1 cells, biphasic $\gamma-$ H2 cells, triphasic $\gamma-$ H3 cells, and $\gamma-$ rod horizontal cells. The photoreceptor types of the zebrafish retina are chromatically sufficient to drive four such horizontal cell types. By combining serial trangential, registered GABA (Fig. 17A), aspartate (Fig. 17B) and taurine (Fig. 17C) signals, we can get a sense of the relative population sizes of the three horizontal cells groups in the zebrafish. A doublet mapping of $\gamma \rightarrow$ red, $\tau \rightarrow$ blue, combined with an aspartate channel displayed as an edge filtered yellow overlay (Fig. 18A) shows that the distal layer of H1 horizontal cells intermeshes tightly with numerous $\gamma-/\tau-$ Hx horizontal cells, but is well separated from the D+ presumed rod horizontal cells that form the proximal margin of the horizontal cell layer. Recoded into a theme map (Fig. 18B), these data allow estimates of cell densities. The rod horizontal cells tile the retina at $\approx$2200/ mm^2, while the H1 horizontal cells are much denser at $\approx$5600/ mm^2. This is much higher than the density of H1 horizontal cells in the goldfish, but it is consistent with the fact that the soma sizes of zebrafish horizontal cells are smaller than those of other cyprinids by a factor of 2. The density of Hx cells is more difficult to estimate as individual somas do not cleanly emerge from the dataset. Even so, they take up twice the area of H1 horizontal cells. If the classes of horizontal cells scale with size and cone density as in other cyprinids, this would argue that the Hx group is a composite of natural classes and that the zebrafish retina likely contains all 4 known classes of cyprinid horizontal cells.

BIPOLAR CELLS

The metabolic profiles of bipolar cells are more complex than in any other cyprinid and, while we have no explanation for this, it does permit better discrimination of bipolar cell superclasses. Subsets of mildly D+ cells (Fig. 19A) reside within the mix of cells with varying glutamate signals (Fig. 19B). Unique to the zebrafish, among cyprinids at least, is a distinct population of presumed bipolar cells with moderate GABA signals (Fig. 19C). Another subset with very weak but distinct GABA signals ($\approx$0.2 mM) is interspersed, but these are also evident in the goldfish retina (Marc, unpublished

Fig. 12. A high-resolution library of registered oblique mosaic channels: ADEGJQ$\tau\gamma$ signals in the dark-adapted retina. A, alanine 01. B, aspartate 02. C, glutamate 03. D, GABA 04. E, glycine 05. F, glutathione 06. G, glutamine 07. H, taurine 08. I, GABA 10. Section thickness: 250 nm. Scale 50 μm.

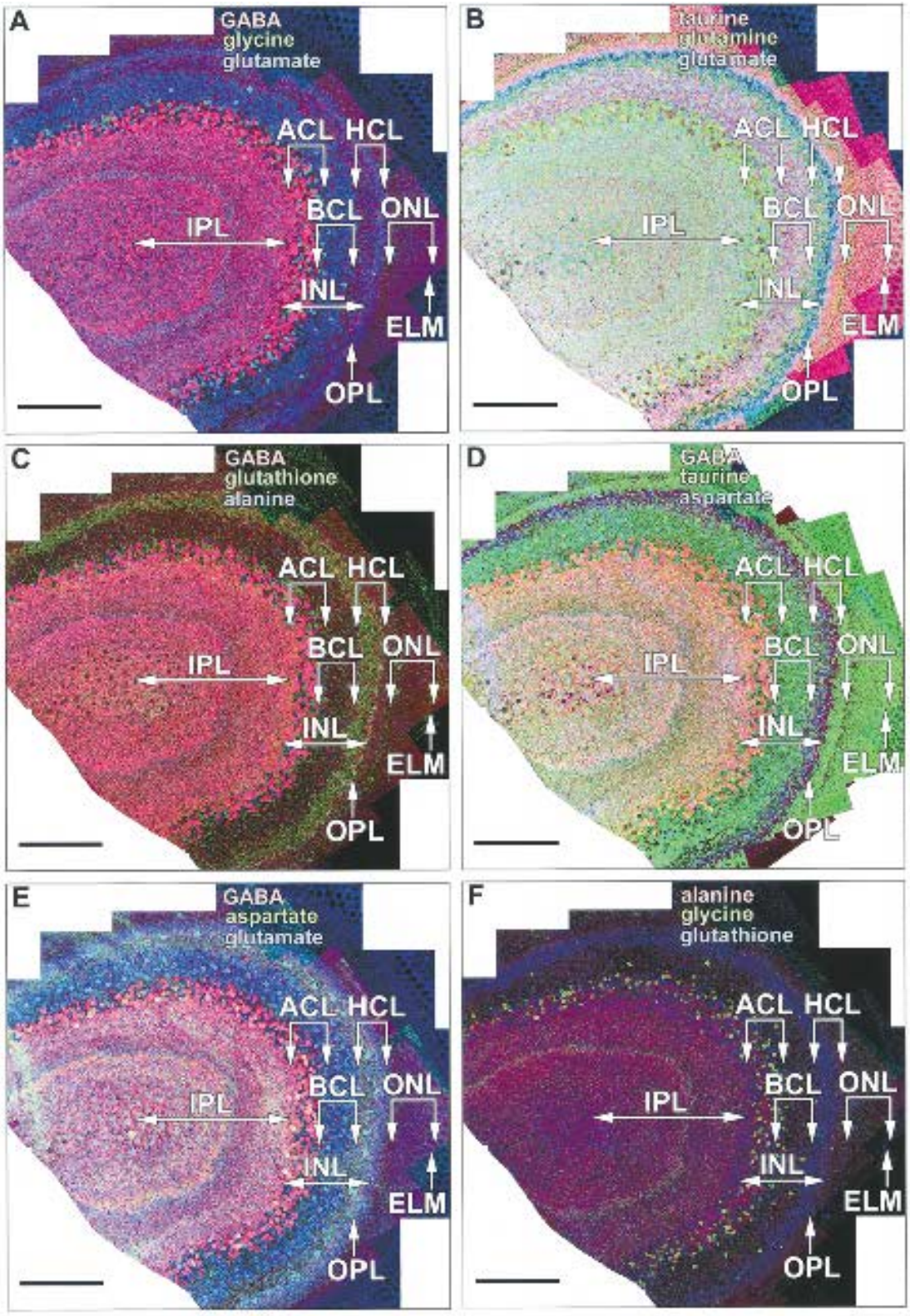

Fig. 13. Triplet mappings of the high-resolution library: ADEGJQ$\tau\gamma$ signals in the dark-adapted retina. A, γGE $\rightarrow$ *rgb*. B, τQE $\rightarrow$ *rgb*. C, γJA $\rightarrow$ *rgb*. D, $\gamma\tau$D $\rightarrow$ *rgb*. E, γDE $\rightarrow$ *rgb*. F, AGJ $\rightarrow$ *rgb*. Scale 50 μm.

data) and we will consider their identities when the terminal arrays of ON-center bipolar cells are described. Some of the cellular space at the proximal margin of the bipolar cell layer is comprised of Müller cell cytoplasm (Fig. 19D). Both glutamine (Fig. 19E) and taurine (Fig. 19F) are extremely varied across bipolar cells, the glutamine signals being weaker and the taurine signals stronger than those of amacrine, ganglion and Müller cells. As revealed by classification and triplet mapping, the $\gamma+$ and D+ sets are completely distinct populations in γDE $\rightarrow$ *rgb* (Fig. 20A), τQJ $\rightarrow$ *rgb* (Fig. 20B), and γDJ $\rightarrow$ *rgb* space (Fig. 20C). The τQJ mapping in particular is important because it captures all cells in the array, and though τQJ signals are not the primary elements of the differentiation, the $\gamma+$ bipolar cells are sufficiently Q− to emerge from the complex display. The $\gamma+$ cells are also very low in glutamate content and, on balance, have molecular phenotypes more reminiscent of H1 horizontal cells (but for the elevated taurine signal) than a classical glutamatergic bipolar cell.

THE AMACRINE CELL LAYER

The real challenge in classification is the amacrine cell layer: the most diverse groups of cells in any retina. This is particularly critical in the cyprinid retina. The roach for example likely has >70 amacrine cell classes (Wagner & Wagner, 1988). Oblique sections through the amacrine cell layer give us a detailed view of the likely molecular phenotypes involved. Figure 21 shows the registered basis set of amacrine cell signals in the dark-adapted zebrafish retina. This provides the most revealing of all views of the distribution of alanine signals (Fig. 21A) showing that it is extremely heterogeneous: many cells maintain no detectable alanine levels (<50 μM), while various cells approach 1 mM. The distribution of aspartate signals (Fig. 21B) shows a greater range, but a more restricted distribution, whereas glutamate signals (Fig. 21C) are extremely complex. Most cells contain some glutamate, but rarely at the levels expressed by bipolar cells. The GABA signals (Fig. 21D) also reveal substantial variation in GABA content across cells. Is this simply metabolic instability within a class, or a metabolic signature across different classes? As with the bipolar cell cohort, classification will provide some evidence that these are stable classes. The G+ amacrine cells (Fig. 21E) are clearly sparser and smaller than $\gamma+$ amacrine cells and partly correlate with the alanine distribution. As in vertical sections, glutathione (Fig. 21F) is consistently and preferentially associated with the Müller cell population in the dark-adapted retina. Both glutamine (Fig. 21G) and taurine (Fig. 21H) display extremely complex distributions within the amacrine cell cohort. Alone, they are too difficult to sort, but triplet mapping and classification shows distinct patterns underlying this complexity. In a triplet mapping of γGE $\rightarrow$ *rgb*, 215 $\gamma+$ amacrine cells are completely segregated from 126 G+ amacrine cells (Fig. 22A). This determination is possible only through quantitative image registration. Aspartate enrichment is exclusive to a subset of the $\gamma+$ amacrine cell cohort (Fig. 22B, γDE $\rightarrow$ *rgb*). Most amacrine cells contain a significant amount of taurine, although less than most bipolar cells and more than all ganglion or horizontal cells, leading to a complex display of τJE mixtures (Fig. 22C). Roughly half of all amacrine cells have elevated alanine signals, and virtually all glycine cells map onto that cohort (Fig. 22D.)

This complexity is partly resolved by classification of molecular phenotypes into a theme map (Fig. 23). Again, seven classes of $\gamma+$ amacrine cells emerge. While it is beyond the scope of this manuscript to also perform a complete morphometric analysis of all these classes, we can assert that the different classes also have distinctive sizes: *e.g.* classes 1 and 2 have smaller mean diameters than classes 3 and 4. Our molecular classification is not informed by structure, and the fact that it discovers cell size groups is an independent proof that the metabolic profiles have a stable biologic origin, and are not just random associations (see Marc & Jones (2002)). This sample of the amacrine cell layer also displays enough glycinergic cells to capture a few cells with exceptionally glycine-weak signals, labeled here as class 2. The two unknown $\gamma-$ G− cells are likely dopaminergic interplexiform cells, as in goldfish (Jones *et al.*, 1999).

THE INNER PLEXIFORM LAYER

The single most dramatic feature of retinal organization is perhaps the functional stratification or lamination of the inner plexiform layer, which is particularly complex in cyprinids (Marc, 1986; Wagner & Wagner, 1988). Figure 24 summarizes the major layers of the zebrafish inner plexiform layer as reflected in the distribution of bipolar cell axon terminals and the positioning of complex signal borders (*e.g.* Fig. 13). As in all cyprinids, the distribution of GABA signals is nearly uniform but for a small mid-retinal dip (Fig. 13A; see also Marc & Liu (2000)). Previous publications suggesting multibanded GABA signals in the inner plexiform layer, with interspersed GABA-free zones, are corrupted by postmortem ischemic release, which is particularly rapid and extreme in the zebrafish. There are no fewer than 12 distinct laminae in the zebrafish inner plexiform layer and, by superposition of additional signals, many more are likely to emerge. The Bb layer between layers 90–100 contains terminals that belong to the homologues of cyprinid mixed rod-cone ON-center bipolar cells, and likely all three are present (Bb1, Bb2, Bb3). The distal border of the inner plexiform layer is a bipolar cell-free gap followed by a broad zone divisible into areas where homologues of two types of cyprinid mixed rod-cone OFF-center bipolar cells terminate (see Marc *et al.*

(1988)). Mixed within and between these specialized zones are the characteristic small terminals of pure cone bipolar cells (Sherry & Yazulla, 1992). Specific size groupings (*e.g.*, C *fine*, C *medium*) are segregated from other bipolar cell terminals bands by three gaps of relative bipolar cell process depletion. These internal gaps are not bipolar cell process-free, but reduced in terminal density. The lower half of layer Ba2 and gap3 are the zones occupied by dendrites of cholinergic amacrine cells in goldfish retina (Tumosa *et al.*, 1984; Marc, 1986; Tumosa & Stell, 1986; Marc & Liu, 2000) and the lower half of layer C *fine* is where the distinctive level 50 G+ amacrine cells terminate. Part of our objective is to provide as much discrimination of bipolar cell types as possible with the basis set of signals. As noted above, a subset of bipolar cells maintains an elevated level of aspartate and this is also expressed in their axon terminals (Fig. 25A). These same bipolar cells are also revealed

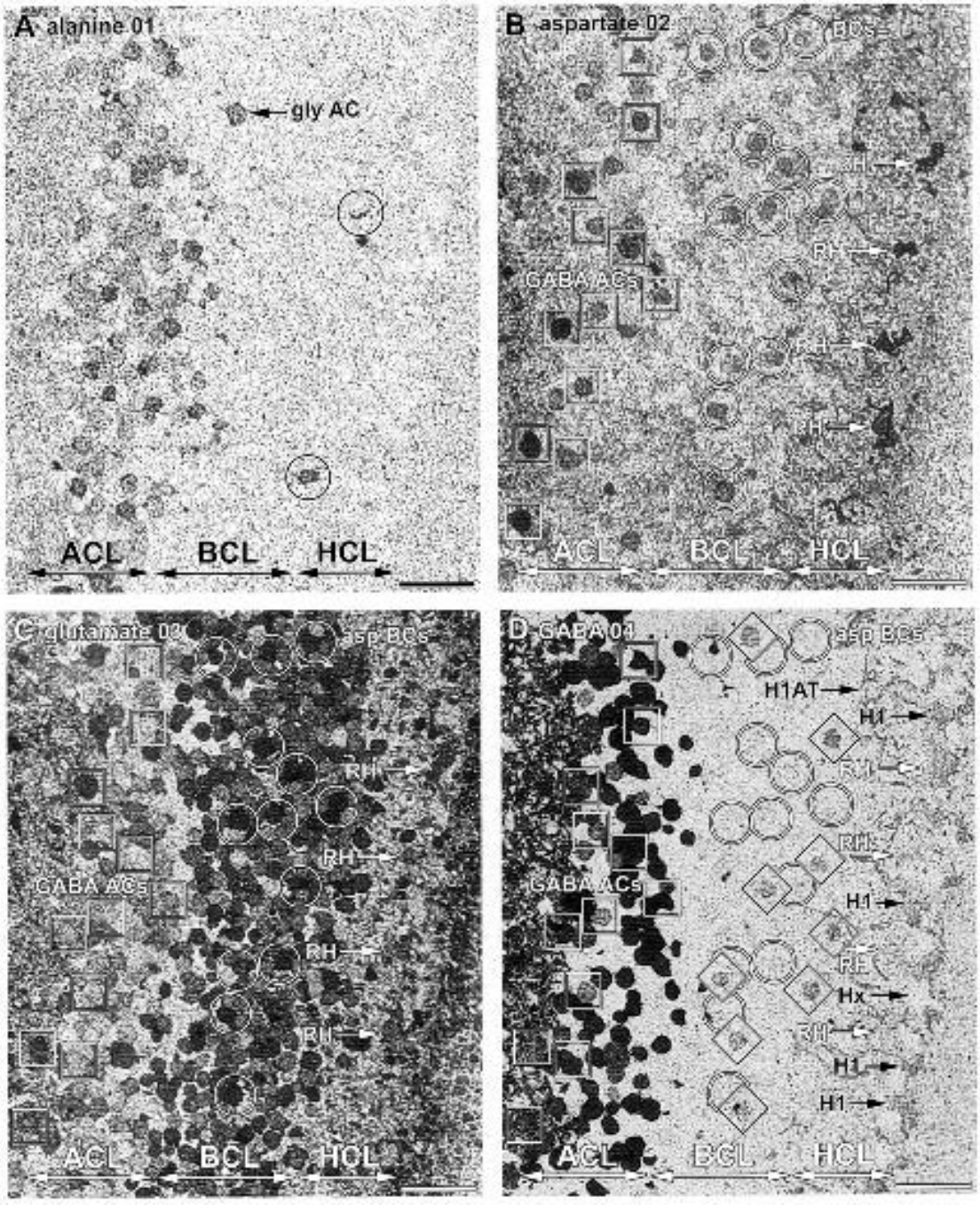

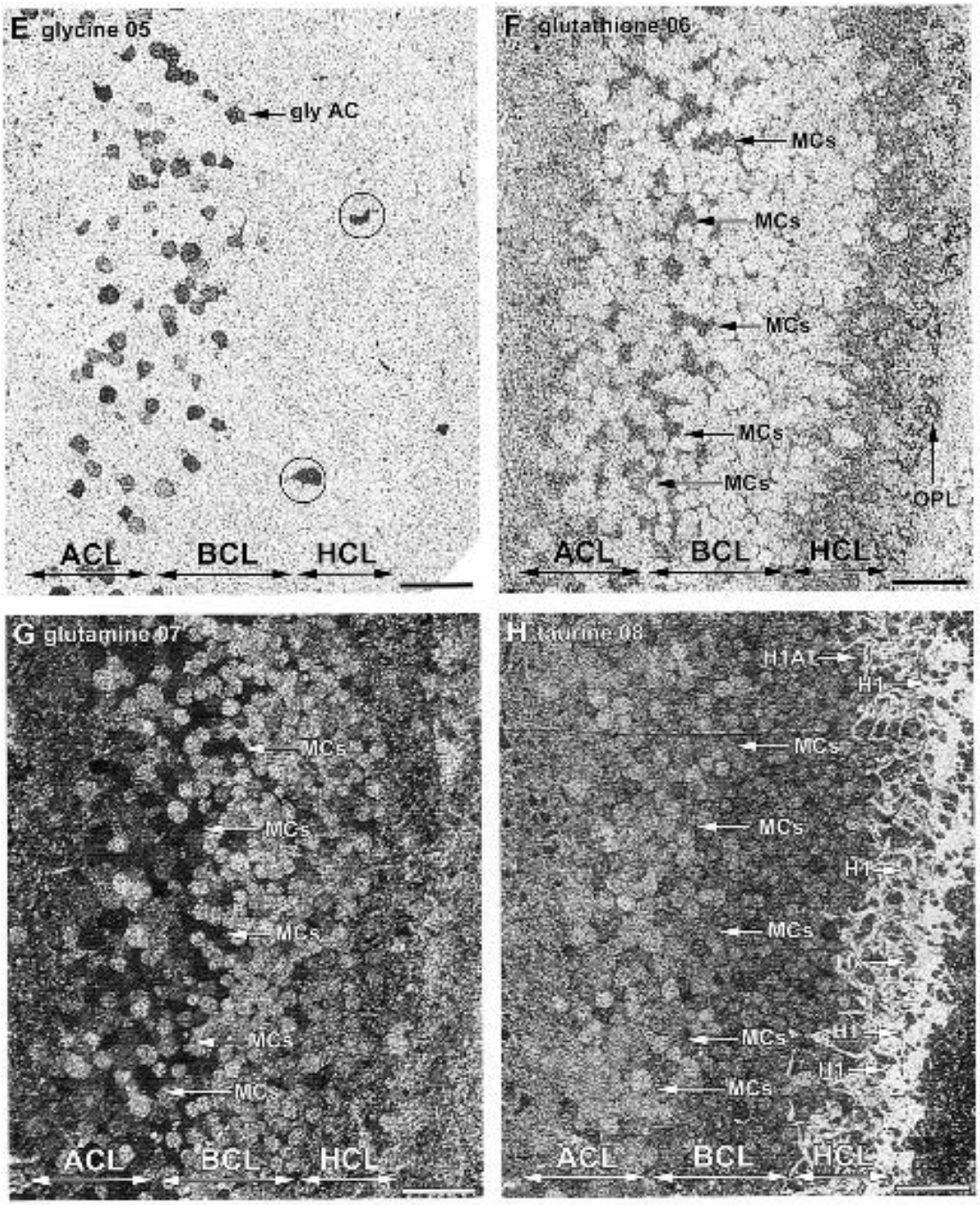

Fig. 14. A high-resolution library of the inner nuclear layer: ADEGJQ$\tau\gamma$ signals in the dark-adapted retina. A, alanine 01. Alanine-rich glycinergic interplexiform cells are circled. B, aspartate 02. Aspartate-rich bipolar cells are circled and a mélange of aspartate+ amacrine cells are boxed. C, glutamate 03. Bipolar and amacrine cells are marked as in panel B. D, GABA 04. Bipolar and amacrine cells are marked as in panel B. GABA+ presumed bipolar cells are marked by diamonds. Both H1 and Hx horizontal cells are indicated, as well a fine, strand-like horizontal cell axon terminals (H1AT). E, glycine 05. Glycinergic interplexiform cells are circled. F, glutathione 06. Large, glutathione-deficient bipolar cell somas that protrude into the horizontal cell layer are circled. G, glutamine 07. H, taurine 08. Section thickness: 250 nm. Scale 20 μm.

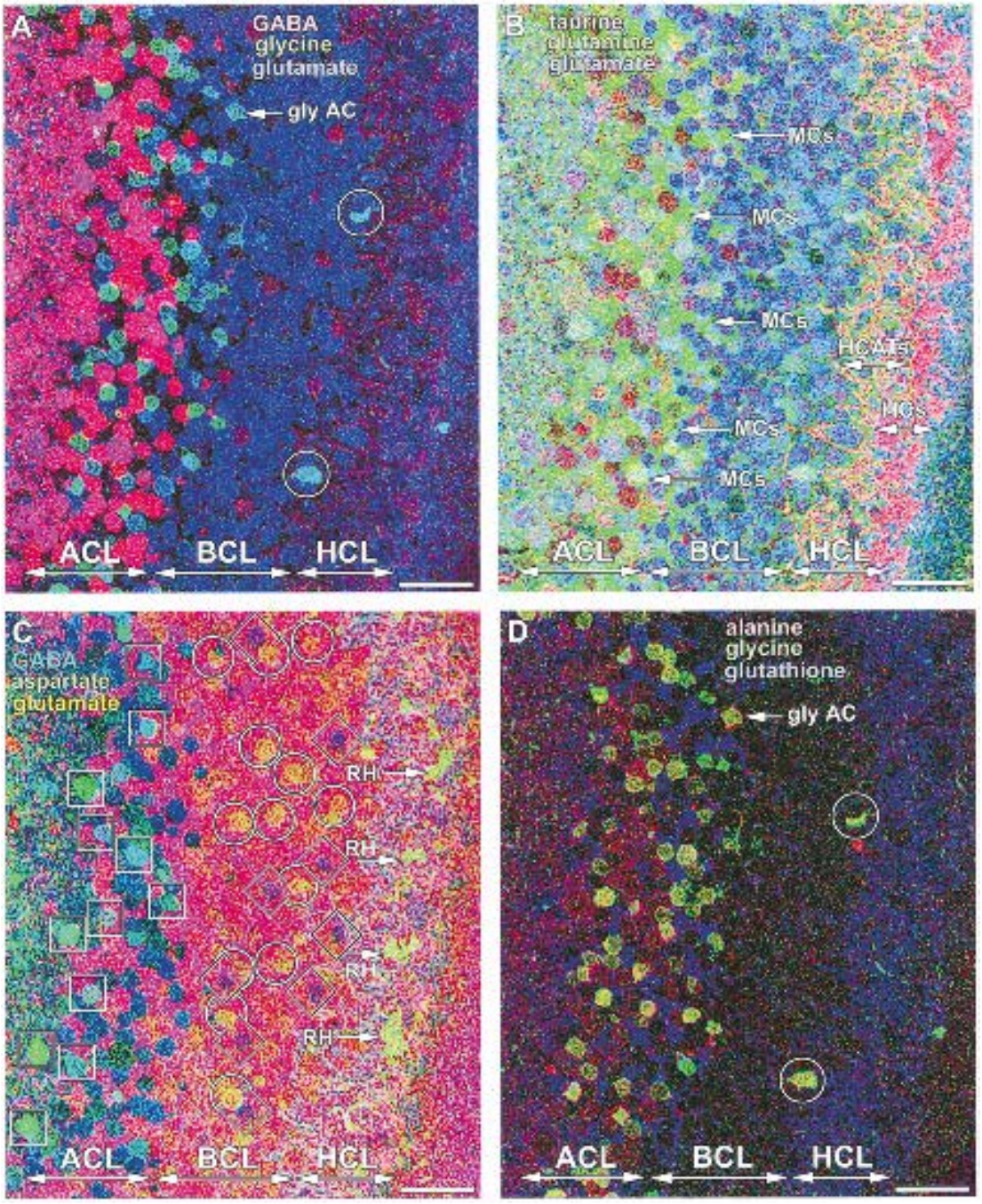

Fig. 15. Triplet mappings of a high-resolution library of the inner nuclear layer. A, γGE → *rgb*. B, τQE → *rgb*. C, γJA → **cgy** complex mapping. D, AGJ → *rgb*. Abbreviations and symbols as in Figure 14. Scale 20 μm.

by glutamate, GABA and taurine signals (Fig. 25B–D) but with subtle differences. The array can be visualized as a conventional γDτ → *rgb* mapping and enhanced in a γDτ → **cmy** mapping (Fig. 26A and B). The key result is that a subset of terminals shows a slightly elevated GABA content, as do some cell bodies in the outer nuclear layer (*e.g.* Fig. 19C), and they comprise a well-patterned array of irregular, rather than circular terminal profiles. This subset is likely to be class Bb3 (Ishida *et al.*, 1980b) and has a density of 1300/ mm^2:

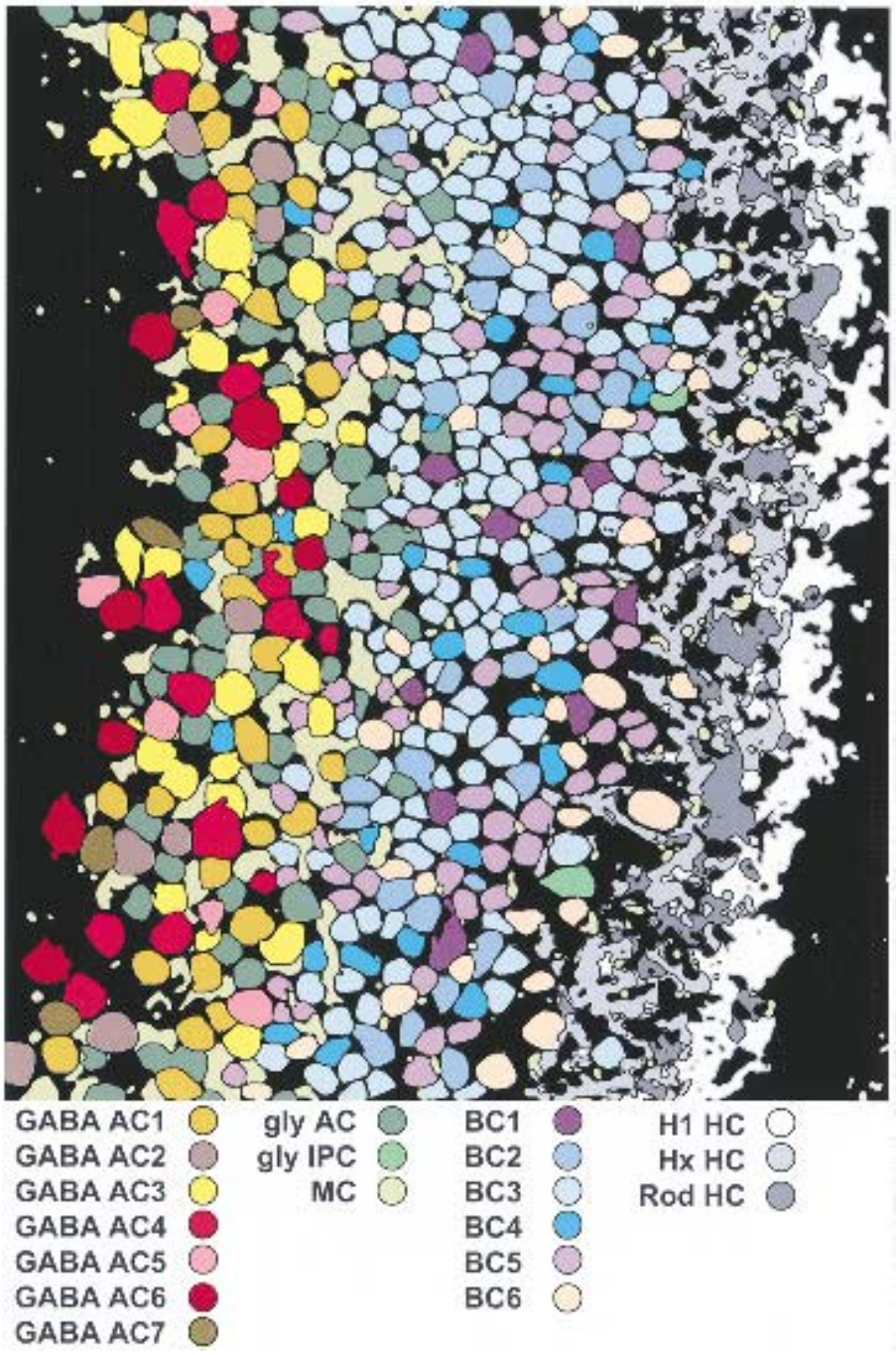

Fig. 16. A formal theme map of the dark-adapted inner nuclear layer. Each cell type is color coded by class membership based on isodata clustering and histogram deconvolution. The precise stratification of the inner nuclear layer into horizontal, bipolar, Müller and amacrine cell layers in the theme map is derived purely from the basis set (chemical space) and not morphological indices.

it corresponds to class BC6 in the theme map of Figure 16. The remaining arrays are likely a mixture of structural classes Bb1 and Bb2 (3700/ mm^2) submerged in the molecular superclasses BC4 or BC5.

THE GANGLION CELL LAYER

The ganglion cell layer is a monolayer just beneath the inner plexiform layer and harbors a mixture of ganglion cell classes and displaced amacrine cells. All

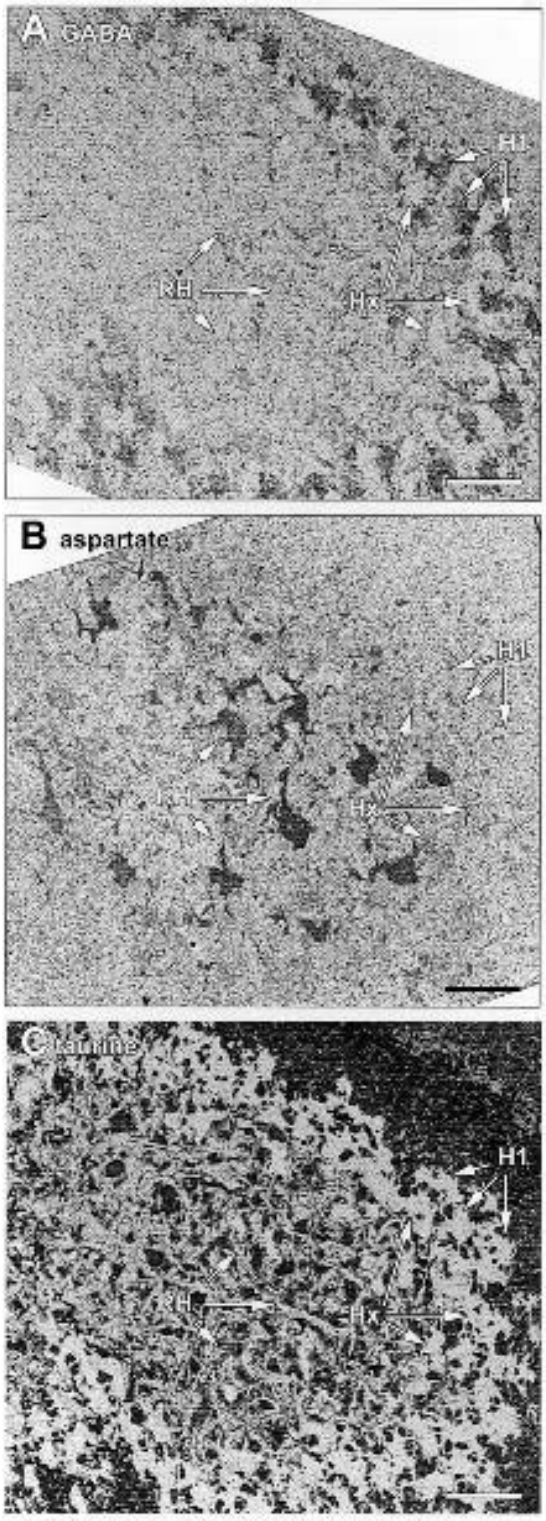

Fig. 17. A high-resolution library of the horizontal cell layer: $\gamma D\tau$ signals in the dark-adapted retina. A, GABA. B, aspartate. C, taurine, 03. Section thickness: 250 nm. Scale 20 μm.

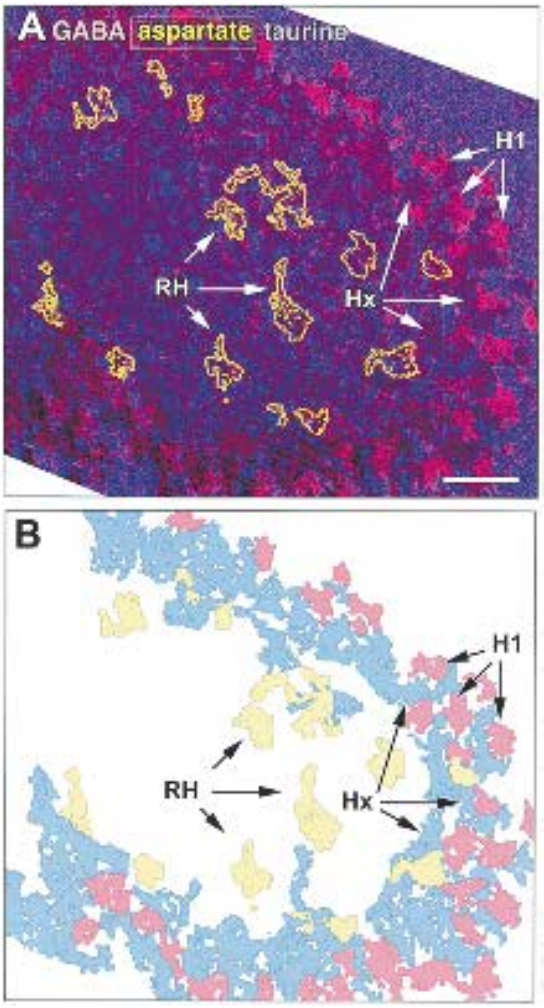

Fig. 18. A composite mapping of the horizontal cell layer. A. $\gamma\tau \rightarrow rb$ signals in the dark-adapted retina with edge-filtered D+ rod horizontal cells superimposed in yellow. B, theme map of horizontal cells: H1 red, Hx blue, RH, yellow. Scale 20 μm.

ganglion cells are strongly E+, while the distinct set of displaced amacrine cells and occasional misplaced amacrine cells have very low E signals (Fig. 27A). The taurine signal of the ganglion cell layer is, in effect, the inverse of the glutamate signal with very low signals in ganglion cells and elevated signals in amacrine cells (Fig. 27B). The optic fiber layer presages the massive τ+ signature of the optic nerve proper (see below), due to optic nerve astrocytes and not the optic fibers themselves. The GABA signal selectively displays displaced and misplaced amacrine cells. The simultaneous segregation of these signals are best displayed as γGE $\rightarrow$ *rgb* and **cmy** mappings (Fig. 28). In these mappings it is clear that ganglion cells display minor

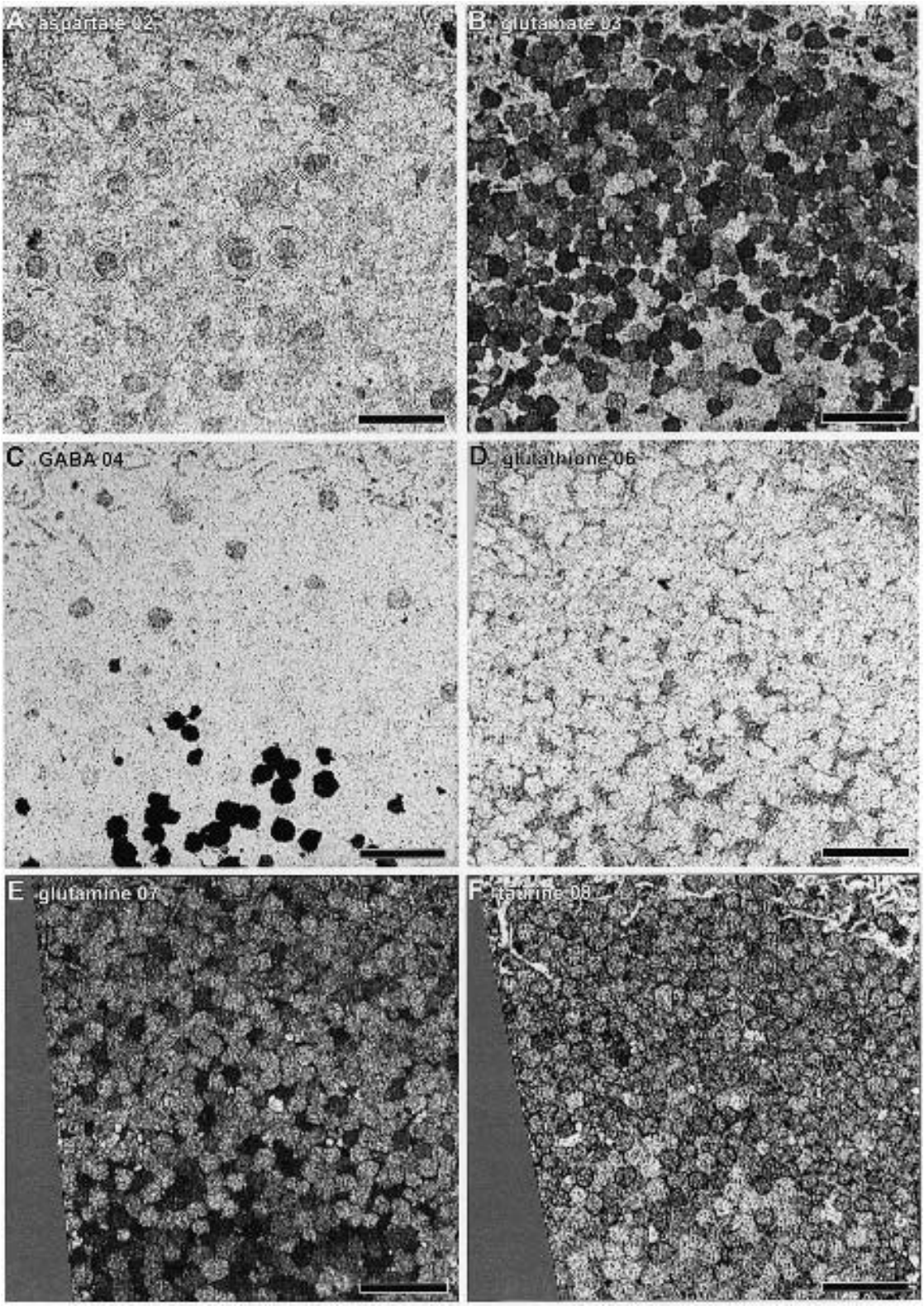

Fig. 19. A high-resolution library of the bipolar cell layer: DEJQ$\tau\gamma$ signals in the dark-adapted retina. A, aspartate 02. Aspartate-rich bipolar cells are circled. B, glutamate 03. C, GABA 04. Both strong and weak $\gamma+$ bipolar cell-like somas are evident. D, glutathione 06. E, glutamine 07. F, taurine 08. Section thickness: 250 nm. Scale 20 μm.

variations in their low taurine contents and that displaced and misplaced amacrine cells belong to different $\gamma+$ classes.

SUMMARY N-PLOTS

The arrays of registered monochrome and triplet mappings are the physical evidences of diverse molecular phenotypes between and within retinal cell types. Without such precision signal archives, decomposition of types cannot achieved. Even theme maps, such as in Figure 16, are difficult, if not impossible, to interpret by back-and-forth comparison with the source data. N-plots of signatures for each bipolar, horizontal, and ganglion cell class/ superclass are summarized in Figure 29. Six separable classes of bipolar cells emerged from isodata clustering. BC1 is the most remarkable and is a $\gamma+$ BC patterned in an array with a conformity ratio of >3, arguing that it is a singular type comprising but 3% of the entire bipolar cell cohort. The GABA content is only about 1 mM, much lower than that of any amacrine cell but equivalent to H1 horizontal cells. And the glutamate content is submillimolar, 2–10× lower than any other bipolar cell, but equivalent to the contents of light-adapted cones. What is the likely neurotransmitter of this cell? Arguably, it could be GABA or glutamate. The remaining bipolar cells are separable based on their characteristic, complex mixtures of glutamate, aspartate, glutamine and taurine. The ON-center mixed rod-cone Bb bipolar cells are likely contained in classes BC5 (Bb1, Bb2) and BC6 (Bb3), each comprising about 12% of the entire bipolar cell cohort. The remaining bipolar cells are all contained in classes BC2,3,4. Superclass BC3, the lowest DQ composite signal group in the E+ bipolar cells, makes up 46% of all bipolar cells and likely contains most or all of the cone bipolar cells. It is also a collection of the smallest cells in the inner nuclear layer, which matches well with the cone bipolar cell profiles of other cyprinids. Using the class/ superclass minimum fractions as a representative size for pure cone bipolar cells, it is clear that this diversity could harbor over 20 classes: easily accomodating the estimated 15 cell classes described for other cyprinids (Sherry & Yazulla, 1992).

The ganglion cell population is likely as complex as in the goldfish (Hitchcock & Easter, 1986), but similar to the goldfish, the signatures do not segregate them effectively into classes or superclasses. Ganglion cells display a remarkably stable and distinctive signature, with a high DQ composite and very low AJ and Gτ

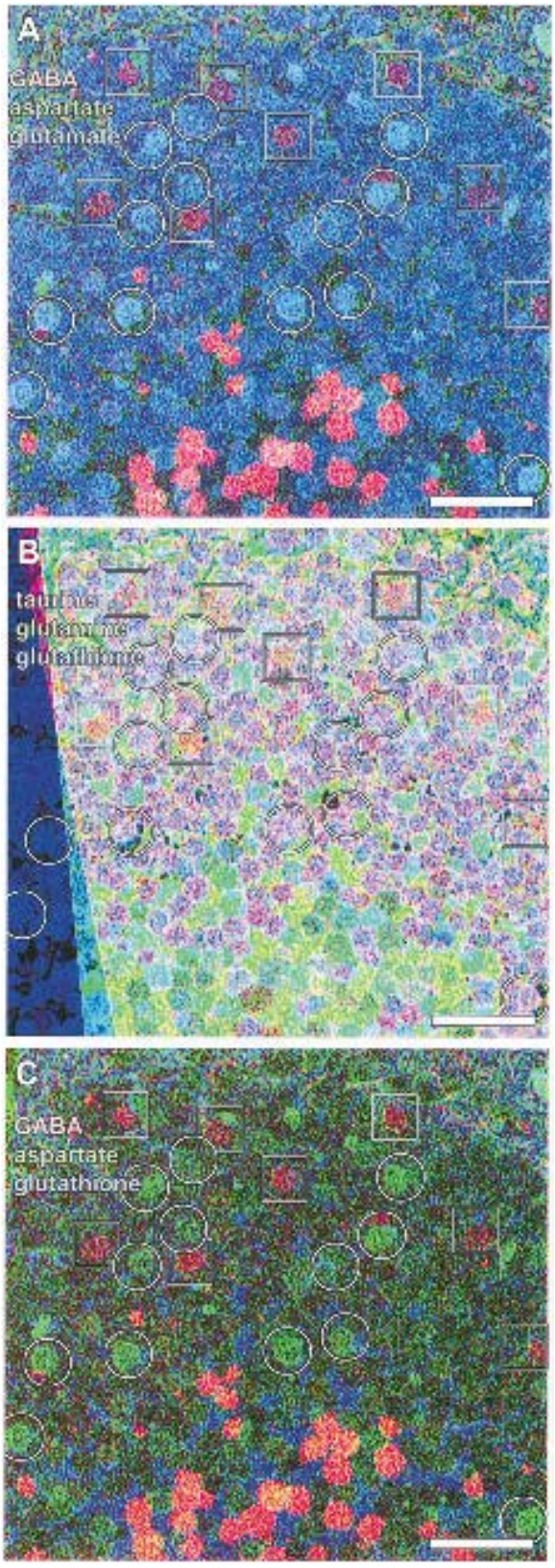

Fig. 20. Triplet mappings of the bipolar cell layer: A, γGE → *rgb*. Aspartate-rich cells are circled, GABA-rich cells are boxed. τQE → *rgb*. C, γDJ → *rgb*. Scale 20 μm.

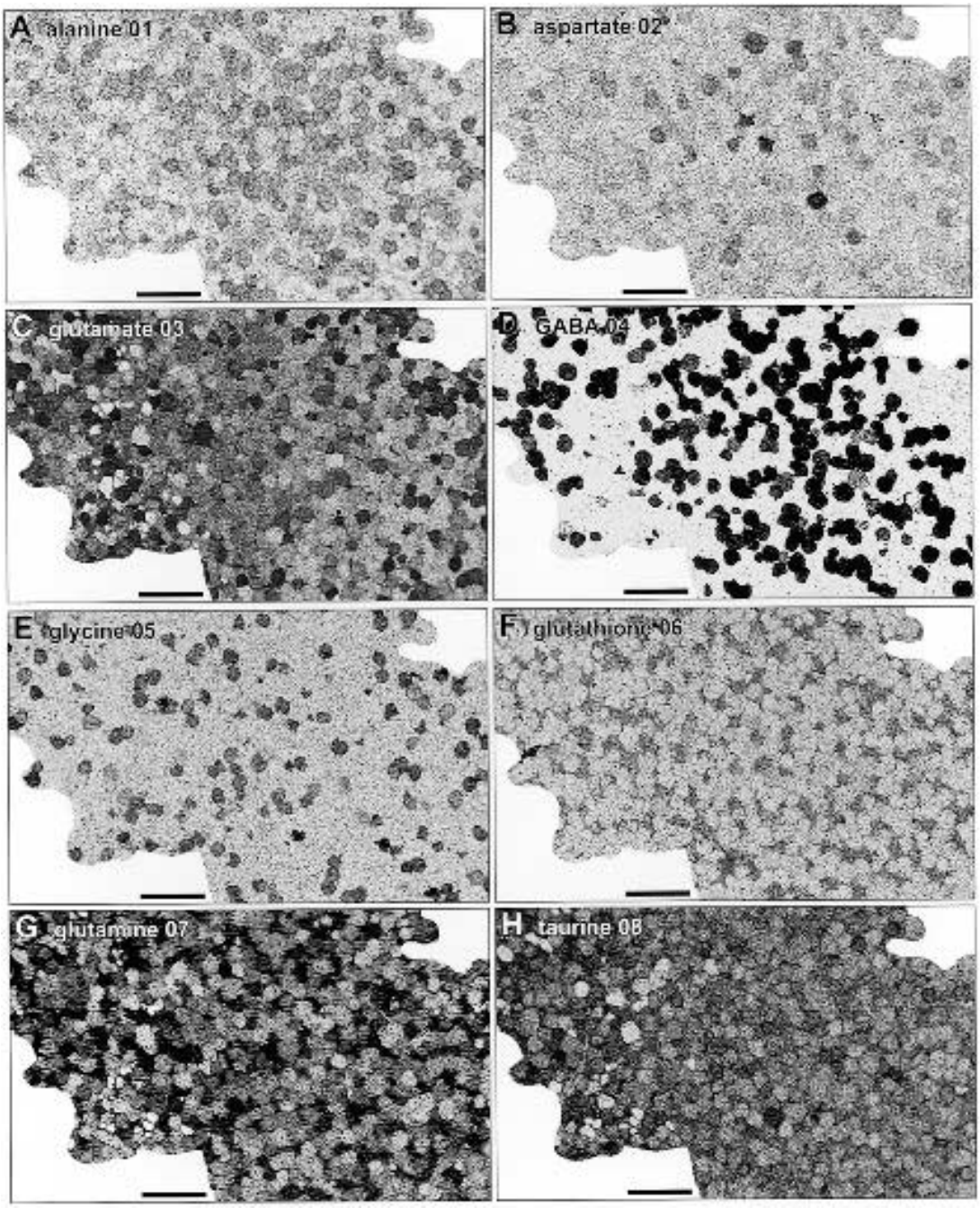

Fig. 21. A high-resolution library of the amacrine cell layer: ADEGJQ$\tau\gamma$ signals in the dark-adapted retina. A, alanine 01. B, aspartate 02. C, glutamate 03. D, GABA 04. E, glycine 05. F, glutathione 06. G, glutamine 07. H, taurine 08. Section thickness: 250 nm. Scale 20 μm.

composites. This signature is also characteristic of displaced ganglion cells in the goldfish (Marc *et al.*, 1990), and examples of similar cell signatures were detected in the zebrafish.

The neurochemistry of presumed lateral "inhibitory" horizontal cells remains one of the mysteries of retinal processing. There are three major horizontal cell signatures in the zebrafish retina. H1 horizontal cells are the $\gamma+$ cells of the horizontal cell layer, but might as well be termed E+, as they contain up to 1 mM glutamate, as in goldfish and other cyprinids. Based on signal content and the presence of H1 horizontal cell

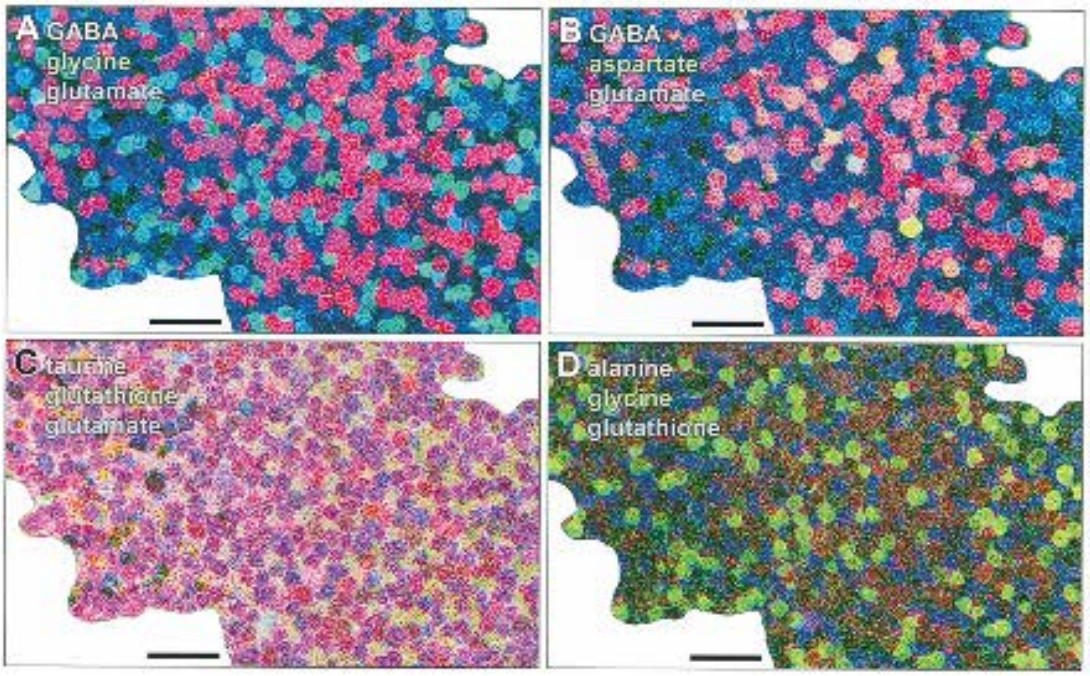

Fig. 22. Triplet mappings of the amacrine cell layer: A, γGE → *rgb*. B, γDE → *rgb*; C, τQE → *rgb*. D, AGJ → *rgb*. Scale 20 μm.

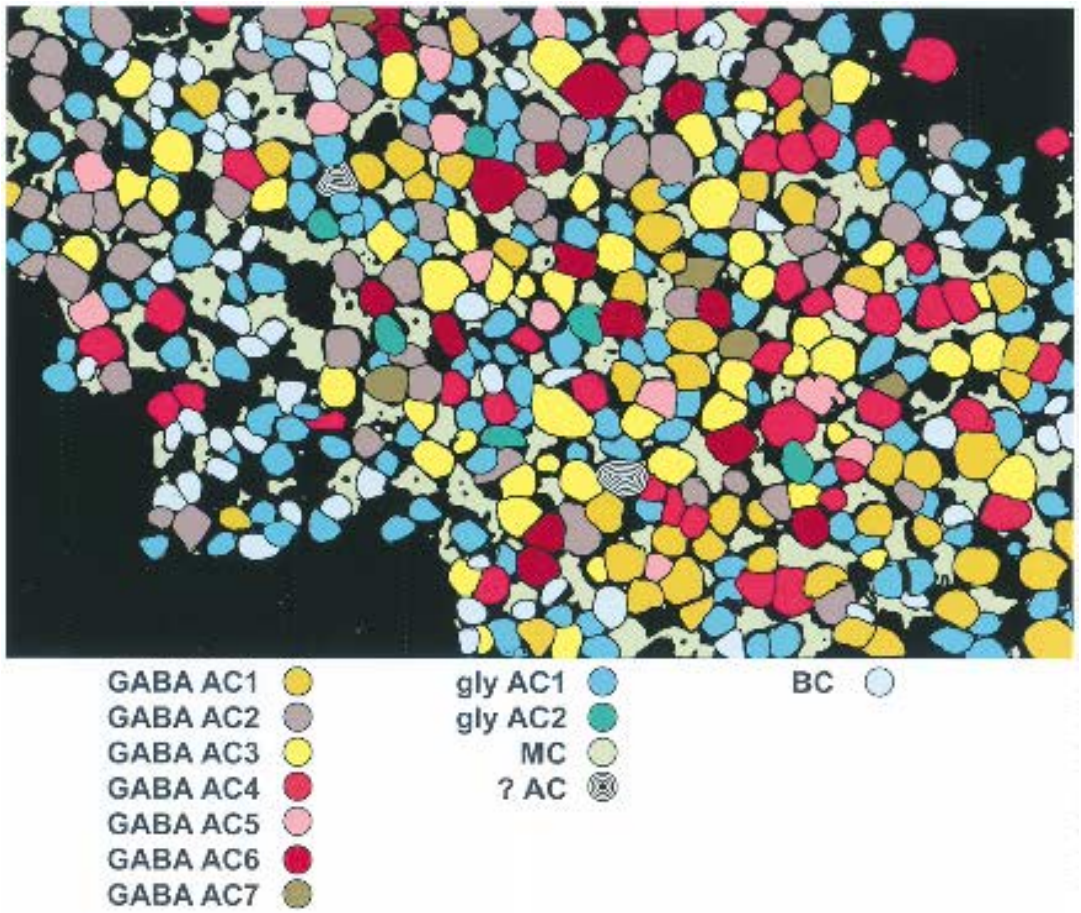

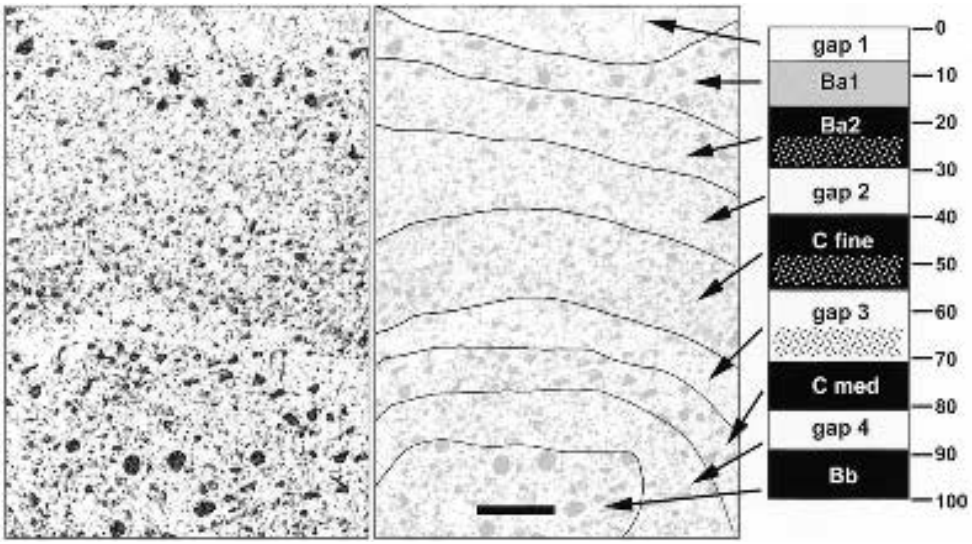

Fig. 24. Bipolar cell axon terminal arrays in the inner plexiform layer. Different morphological types of bipolar cells target distinct levels in the inner plexiform layer and, in combination with other signals, a formal lamination can be extracted. Left panel, the median-filtered γ-E difference signal in an oblique, high-resolution section isolates bipolar cell terminals. The center panel superimposes lamination borders on a brightness remapped image. The right panel is a formal lamination scheme where white *gap* boxes indicate a relative paucity of bipolar cell terminals. Dark boxes indicate bipolar cell rich zones: Ba1, class Ba1 OFF-center bipolar cells; Ba2, class Ba2 OFF-center bipolar cells; C fine, fine cone bipolar cell terminals; C med, coarser cone bipolar cell terminals; Bb, class Bb ON-center bipolar cell terminals. Stippling denotes finer scale subdivision of a region: levels 25 and 65 are zones where pairs starburst and pyriform radiate cholinergic amacrine cells arborize; level 50 is where a unique set of glycinergic amacrine cells terminate.

synaptic specializations in the outer plexiform layer targeting glycinergic interplexiform cell, H1 horizontal cells could as readily use glutamate as GABA, or both, as a signal molecule, in addition to pure biophysical signal modes (Kamermans & Spekreijse, 1999). The case for a specific molecule is far from established and becomes more complicated when the modes of signaling of Hx or RH cells are considered: both contain little GABA, but rod horizontal cells in particular contain about 3 mM aspartate and glutamate. So even though distinctive signatures are evident from the N-plots, the neurochemistry of horizontal cells in general remains puzzling. As noted earlier, the size of the Hx group is large enough to justify the speculation that more than one class of horizontal cell is submerged in the set.

There are seven groups of $\gamma+$ and two of G+ amacrine cells (Fig. 30). Classes γ AC1 and γ AC3 each comprise $\approx$30% of the $\gamma+$ amacrine cell cohort and are thus likely to be superclasses. Among several differentiating features, class γ AC1contains 5–10$\times$ less glutamate than class γ AC3. Class γ AC3 is also one of the low-taurine cells so evident in the triplet displays of the amacrine cell layer. The next largest classes are γ AC4 (14%) and γ AC6 (10%). Class γ AC4 is unique in a mathematical sense: no single signature sets it apart, but N-dimensional vector mapping segregates it from other classes. Class γ AC6 is the high-aspartate cohort of the amacrine cell layer. The smallest classes, γ AC2 (6%), γ AC5 (6%) and γ AC7 (4%) each have a unique signature, with γ AC5 being the lowest γ signal population in the $\gamma+$ cells of the amacrine cell layer. The glycine signals of G+ amacrine cells are modest compared to the primary signals of other neurons and they also contain significant glutamate signals. As noted above, the G AC1 group is certainly a superclass, as evidenced by multimodal DQ components of the N-plot. This illustrates that even univariate deconvolution has limits, as segregating the DQ cluster would require a bivariate deconvolution algorithm, which we have not yet implemented. Class G AC2 is a very small group (5% of the G+ cohort, only 1% of the amacrine cell type) with weak but significant glycine levels, $\approx$800 μM. We place

Fig. 23. A formal theme map of the dark-adapted amacrine cell layer. This map displays the dataset from Figures 22 and 23. Color-code as in Figure 16, with additional codes for unidentified cells. Bipolar cells are grouped as a single type and not classified for simplicity.

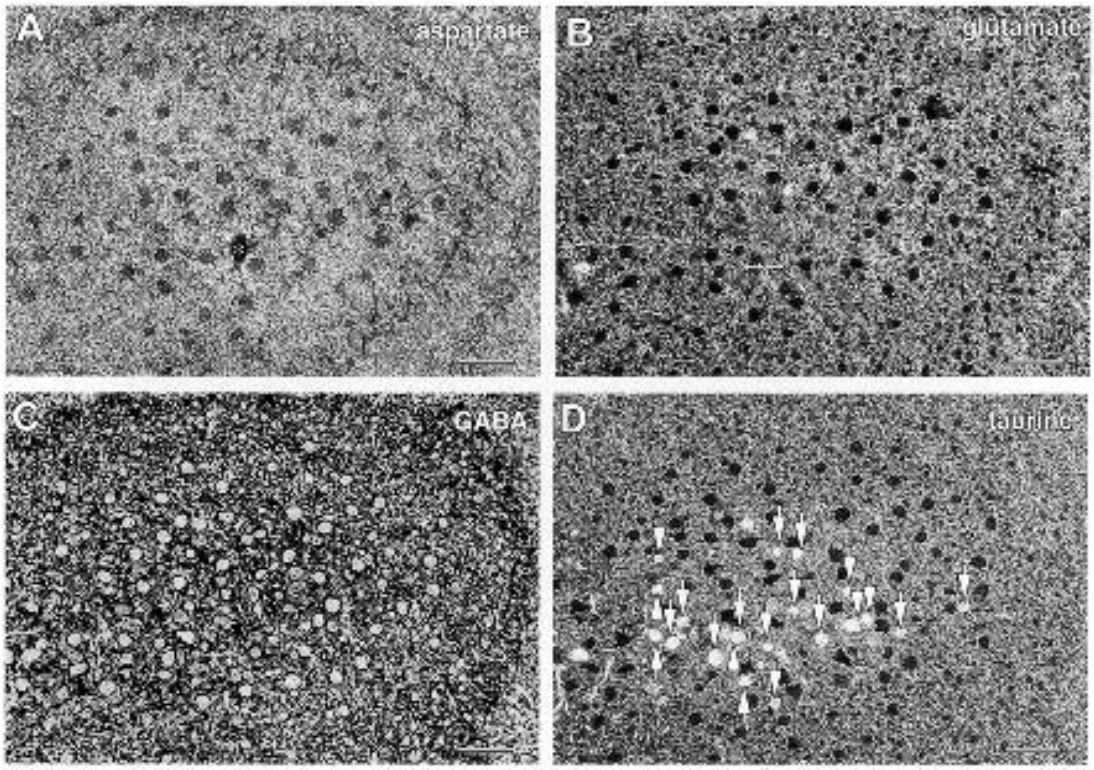

Fig. 25. A high-resolution library of the Bb bipolar cell terminal layer at level 90 of the inner plexiform layer: DE$\tau\gamma$ signals in the dark-adapted retina. A, aspartate. Asterisk denotes an image defect. B, glutamate. C, GABA. D, taurine. Arrows indicate ganglion cells. Section thickness: 250 nm. Scale 20 μm.

it in the G+ group for circumstantial reasons: (1) the GABA content is nil; (2) although it has significant glutamate content, so does many an amacrine cell; (3) it does not seem likely to be a bipolar cell based on its slightly lower τ and higher J signals; (4) it is not likely to be a dopaminergic cell, due to its high frequency and small soma size; (5) it is unlike any ganglion cell in its taurine content. We must admit, however, that we really do not know what it is. Even discounting these cells, γ+ amacrine cells comprise 63% and G+ amacrine cells 35% of the neurons in the amacrine cell layer proper. Thus any developmental, experimental or pathologic processes that differentially impact these populations can easily be tracked in terms of their effects on the proportions of γ+ and G+ cells.

SIGNALS IN THE LIGHT-ADAPTED NEURAL RETINA

On the whole, there is little *obvious* difference in the signals of light and dark-adapted retinas, but since there are real changes in the signatures of LD and SD cones, it was obviously necessary to screen the neural retina. Subtle patterns of signal alteration were detected with, we believe, interesting consequences for the physiological properties of amacrine cells in particular. Most basis signals viewed in single-channel mode for light-adapted retinas (Fig. 31) were indistinguishable from dark-adapted specimens (Fig. 10). Alanine (Fig. 31A), glutamate (Fig. 31C), GABA (Fig. 31D), glycine (Fig. 31E), glutamine (Fig. 31G) and taurine (Fig. 31H) signals display the same patterns and signal strengths appeared unchanged. In three of five samples, the glutathione levels (*e.g.* Fig. 31F) appear slightly higher in the inner plexiform layer, as though the overall Müller cell content was enhanced. The aspartate signals were dramatically different in all cases (Fig. 31B): all horizontal cell aspartate levels dropped, and the levels in ganglion cells and bipolar cells rose. The significance is unknown, of course. One major change is invisible in this mode, however, and required triplet mapping (Fig. 32) before it was found. In the light-adapted retina, there is strong dual G+ γ+ signal localization (Fig. 32A) in cells found to be purely G+ when dark-adapted (Fig. 11A). In fact, nearly all G+ amacrine cells showed some suprathreshold GABA signal, usually at the 300–500 μM level. However, one set of cells showed much stronger GABA signals ($\approx$1 mM) combined with 3–5 mM glycine (Fig. 32A). These may be the homologues of the Gγ amacrine cells in the goldfish retina (Marc *et al.*, 1995). There are even

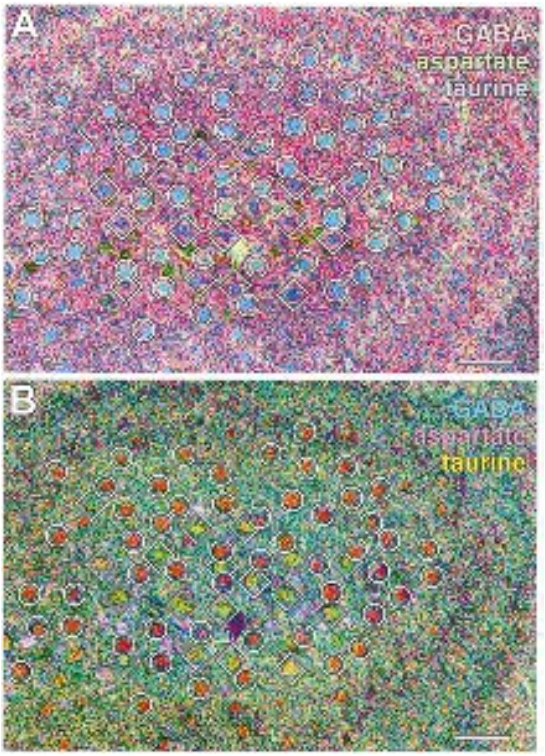

Fig. 26. Triplet mappings of the Bb bipolar cell terminal layer: A, γDτ → *rgb*. Circles denote Bb1 and Bb2 bipolar cell terminals. Diamonds denote Bb3 bipolar cell terminals. B, γDτ → **cmy**. Scale 20 μm.

some very strong γ+ amacrine cells and E+ bipolar cells that show enhanced glycine signals, and the latter have also been detected in the goldfish retina. These are subtle phenomena, not obvious without detailed signature analysis and N-plots, and their significances will be addressed in the discussion. Even with this change in signature, G+ amacrine cells remain strongly A+ (Fig. 32B, AGJ → *rgb*), continuing the theme of alanine/ glycine association. Moreover, the light-adapted τQE → *rgb* mapping is indistinguishable from the dark-adapted retina, supporting the idea metabolic changes are selective, not global. The inclusion of the aspartate channel (Fig. 32C, γDE → *rgb*) does produce a different and unique image, lacking the distinctive horizontal cell band and with more pronounced bipolar cell and ganglion cell definition. The role of elevated aspartate levels in any cells, much less neurons, is without explanation.

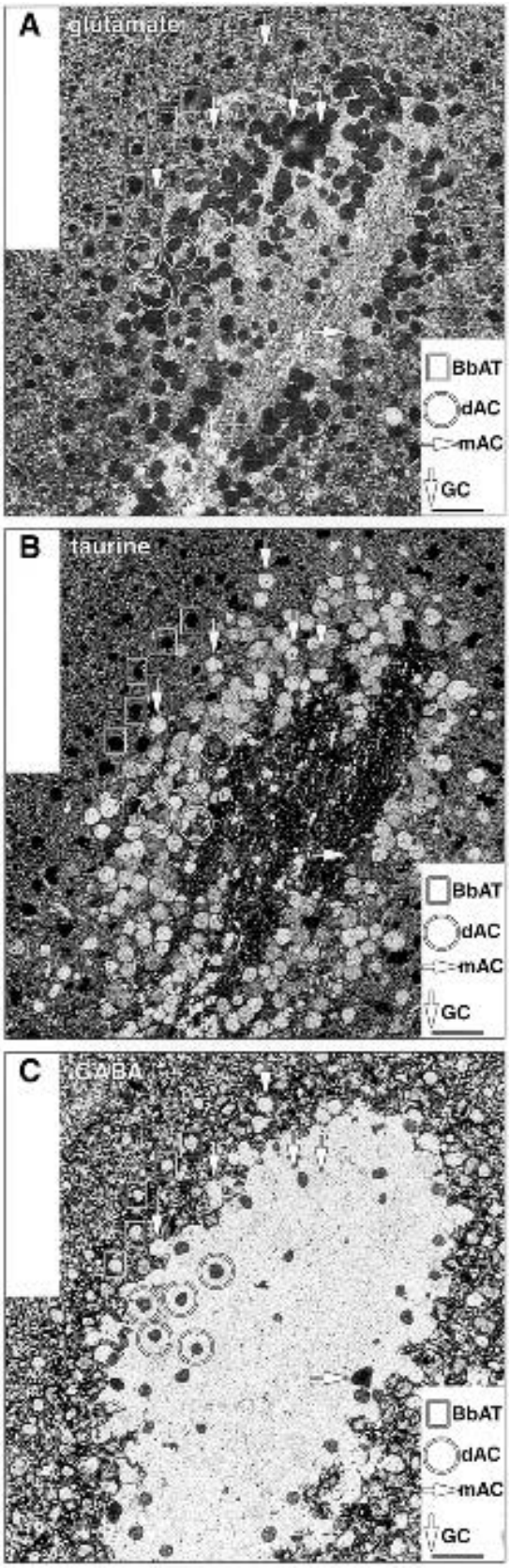

Fig. 27. A high-resolution library of the ganglion cell layer: E$\tau\gamma$ signals in the dark-adapted retina. A, glutamate. B, taurine. C, GABA. Abbreviations: dAC, displaced amacrine cell; mAC, misplaced amacrine cell. Section thickness: 250 nm. Scale 20 μm.

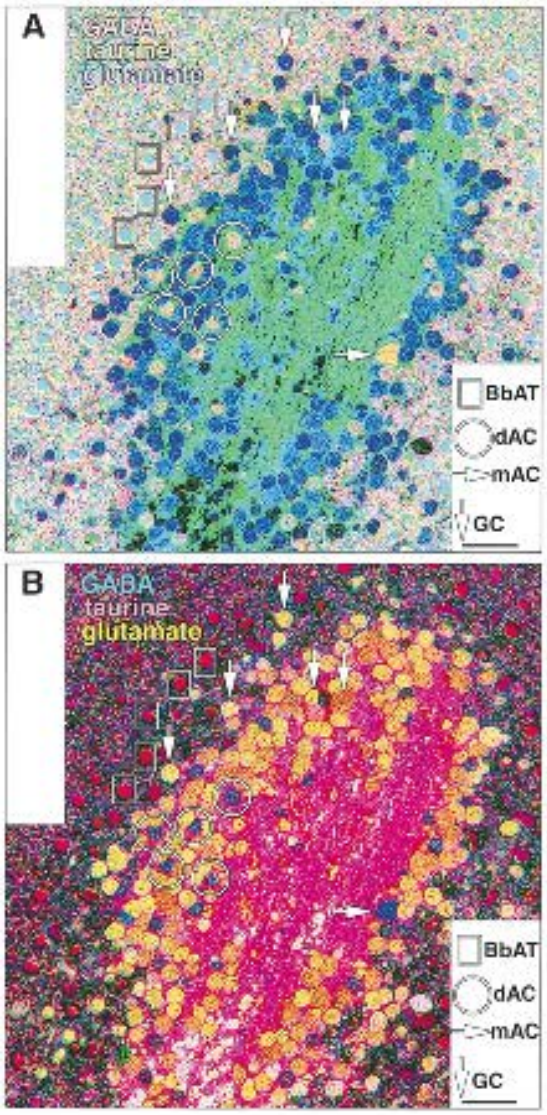

Fig. 28. Triplet mappings of the ganglion cell layer: A, $\gamma\tau$E → *rgb*. B, $\gamma\tau$E → **cmy**. Scale 20 μm.

SPECIALIZED AREAS OF THE RETINA: THE OPTIC NERVE HEAD AND OPTIC NERVE

The ganglion cell axon outflow into the axon fascicles of the peripheral retina, merging into the optic fiber layer, the optic nerve head and the heavily fasciculated optic nerve (Easter *et al.*, 1981), a rough folded ribbon, also have distinctive phenotypes. Figure 33 displays a registered data set from a dark-adapted zebrafish retina encompassing all of these structures, the vasculature of the optic nerve proper and the choroidal rete. Even relatively weak patterns such as alanine and aspartate signals (Fig. 33A and B) illustrate the delicate changes in molecular signatures of the optic fiber layer, head and nerve change; various signals are graded accross the path of the folded ribbon. The optic nerves of many fishes resemble flat ribbon cables crumpled into compact bundles. The thick, most extended portion is made of axons from the central retina which is the oldest part of the eye: this organization is largely chronotopic, not precisely retinotopic. The thinnest, most folded segment ends in axons from the peripheral retina. The glutamate image (Fig. 33C) validates the expectation that the axons of ganglion cells ought to contain high glutamate signals, but also shows a surprising glutamate-rich cap at the peripheral end of the ribbon, which may be the pale nonmyelinated fiber tract (the newest axons) in goldfish (Easter *et al.*, 1981) or a zone nearby. Vascular endothelia of vitreal vessels, optic nerve vessels, the choroidal rete, the choroids and choriocapillaris all have glutamate levels as high as any retinal neuron. Conversely, high glycine signals seem to be the signature of *bona fide* glycinergic neurons, and no element in the optic nerve or its associated tissues has any significant glycine content (*i.e.* all levels must be below 50 μM). Glutathione signals (Fig. 33E) display some intriguing specializations. The glutamate-rich cap at the peripheral limit of the optic nerve ribbon is extremely J+, second only to the RPE, which suggests that this cap contains glial cells. There is also a subtle increase in glutathione levels within the body of the ribbon, following the same gradient as alanine and aspartate. Finally, the glial (or perhaps ependymal) derivatives that form the margin of the optic nerve head in the retina also display significant elevation in glutathione. GABA levels in the optic nerve and associated tissues are nil, except for a subtle elevation in the cap (Fig. 33F). Glutamine levels are massive throughout the optic nerve and in the cap, consistent with both axonal and glial sources (Fig. 33G). It is again worth noting that endothelial glutamine levels are quite low (as are aspartate levels), perhaps suggesting that these metabolites are not the prime sources of endothelial glutamate. Finally, taurine signals create a rich tableau (Fig. 33H). Taurine levels in the optic fiber layer rival those of the outer retina, and are likely representative of intraretinal fiber layer astrocytes. But as the axons flow into the optic nerve head, taurine signals weaken by nearly 100-fold, suggesting that glia (astrocytes) with an entirely different metabolic program now support the axonal extracellular regime. The optic nerve is reticulated with τ+ elements (especially near the surface of the nerve), but no central → peripheral signal gradient is evident. Again, the unmyelinated cap has extremely high taurine signals, approaching 10 mM or higher. Triplet mapping uncovers a wealth of signatures unmatched by any other visualization process or probe set. The standard γGE → *rgb* mapping is unremarkable, but for the enhancement of the subtle signals in the peripheral optic nerve glial cap (Fig. 34A). In contrast, the τQE → *rgb* and τQJ → *rgb* triplets (Fig. 34B and C) reveals a rich polychromatic display of signatures. Only one area will be noted here: the fine discrimination

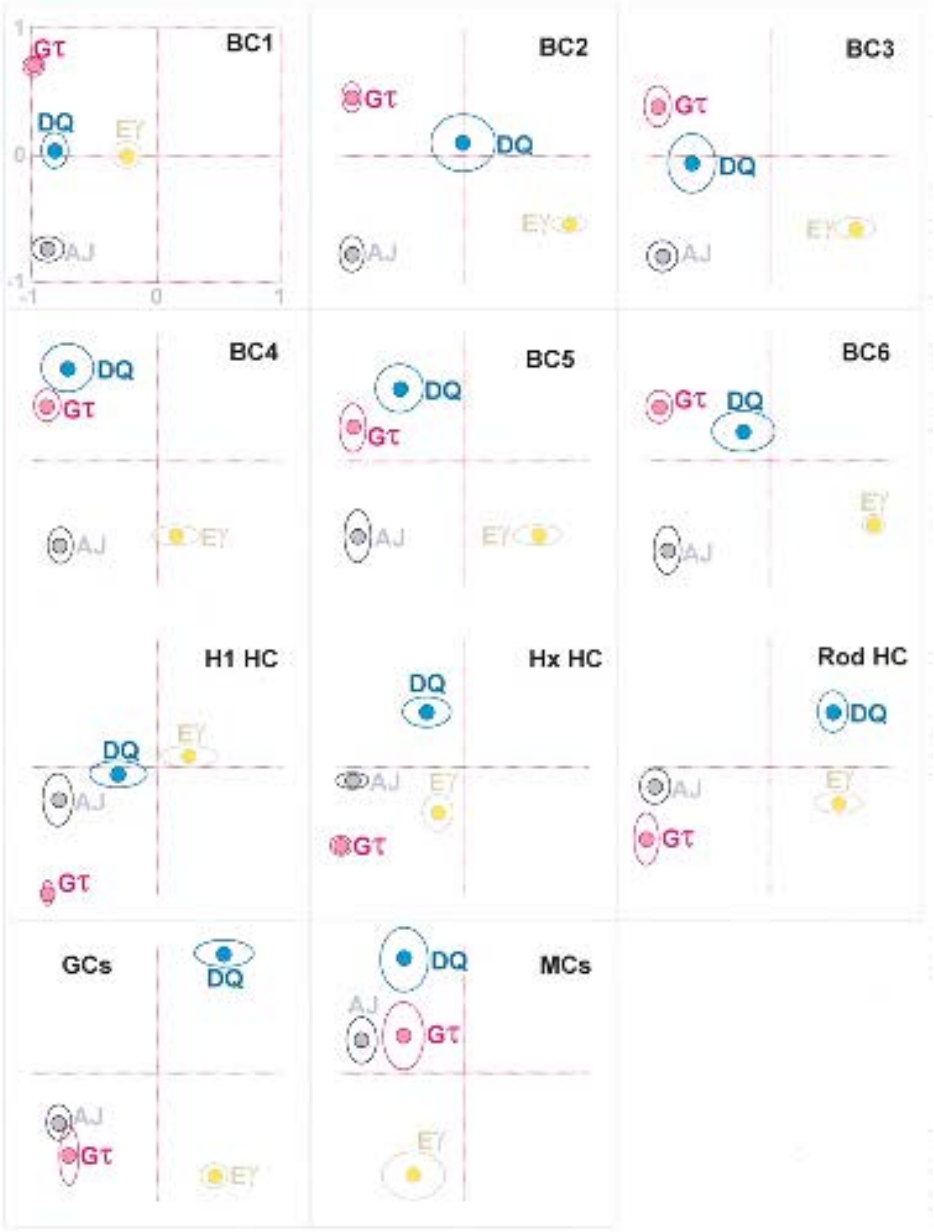

Fig. 29. Horizontal, bipolar, ganglion and Müller cell molecular phenotyping N-plots. Each plot is coded as in Figure 2 and is derived from dark-adapted retina.

of molecular phenotype signals of the axonal core, the glial sheath and terminal glial cap of the peripheral optic nerve. The cap displays a unique mixture of maximal glutamate, taurine, glutamine and glutathione signals. No neural or glial element in the retina and no epithelial or endothelial cell has a similar signature. These strong signals obscure the fine gradient of minor metabolites, which can be easily expressed with a $\gamma D\tau \rightarrow rgb$ mapping (Fig. 34D). As various insets display (Fig. 34A, C and D), the retinal signatures remain precise across specimens, preserving characteristic neuronal and epithelial signals.

SPECIALIZED AREAS OF THE RETINA: THE MARGINAL ZONE

Of all regions, the circumferential marginal zone (also known as the germinal zone) of cyprinid retinas is perhaps the most provocative, as it contains adult retinal stem cells from which new photoreceptors and neurons

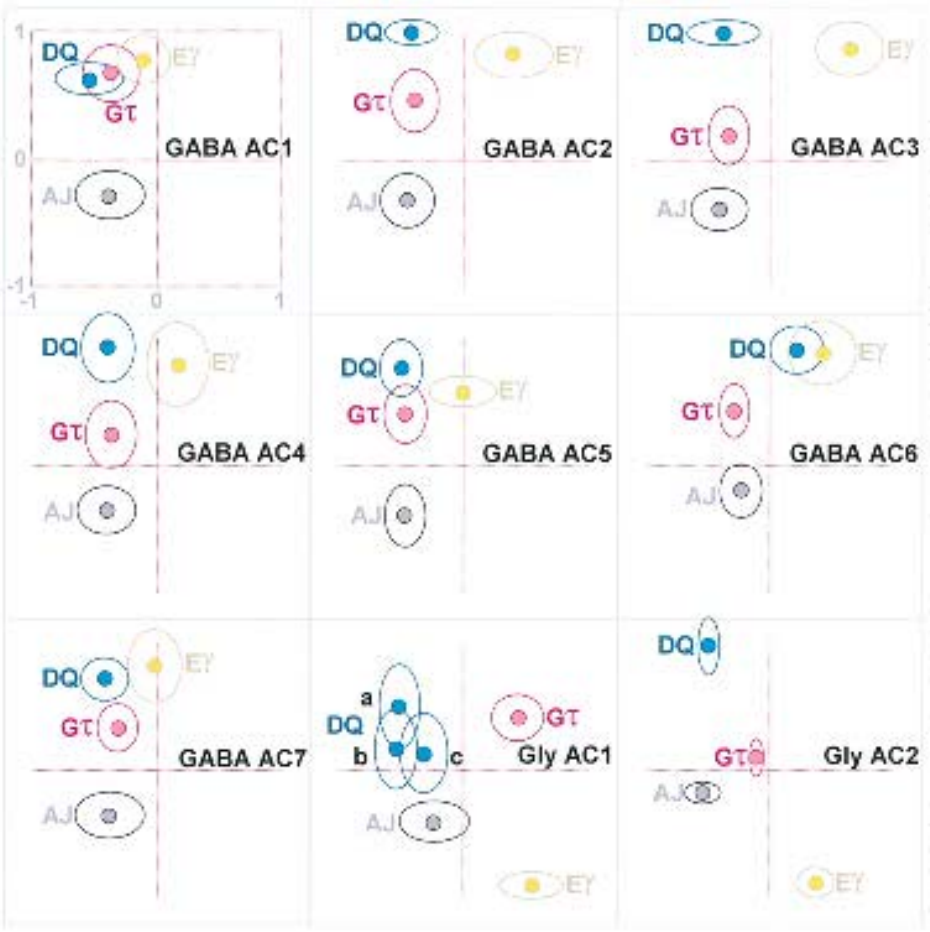

Fig. 30. Amacrine cell molecular phenotyping N-plots for 7 GABA and 2 glycine amacrine cell classes. Each plot is coded as in Figure 2 and is derived from dark-adapted retina.

are generated. We performed molecular phenotyping with the same approaches as described for all other retinal loci and the optic nerve. The entire region can be visualized as the marginal retina abutting the marginal zone and the continuous transition from retina to the epithelial ciliary zone and iris (Fig. 35: A, alanine; B aspartate; C, glutamate; D, glycine; E, GABA; F, glutathione; G, glutamine; H, taurine). The interface between the neural retina proper and the formal marginal zone is abrupt, with no detectable gradients on first examination. The processes of amacrine cells (Fig. 35D and E), bipolar and ganglion cells (Fig. 35C) do not invade the marginal zone. The retina itself appears largely mature right up to the marginal zone, with some exceptions. Aspartate signals (Fig. 35B) in the outer plexiform layer seem not to be stable for all horizontal cells until 75–100 μM away from the marginal zone and the precise G+ amacrine cell lamina at level 50 of the inner plexiform layer seems absent until 50 μM from the marginal zone. Cells likely to be ganglion cells based on their EQ signatures (Fig. 35C and G) are present in the ganglion cell layer right up to the border and within the proximal part of the marginal zone. The marginal zone itself is an apparently continuous flattened torus, about 50–60 cells in cross-section: only a fraction are likely neuronal precursors. The zone is particularly well-delineated by its moderate glutamine and taurine signals. Proceeding further anteriorly, the marginal zone gives way to the ciliary body. In the zebrafish this is an uncomplicated area comprised of the distal PCE and proximal NPCE bilayer. The signals of these epithelial sheets generally resemble the RPE, but some clear differences emerge, especially in glutathione, glutamine and taurine content. As the RPE approaches the peripheral retina its glutathione signals get slightly weaker, though they are still far elevated above any retinal cell. This signal is contiguous with the pigmented ciliary epithelium and the pigmented epithelium abutting the distal surface of the marginal zone. However, the NPCE emerges at the anterior edge of the marginal zone and

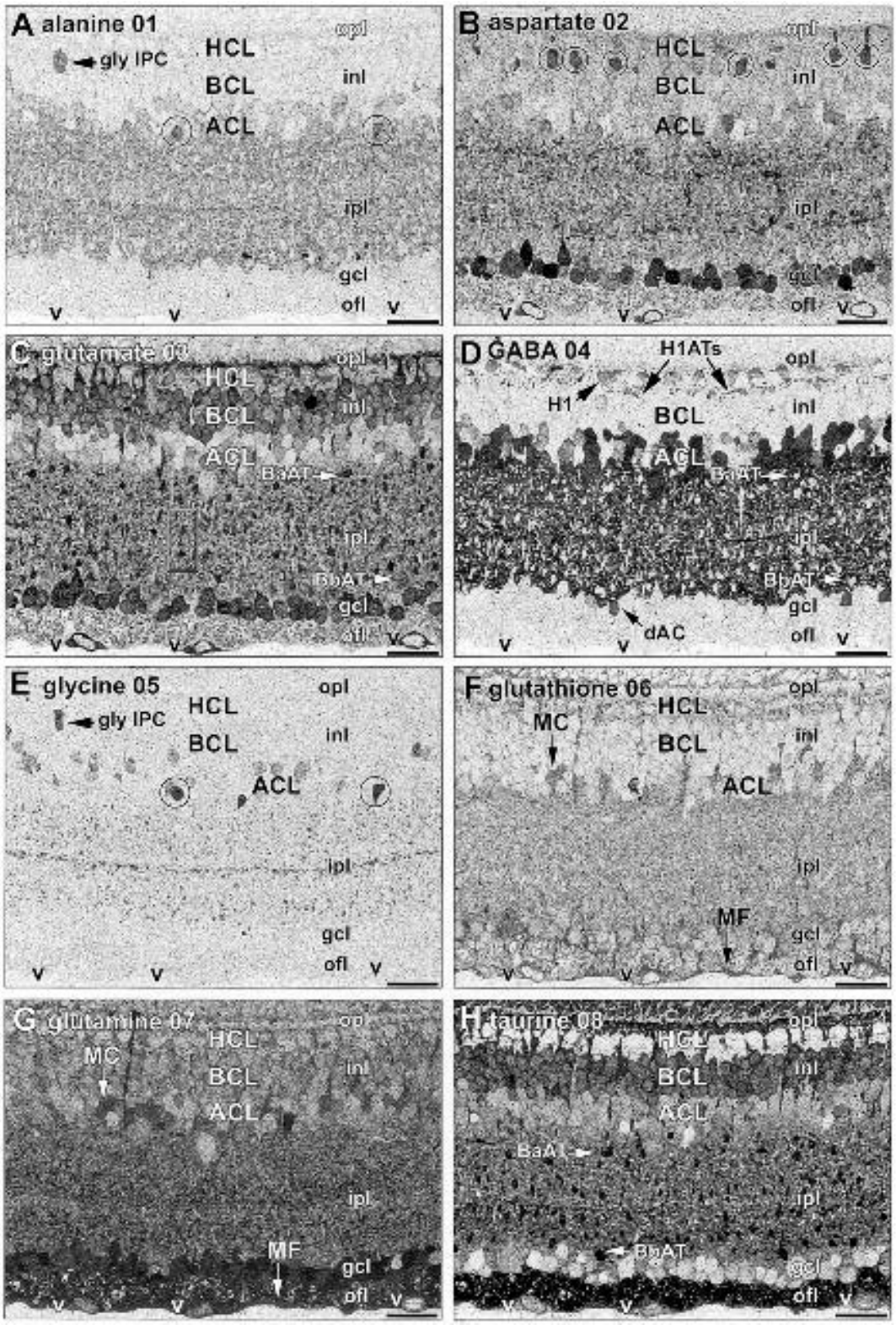

Fig. 31. Single channel, registered ADEGJQ$\tau\gamma$ signals in the light-adapted inner retina. A, alanine 01. B, aspartate 02. C, glutamate 03. D, glycine 04. E, glutathione 05. F, GABA 06. G, glutamine 07. H, taurine 08. Section thickness: 250 nm. Scale 20 μm.

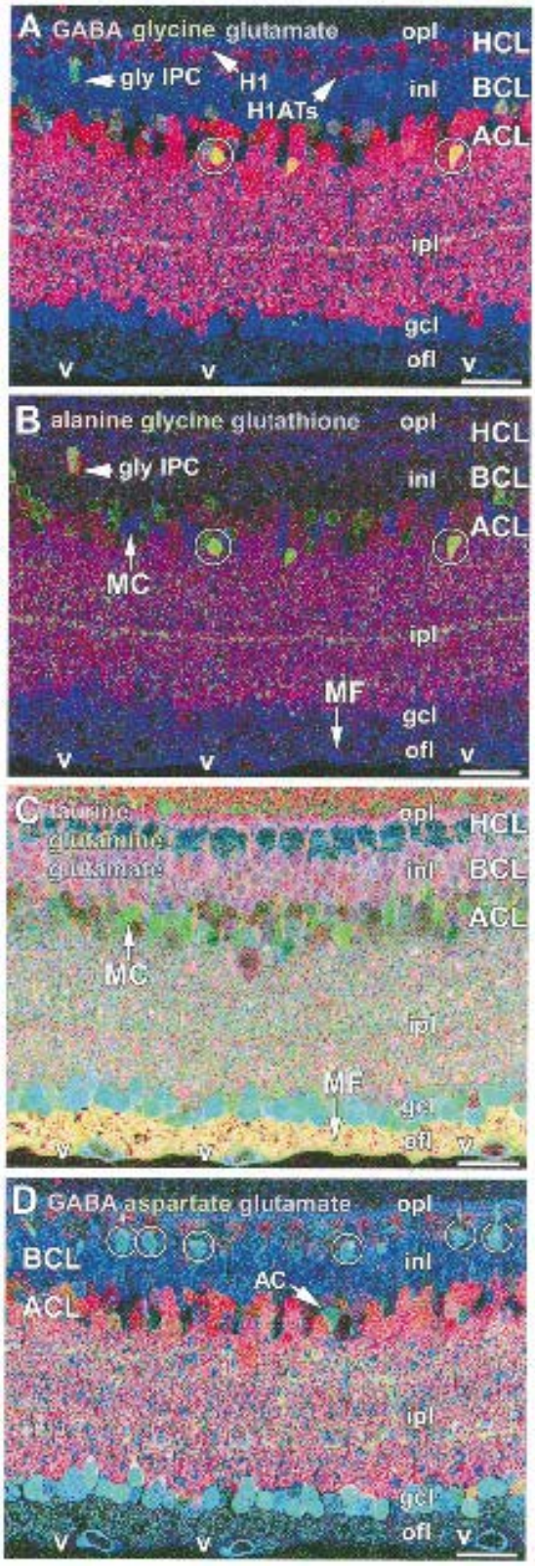

Fig. 32. Triplet mappings of the light-adapted inner retina. A, γGE → *rgb*. B, τQE → *rgb*. Scale 20 μm.

clearly has lower glutathione, higher glutamine and higher taurine signals (Fig. 35F, G and H). Since the PCE and NPCE are supposedly coupled by gap junctions at their interface (both apical surfaces point toward each other, unlike conventional transport monolayer epithelia), this signature difference must reflect either modulation of coupling or steady-state gradient differentials. The transition between the ciliary body and the iris epithelium becomes particularly evident in the glutamine signals (Fig. 35G). The choroid and the reflective tapetal layers of the eye have their own unique signatures, the most dramatic signal being the high glutamate enrichment (Fig. 35C). Taken together these signals allow the formation of a tissue-scale theme map (Fig. 36A) delimiting the cellular compartments of this complex area. The neural retina appear to possess its complete normal set of signatures (Fig. 36B, γGE → *rgb*; 36C, τQE → *rgb*), including the emergence of presumptive rod and cone horizontal cells at the retina:marginal zone interface (Fig. 36D, ADJ → *rgb*; 36E, τQD → *rgb*; 36F, γDτ → *rgb*). We define four sub-regions in and four epithelial types adjacent and anterior to the marginal zone.

Closer examination reveals substructure of the marginal zone and the young neurons apparently emerging from it (Fig. 37). In particular, the glutamate signals of the retina appear to fuse with or enter the distal half of the marginal zone, with diverse signal strengths evident within one cell of the marginal epithelium (Fig. 37C). The signatures of amacrine and ganglion cells (Fig. 38A, γGE → *rgb*) provide evidence that both cell populations develop distinctive, immature signatures within the marginal zone before being displaced into the neural retina proper and developing arbors. And perhaps more importantly, laminar position is already specified in the marginal zone. No cells with inappropriate laminar signatures appear in the the normal peripheral retina, even at the border with the marginal zone. Glutamate signals, combined with the glutathione (Fig. 37F), glutamine (Fig. 37G) and taurine signals (Fig. 37H), as well as τQE → *rgb* mapping (Fig. 38B) also suggest that most of the distal marginal zone cells apposed to the marginal epithelium are destined to be photoreceptors. The horizontal cell layer inserts deeply into the marginal zone where new rod horizontal cells also develop next to the photoreceptor precursors (Fig. 38C). The early maturation of ganglion cell-like signatures is particularly evident. In the proximal marginal zone, cells with strong glutamate signals (Fig. 37), but inappropriately low glutamine and high taurine and glutathione signals abut the true ganglion cell layer: these are likely immature ganglion cells. Within the ganglion cell layer, a few unequivocal ganglion cells show the same inappropriately high glutathione signals, but are also now developing the high glutamine contents of normal ganglion cells. The most peripheral of these still display

inappropriate taurine signals, but neighboring cells lack taurine. We term these *maturing* ganglion cells. It is also quite obvious that different morphological types of ganglion cells emerge within 50 μm of the marginal zone. Taken together with classification, a detailed map of the marginal zone (Fig. 39) suggests that it is completely stratified into at least five distinguishable cohorts. Marginal zone class 1 cells (MZ1Cs) are those abutting the marginal epithelium (with their distal faces) and lined up next to the photoreceptor layer. They appear to be the transitional cell type already specified as photoreceptors. Next to those cells are class 2a (MZ2aCs) cells from marginal zone 2: cells both abutting the marginal epithelium and forming the core of the marginal zone. Class 2b cells are sandwiched between class 2a cells and the retina, appearing to be zone within which near-mature inner nuclear layer molecular phenotypes of horizontal, bipolar, γ+ amacrine, and G+ amacrine cells are activated. A thin class 2a strand only 1–2 cells wide emerges from the proximal cluster of 2a cells and is contiguous with the emerging ganglion cell layer. The proximal cluster of marginal zone cells in contact with the marginal epithelium, class 3 cells (MZ3Cs), evinces molecular phenotypes subtly different from the other zones and more like the marginal and ciliary epithelia. Thus we suspect it is the precursor pool for those transport layers. Finally, a complex of cells emerges from the vitreal surface of the marginal zone and protrudes slightly past the retina into the vitreous and in front of the NPCE. It appears sealed from the rest of the marginal zone by an interposed block of tissue with Müller cell signatures. Though we refer to it as marginal zone 4 and its associated class 4 cells, it may have nothing to do with the marginal zone. The signatures in MZ4 are extremely complex and contain nondescript cells with signal patterns very similar to vascular cells (Fig. 38). In sum, we find the marginal zone pre-laminated and detect no evidence of radial migration after emergence of maturing cell types into the retina proper. Additionally, arborization does not ensue until the cells enter the retina and even then new arbors never spread back into the marginal zone.

Discussion

Some 24 neural and 19 non-neural molecular phenotypes can be detected in the zebrafish retina and associated tissues (summarized in Tables 1 and 2). The zebrafish is, in most respects, a classic cyprinid. The only major differences between the zebrafish and its carp relatives are: (1) the better mosaic organization of the retina, with no LS cones filling in spaces between mosaic elements; (2) more distinctive laminar markers in the inner plexiform layer, especially the G+ band at level 50; (3) more diverse cellular signatures. The cells of the adult zebrafish retina are unfortunately about 20–50% smaller than those of other adult cyprinids, rendering physiological and some structural analyses more difficult. Nevertheless, clear homologies with the various neuronal and glial cohorts of other cyprinids are easily made.

PHOTORECEPTOR COHORTS AND MOLECULAR PHENOTYPES

The zebrafish ppears to lack the red LS, green LS and red miniature LS cones of goldfish, rudd, roach, carp and koi. The double cone mosaic is more compact and orderly than other cyprinids, with little room for these additional cell types. This is consistent with comparisons of mosaic structure in other teleost families: bottom grazers and predominant vegetarians (*e.g.* carp) have loose mosaics with additional "fill-in" cones and clear water predators have crystalline mosaics with exceptional conformity ratios. The blue SS cones of zebrafish have been termed LS cones by previous workers and this was reasonable in the sense that they are the largest of the "single" cones. However, the blue cones of the zebrafish are not homologous to LS cones but rather to the SS cones of other cyprinids; they match in shape, mosaic position, general pigment content and molecular phenotype. Similarly UV cones of the zebrafish, elsewhere termed SS cones, are the homologues of cyprinid UV-sensitive MSS cones in general, and not SS cones. The mosaic is unlike the loose square mosaic of the goldfish and is a row mosaic with precise interdigitation of double cones due to the 1/ 2 cycle offset of neighboring rows.

It appears that cyprinids share the same pattern of photoreceptor signatures and the same, somewhat unusual adaptation dynamics. Light-adapted rods and cones maintain very low levels of intracellular glutamate which increase dramatically (3–6×) in rods and double cones, along with a decrease in both glutamine and taurine, upon dark-adaptation. The fact that both rods and cones respond in the same direction suggests that this metabolic change may have less to do with synaptic transmission than with some other regulatory process, such as changes in metabolic demands during sleep or in osmoregulation during the photomechanical responses. Since all photoreceptor signaling is glutamatergic, it is evident that cone synapses must be able to function and reload synaptic vesicles with a steady-state glutamate level of about 300 μM.

Connaughton *et al.* (1999) reported high glutamate levels in cones, apparently equivalent to bipolar and ganglion cells, but this was due to superposition saturation.

Both cones and rods contain high taurine signals. It is generally thought that the role of taurine, along with betaine and myo-inositol, is to act as part of a large pool of channel-permeant and transportable molecules for osmoregulatory adjustment in virtually all living systems (Moeckel *et al.*, 1997; Roberts, 2000; Schaffer

et al., 2000) and particularly in the retina (Morimura *et al.*, 1997). Taurine is the most abundant photoreceptor amino acid in light-adapted photoreceptors, ranging from 3–10 mM. Dark-adapted cones display up to a three-fold loss of taurine. The concomitant loss of glutamine is more explicable in terms of partial conversion to glutamate, though it is not simply stoichiometric: in LD cones, the actual drop in glutamine is about 500 μM while the increase in glutamate is some 4 mM. It is important to think of amino acid pools as open networks and the signals captured in any one state as reflective of steady states far from equilibrium. Simple additivity is unlikely to explain changes in most metabolic signatures. The general metabolic signature of zebrafish photoreceptors is similar to that of most vertebrates: a modest glutamate content and high taurine levels. The major differences with tetrapod and mammalian photoreceptors in particular are that the latter generally maintain low millimolar rather than micromolar glutamate, and show no adaptation dynamics.

HORIZONTAL CELL COHORTS AND MOLECULAR PHENOTYPES

Molecular phenotyping is particularly useful with inner retinal neurons, as it is one of the most incisive and general of tools for establishing homologies. The horizontal cells of the zebrafish retina are extremely small, with soma diameters of about 10 μm and population densities 2–2.5× those of other cyprinids. But it is clear that at least three distinctive populations are present with signatures similar to other cyprinids and non-mammalians. H1 horizontal cells are weakly $\gamma+$ E+ and $\tau-$, as are the presumed long-wave cone

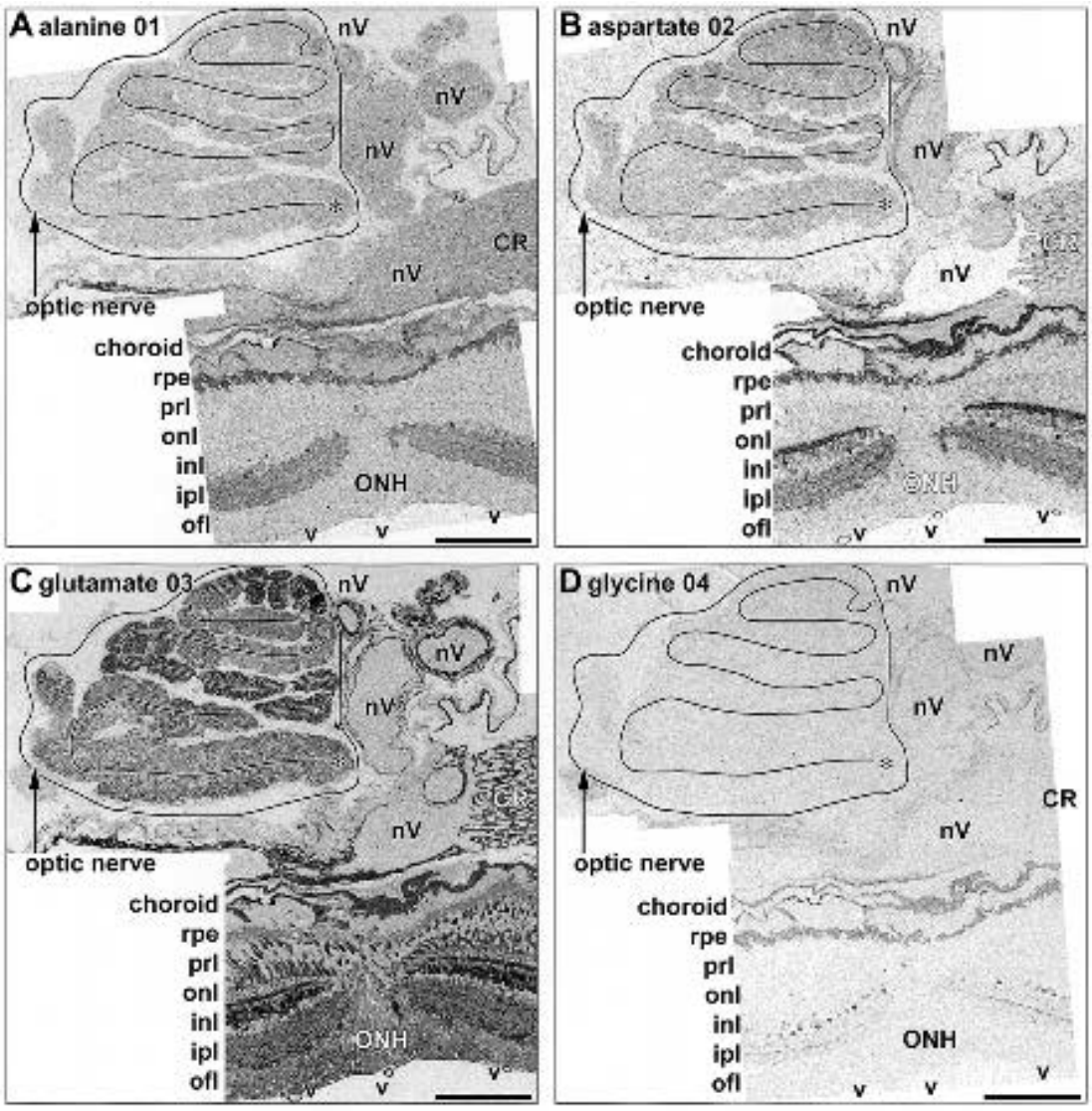

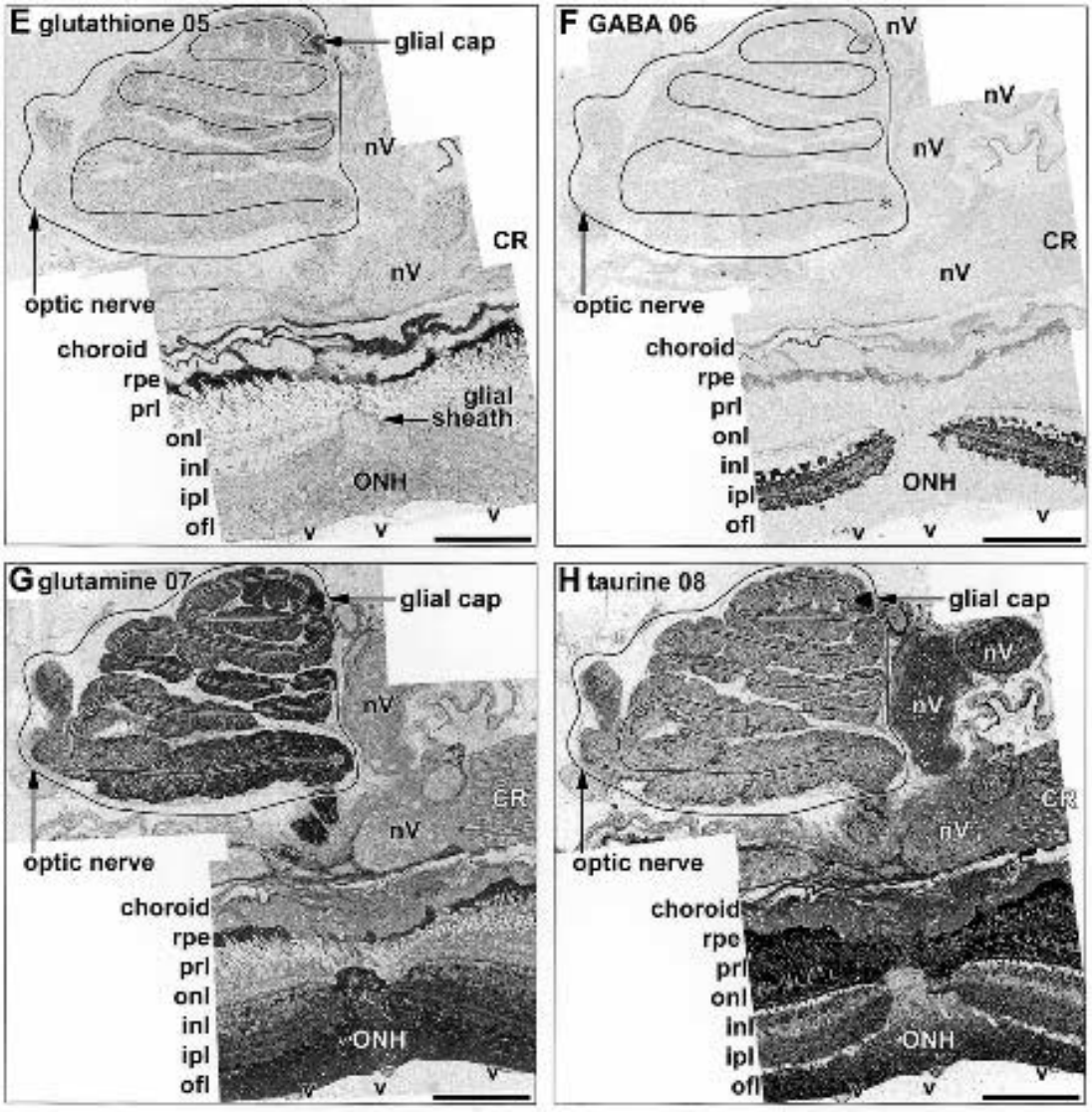

Fig. 33. A high-resolution library of the optic nerve head and folded optic nerve ribbon. A, alanine 01. B, aspartate 02. C, glutamate 03. D, glycine 04. E, glutathione 05. F, GABA 06. G, glutamine 07. H, taurine 08. Asterisk denotes the portion of the optic nerve ribbon (outlined) that arises from central retina and maps to increasingly peripheral loci (folded line) to end at the newest, most peripheral ganglion cell axons near the glial cap. Abbreviations: CR, choroidal rete; ofl, optic fiber later; ONH, optic nerve head; prl, photoreceptor layer; nV, vasculature of the optic nerve, Section thickness: 250 nm. Scale 100 μm.

horizontal cells of all non-mammalians (see review by Marc (1992)). Previous description of GABA signals in the zebrafish outer plexiform layer detected weak horizontal cell signals but did not resolve subtypes (Connaughton *et al.*, 1999). H1 horizontal cells are the only teleost horizontal cell type expressing a GABA transporter (Marc *et al.*, 1978; Marc, 1992; Verweij *et al.*, 1998; Watt *et al.*, 2000) or GAD (Lam *et al.*, 1979; Brandon, 1985; Marc, 1992). So we might expect zebrafish H1 horizontal cells to behave similarly. Color opponent horizontal cells in zebrafish and other teleost fishes lack significant GABA signals, though they do have the characteristic $\tau-$ signature of horizontal cells in general and maintain the same glutamate contents as light-adapted cones. Rod horizontal cells also lack any GABA signal, but have a characteristic D+E+ signal with millimolar glutamate content. The population sizes of H1, Hx and rod horizontal cells in the zebrafish retina suggest that the Hx population must be similar to that of the goldfish, which is known to harbor both H2 and H3 cone horizontal cells (*e.g.* Miyachi *et al.* (1999)). If the circuitry of zebrafishes matches that of

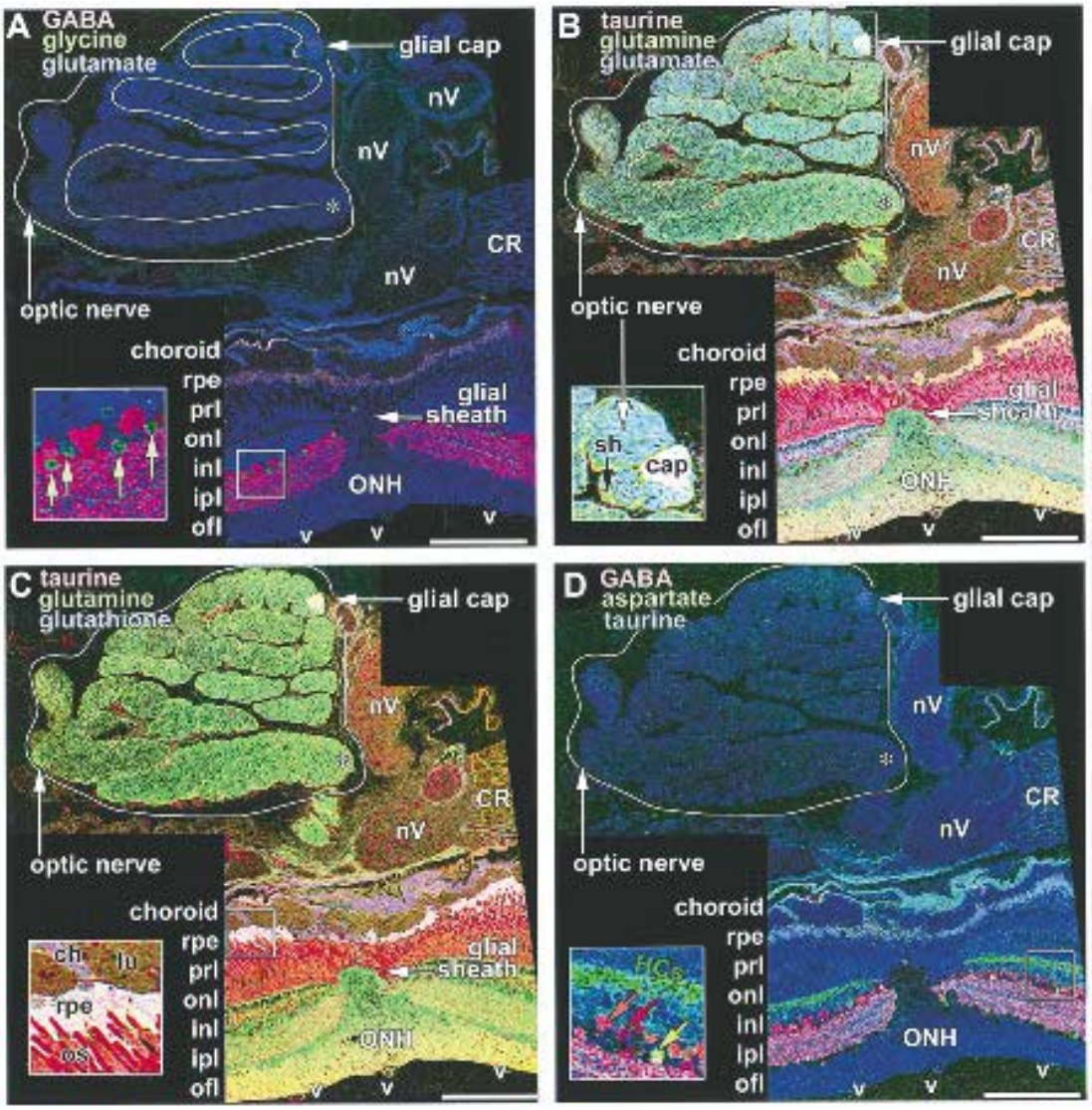

Fig. 34. Triplet mappings of the optic nerve head and folded optic nerve ribbon: A, γGE $\rightarrow$ *rgb*. The two inset boxes are 50 μm square and show the complete separation of $\gamma+$ and G+ amacrine cells. B, τQE $\rightarrow$ *rgb*. The two inset boxes are 50 μm square and show the separate signal patterns of the peripheral optic nerve glial cap (white, high τQE signal) and the normal nerve sheath glia (yellow, high τQ signal). C, τQJ $\rightarrow$ *rgb*. The two inset boxes are 50 μm square, showing the strong spectral, and hence metabolic, differentiation of rod outer segments (red), the RPE (white), choroidal endothelium (lavender), and the choriocapillaris vascular lumen (brown). D, γDτ $\rightarrow$ *rgb*. The two inset boxes are 50 μm square, showing the high D+ signal of the horizontal cell layer (green) and three aspartate-differentiated classes of amacrine cells (arrows). Scale 100 μm.

other cyprinids, both H2 and H3 horizontal cells should exist to service the green and blue cones respectively. The signatures of non-H1 horizontal cells are challenging, for they do not fit any conventional view of lateral inhibitory transmission. Marc *et al.* (1990, 1995) noted the elevated glutamate contents of rod horizontal cells and suggested that they may use glutamate rather than GABA to signal to their targets. Kamermans and his colleagues have argued that horizontal cell feedback to cones may not be exclusively chemical but rather an ephaptic signaling, perhaps involving current leaks through connexin-based hemijunctions in horizontal cell dendrites (Kamermans & Spekreijse, 1999; Kamermans *et al.*, 2001). That may solve the communication problem with cones at least, but it does not help us explain why cyprinid horizontal cells should have such distinct molecular signatures. And we do know that many horizontal cells form conventional chemical synapses with non-photoreceptor targets (Marc & Liu, 1984; Marshak & Dowling, 1987; Van Haesendonck

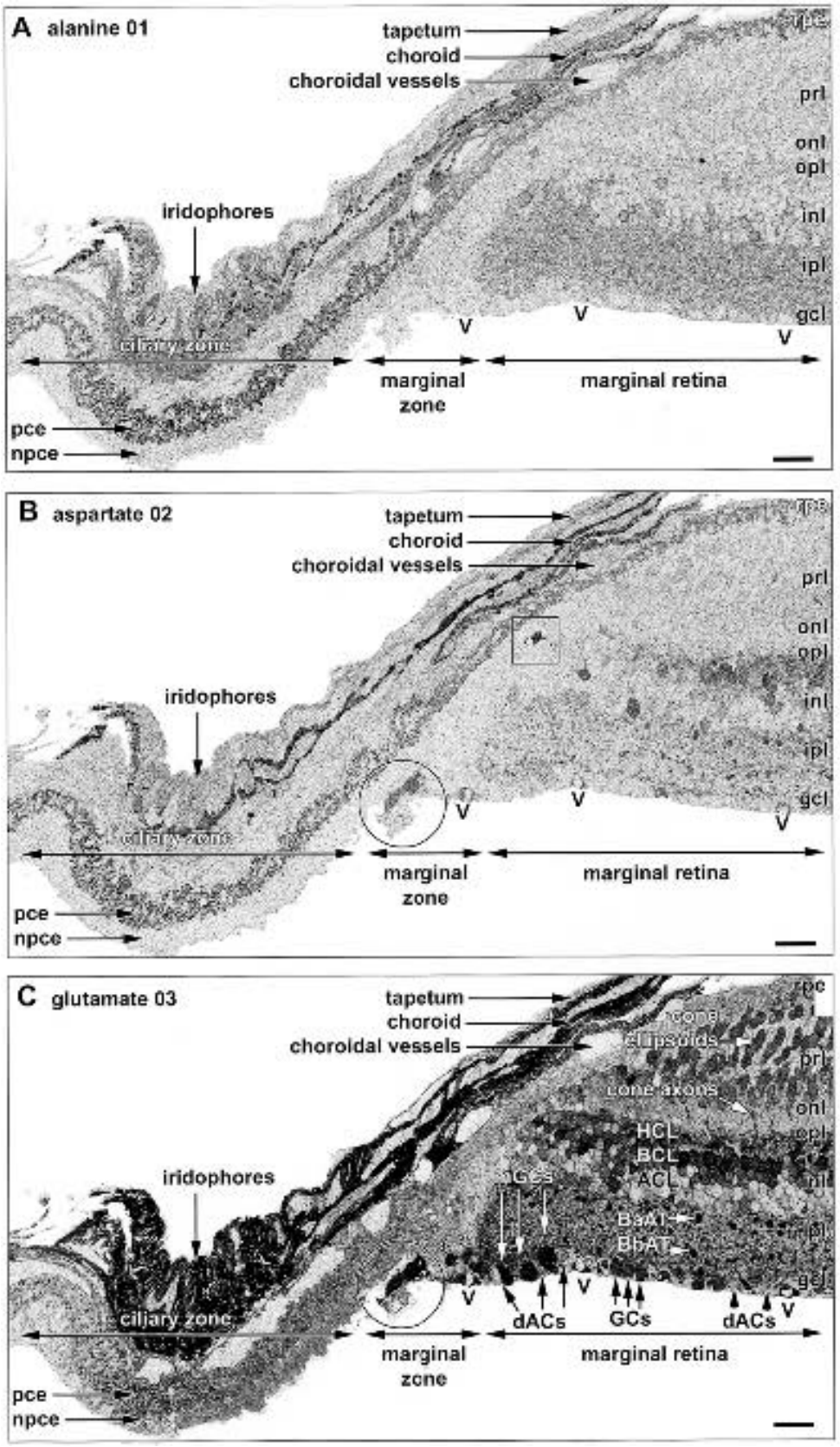
A alanine 01
tapetum
choroid
choroidal vessels
rpe
prl
onl
opl
inl
ipl
gcl
iridophores
ciliary zone
marginal zone
marginal retina
pce
npce
B aspartate 02
tapetum
choroid
choroidal vessels
rpe
prl
onl
opl
inl
ipl
gcl
iridophores
ciliary zone
marginal zone
marginal retina
pce
npce
C glutamate 03
tapetum
choroid
choroidal vessels
rpe
cone ellipsoids
prl
cone axons
onl
opl
HCL
BCL
ACL
inl
iridophores
GCs
BaA1
BhAT
ipl
gcl
ciliary zone
dACs
GCs
dACs
marginal zone
marginal retina
pce
npce

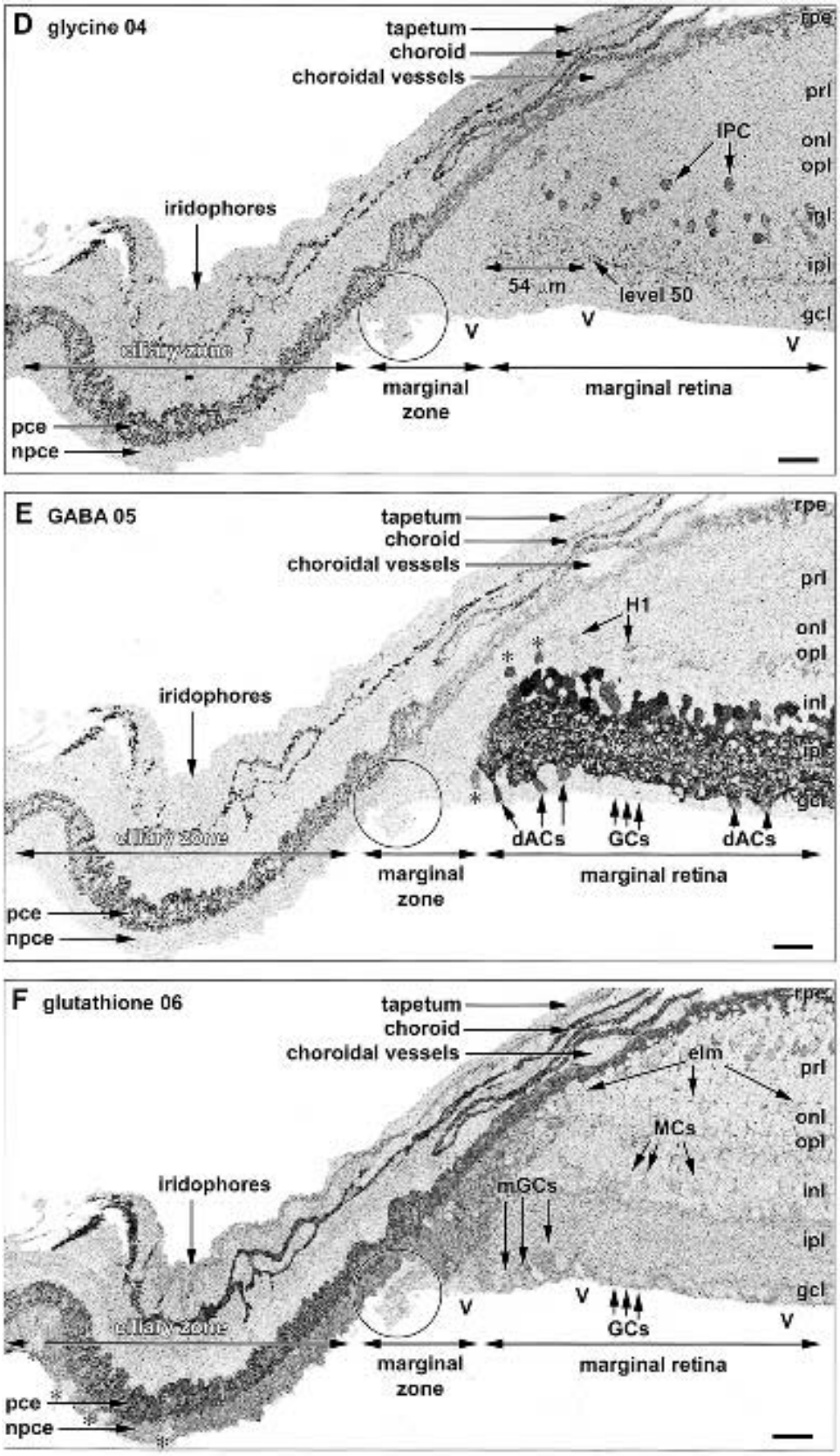
D glycine 04
tapetum
choroid
choroidal vessels
rpe
prl
IPC
onl
opl
iridophores
inl
ipl
54 µm
level 50
gcl
V
V
V
ciliary zone
marginal zone
marginal retina
pce
npce
E GABA 05
tapetum
choroid
choroidal vessels
rpe
prl
H1
onl
opl
iridophores
inl
ipl
gcl
dACs
GCs
dACs
ciliary zone
marginal zone
marginal retina
pce
npce
F glutathione 06
tapetum
choroid
choroidal vessels
rpe
elm
prl
MCs
onl
opl
iridophores
mGCs
inl
ipl
gcl
V
V
GCs
V
ciliary zone
marginal zone
marginal retina
pce
npce

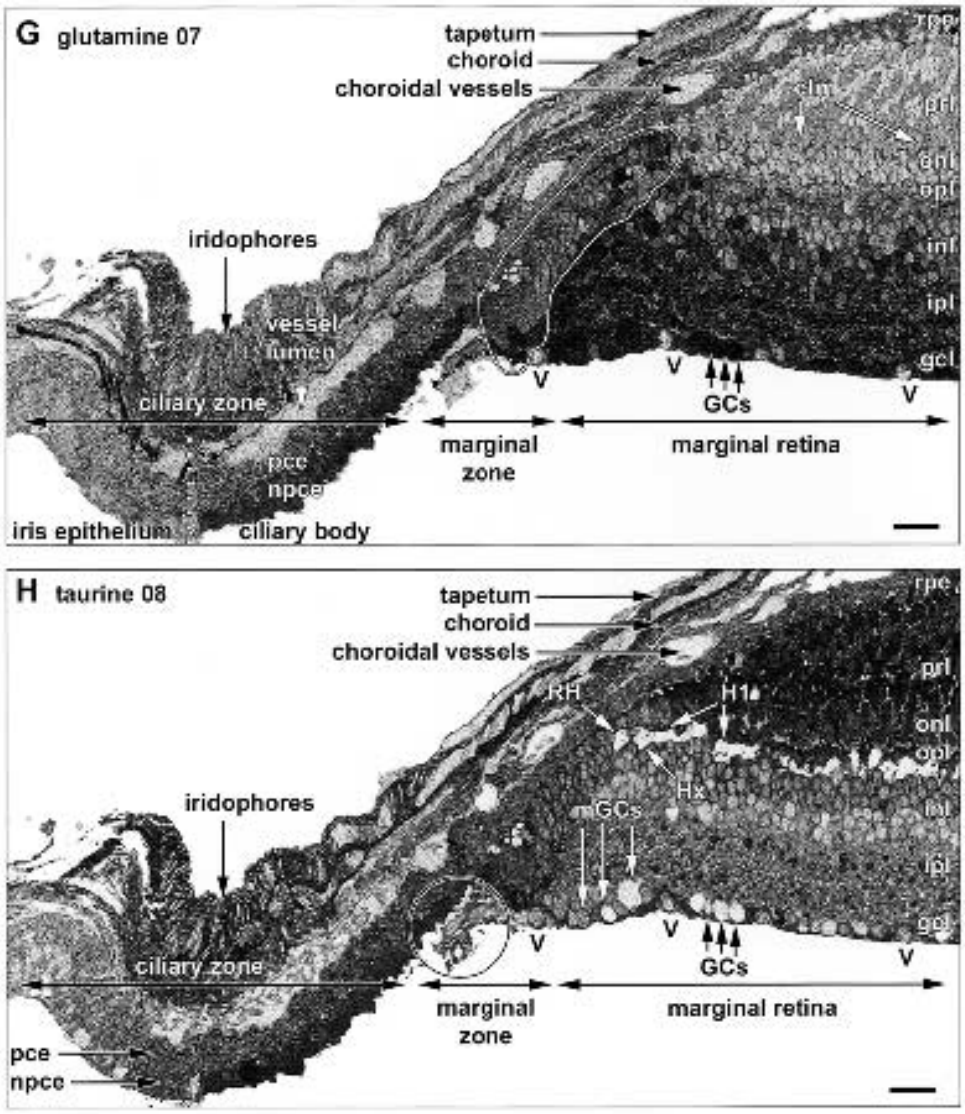

Fig. 35. A high-resolution library of the marginal retina, the marginal zone, and the ciliary zone. A, alanine 01. B, aspartate 02. Two unknown cell types display high D signals (circle), while a presumed maturing RH cell in the marginal zone is boxed. C, glutamate 03. Asterisks denote two presumed immature ganglion cells in the marginal zone. D, glycine 04. Two glycinergic interplexiform cells are marked (IPC). The characteristic level 50 glycinergic band approaches within 54 μm of the marginal zone. E, GABA 05. Asterisks denote presumed maturing conventional and displaced amacrine cells in the marginal zone. F, glutathione 06. Asterisks mark glutathione-deficient cells in the non-pigmented ciliary epithelium. G, glutamine 07. The distinctive, low glutamine marginal zone is outlined. There is a distinct molecular border (dotted) between the ciliary body and iris epithelium. H, taurine 08. Horizontal cells are clearly emerging from the marginal zone in their proper laminar position. Abbreviations: mGCs, maturing ganglion cells; npce, nonpigmented ciliary epithelium; pce, pigment ciliary epithelium; Section thickness: 250 nm. Scale 100 μm.

et al., 1993), so their signatures might still need to be coupled to their neurotransmitter function.

Another puzzling feature of teleost cone horizontal cells are their specialized axon terminal expansions, which are unbranched, nematode-shaped processes filled with microtubules (and occasional conventional synapses) that do not contact photoreceptors and course through the inner nuclear layer. The zebrafish does, in fact, have these processes but they are some 100-fold smaller in volume than those of the carp relatives and form a distinct layer just proximal to the horizontal cell layer proper. Whether they actually perform any network operations remains to be seen, and their only likely functions would seem to be lateral homotypic coupling with other horizontal cell axons or feedforward synapses onto bipolar cell proximal

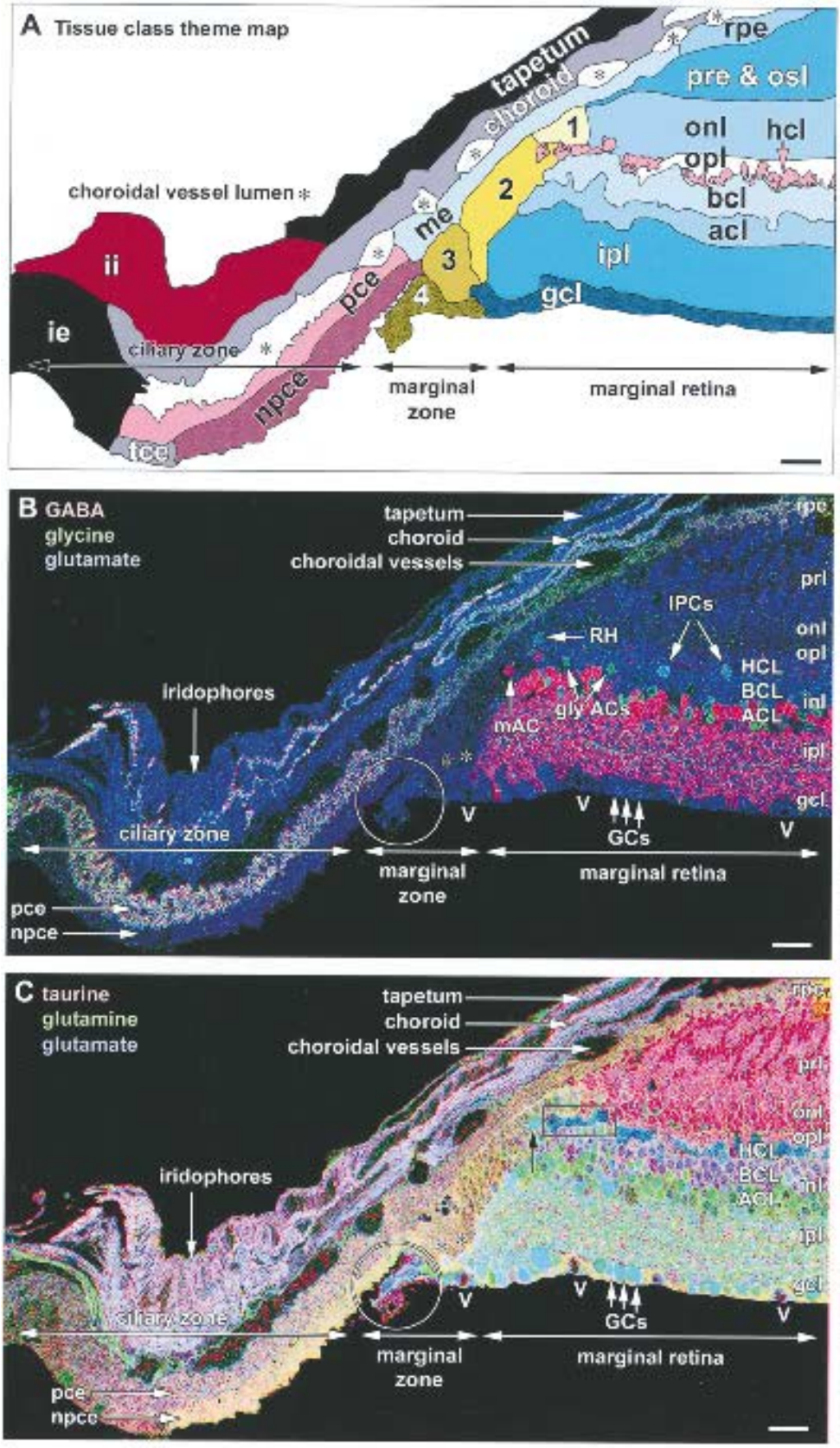
A Tissue class theme map
tapetum
choroid
rpe
pre & osl
onl
hcl
opl
bcl
acl
ipl
gcl
choroidal vessel lumen
ii
ie
me
pce
ciliary zone
npce
fce
1
2
3
4
marginal zone
marginal retina
B GABA
glycine
glutamate
tapetum
choroid
choroidal vessels
rpe
prl
IPCs
RH
onl
opl
HCL
BCL
ACL
inl
ipl
gcl
iridophores
mAC
gly ACs
ciliary zone
GCs
marginal zone
marginal retina
pce
npce
C taurine
glutamine
glutamate
tapetum
choroid
choroidal vessels
iridophores
ciliary zone
GCs
marginal zone
marginal retina
pce
npce

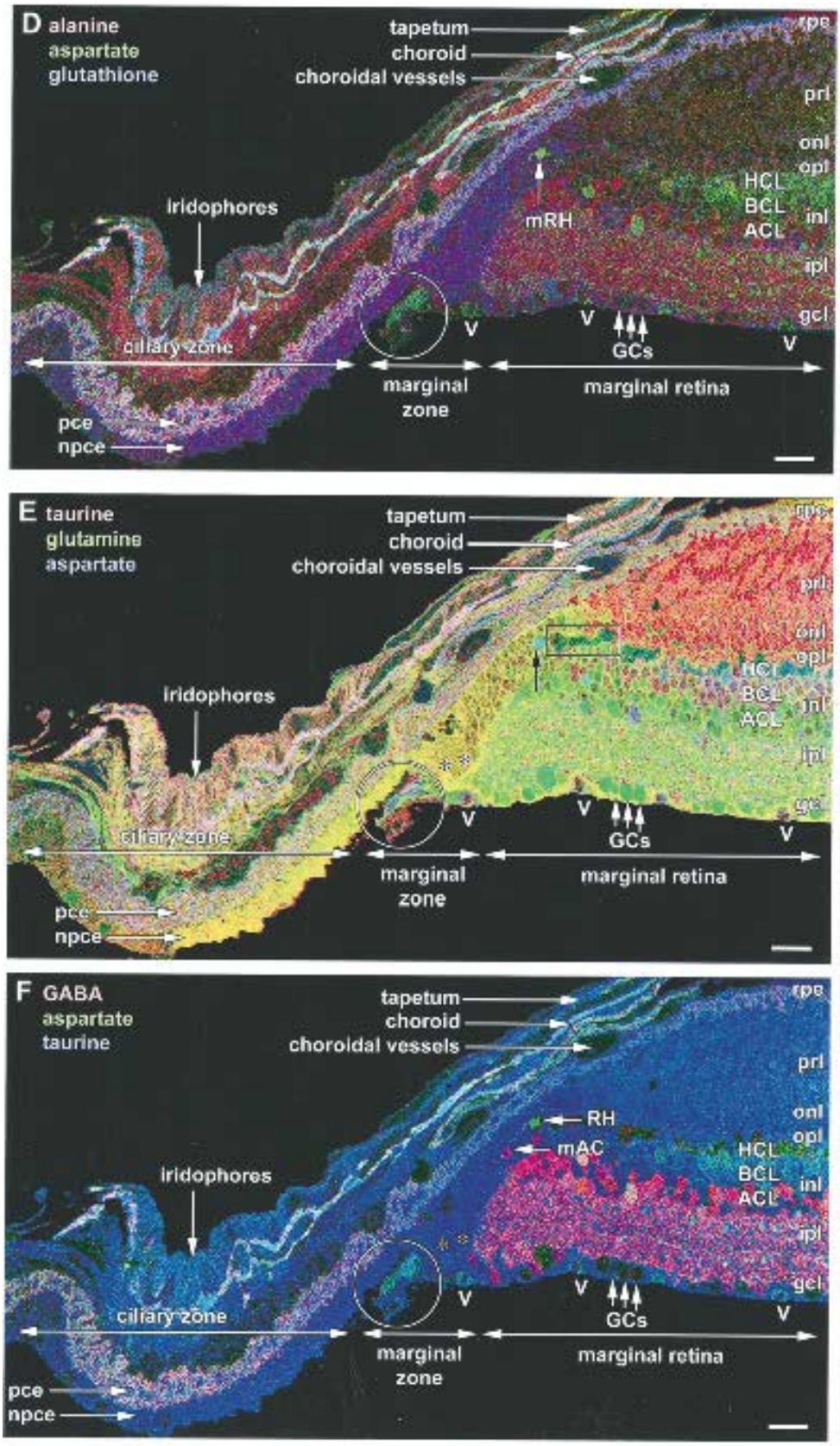
D alanine
aspartate
glutathione
tapetum
choroid
choroidal vessels
rpe
prl
onl
opl
HCL
BCL
ACL
inl
ipl
gcl
mRH
iridophores
V
V
GCs
V
ciliary zone
marginal zone
marginal retina
pce
npce
E taurine
glutamine
aspartate
tapetum
choroid
choroidal vessels
iridophores
ciliary zone
marginal zone
marginal retina
pce
npce
F GABA
aspartate
taurine
tapetum
choroid
choroidal vessels
RH
mAC
iridophores
ciliary zone
marginal zone
marginal retina
pce
npce

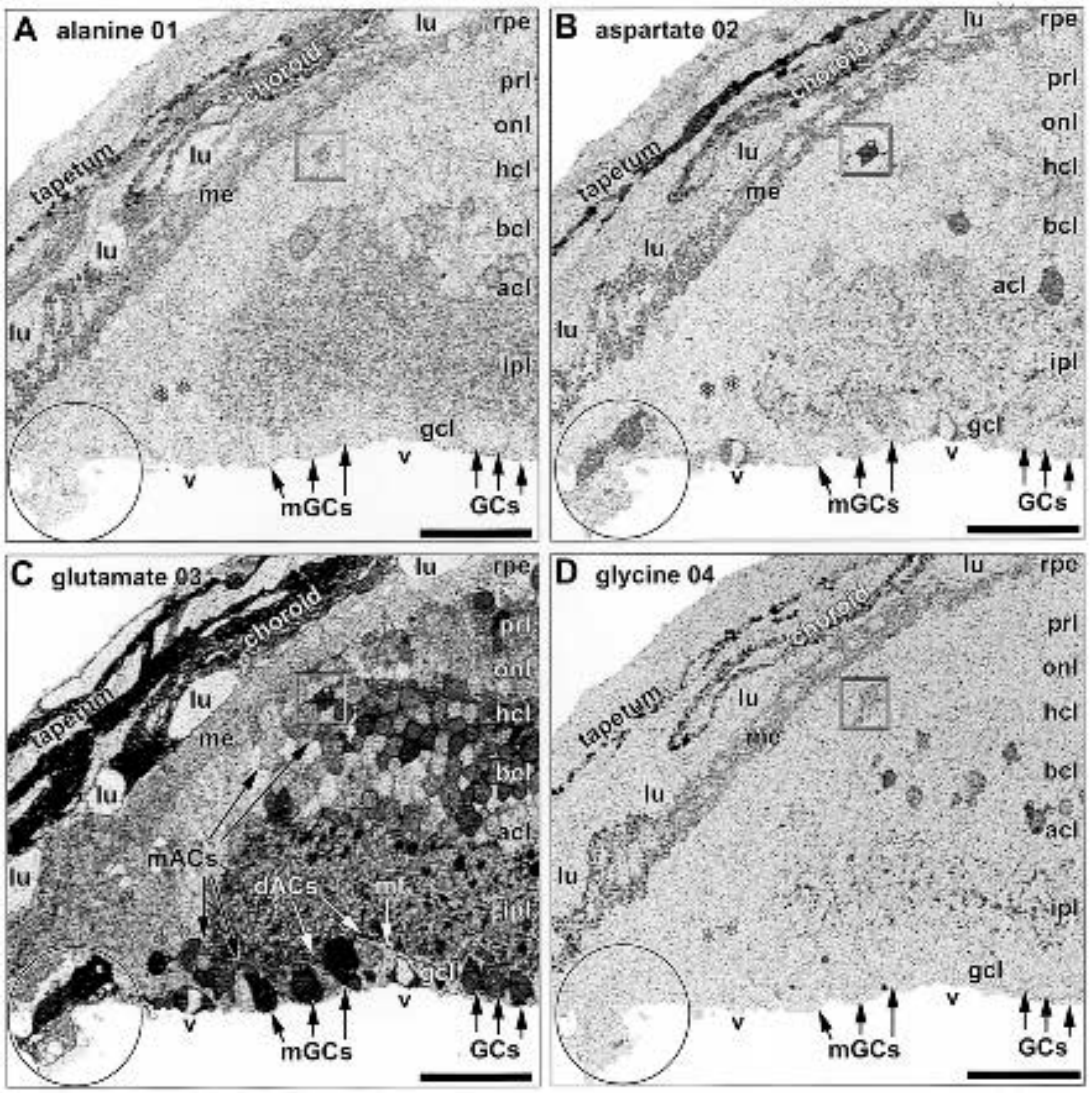

dendrites. Both H1 and Hx horizontal cells have these terminals, but zebrafish D+ horizontal cells seem to lack them. Since they are most proximal, appear to lack axon terminal expansions and have glutamate signals similar to goldfish rod horizontal cells, the D+ horizontal cells are likely to be zebrafish rod horizontal cells, and we have so treated them throughout. Teleost horizontal cells are not strictly homologous to tetrapod horizontal cells, as the latter taxa lack rod horizontal cells and instead express axons from their long-wave driven horizontal cells that contact mixed rods and cones. In non-mammalians, these are still $\gamma+$ horizontal cells. It is quite intriguing that juvenile goldfish horizontal cells are some 20-fold smaller in volume than adult horizontal cells (Raymond, 1990): they are initially like zebrafish and then become cyprinine. Mammalian horizontal cells display a complex and non-homologous pattern. Most, but not all mammals express cone horizontal cells that lack axons, but some of these to express low levels of GABA (such as central rabbit type A horizontal cells). All mammals express a cone horizontal cell with a specialized axon terminal expansion that

Fig. 36. (Previous two pages) Tissue theme map and triplet mappings of the marginal retina, the marginal zone, and the ciliary zone. A, Theme map. Four signature zones of the marginal zone are marked (1,2,3,4). B, γGE $\rightarrow$ *rgb*. C, τQE $\rightarrow$ *rgb*. The inset boxes outlines the emergent horizontal cells and the arrow denotes the RH cell. D, ADJ, the presumed emerging RH cell is indicated. E, τQD $\rightarrow$ *rgb*. F, γDτ $\rightarrow$ *rgb*. Scale 100 μm.

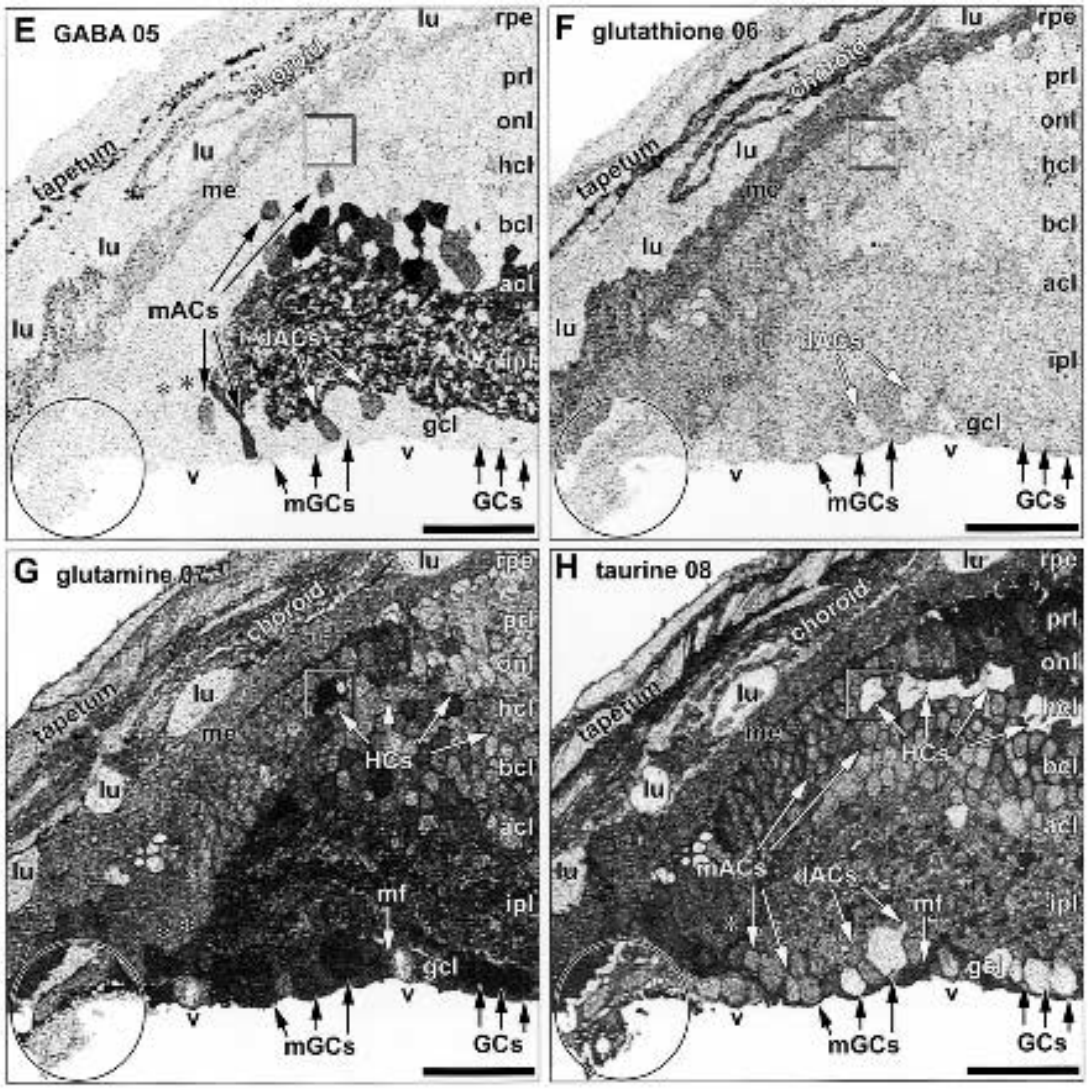

Fig. 37. A high-resolution library of the marginal zone. A, alanine 01. The maturing RH cells is boxed, the marginal zone 4 D+ cells circled and the immature ganglion cells in the marginal zone are marked with asterisks. B, aspartate 02. C, glutamate 03. D, glycine 04. E, GABA 05. F, glutathione 06. Note that the maturing ganglion cells (mGCs) have unusually high glutathione signals. G, glutamine 07. H, taurine 08. Section thickness: 250 nm. Scale 50 μm.

receives input from rods, but with few exceptions, these do not express significant GABA content. The neurochemistry of horizontal cells, after all these years, remains a puzzle.

BIPOLAR CELL CLASSES AND MOLECULAR PHENOTYPES

The bipolar cell populations of cyprinids are complex and divided into mixed rod-cone bipolar cells and pure cone bipolar cells (Stell, 1965, 1967; Scholes & Morris, 1973; Scholes, 1975; Ishida *et al.*, 1980b; Sherry & Yazulla, 1992). This complexity, however, provides a strong basis for testing homology and the zebrafish proves to be virtually identical to all other cyprinids. The rod-cone bipolar cells have been long known to be of two groups, ON-center and OFF-center, further segregated by details of photoreceptor contact patterns into 5. The zebrafish retina expresses generic cyprinid features of distinctive terminal patterning and Eτ bipolar cell signatures. Numerous subtypes were reported by Connaughton *et al.* (1999) based on qualitative examination of glutamate immunoreactivity. There are clearly at least two kinds of Ba terminals as in the goldfish retina. In goldfishes, Ba2 bipolar cells are also distinctively labeled by [^{3}H] serotonin uptake (Marc *et al.*, 1988b) and were proposed to be heterologously coupled to S1 GABAergic/ serotoninergic amacrine cells. While

Table 1. Neuronal cell types, classes and signatures in the zebrafish retina.

Cell code	*Cell type*	*Molecular phenotypes*	*Natural classes*	*Primary signature*	*Primary transmitter class*
Retina		**≈25**	**≈114**		
1.x.x.x	**Vertical channels**	**≈11**	**≈38**	**E**	**E**
1.1.*x*.*x*	*Photoreceptors*	4	5	τE	E
1.1.1.x	Rod photoreceptors	1	1	τE	E
1.1.1.1	Rods	Rod	1	τE	E
1.1.2.x	Cone photoreceptors	3	4	τE	E
1.1.2.1	LD cones	LD/ SD	1	τE	E
1.1.2.2	SD cones	LD/ SD	1	τE	E
1.1.2.3	SS cones	SS	1	τE	E
1.1.2.4	MSS Cones	MSS	1	τE	E
1.2.x.x	*Bipolar cells*	6	18	τE	E
1.2.x.x	γ+BC	BC1	1	τEγ	γ ?
1.2.1.x	Mixed rod-cone BCs	3	5	τED	E
1.2.1.1	Bb1 BC	BC5	1	τED	E
1.2.1.2	Bb2 BC	BC5	1	τED	E
1.2.1.3	Bb3 BC	BC6	1	τED	E
1.2.1.4	Ba1 BC	BC2	1	τED	E
1.2.1.5	Ba2 BC	BC2	1	τED	E
1.2.3.x	Cone BCs	2	≈12	τE, τEQ	E
1.2.3.x	C BC	BC3,4	≈12	τE, τEQ	E
1.3.*x*.*x*	*Ganglion cells*	GC	≈15	EQ	E
2.x.x.x	**Lateral channels**	**≈14**	**≈76**	**mixed**	**γ, G, DA**
2.1.*x*.*x*	*Horizontal cells*	3	4	*mixed*	γ ?
2.1.1.x	Cone horizontal cells	2	3	mixed	γ ?
2.1.1.1	H1 cone HCs	H1	1	γ	γ ?
2.1.1.2	H2 cone HCs	Hx	1	τ−	?
2.1.1.3	H3 cone HCs	Hx	1	τ−	?
2.1.2.1	Rod HCs	RH	1	DE	?
2.2.*x*.*x*	*Amacrine cells*	11	≈72	*mixed*	γ, G, DA
2.2.1.x	γ+Amacrine cells	7	?	γ	γ
2.2.1.1	γAC1	γAC1	30%	γτQ	γ
2.2.1.2	γAC2	γAC2	6%	γτEQ	γ
2.2.1.3	γAC3	γAC3	30%	γEQ	γ
2.2.1.4	γAC4	γAC4	14%	γQ	γ
2.2.1.5	γAC5	γAC5	6%	Low γ	γ
2.2.1.6	γAC6	γAC6	10%	γEDQ	γ
2.2.1.7	γAC7	γAC7	4%	High γ	γ
2.2.2.x	G+ Amacrine cells	4	?	G	G
2.2.2.1	GAC1	GAC1 (3)	95%	G	G
2.2.2.2	GAC2	GAC2	5%	QG	G
2.3.*x*.*x*	*Interplexiform cells*		2		G
2.3.1.x	γ+Interplexiform cells		?	?	γ
2.3.2.x	G+ Interplexiform cells		1		G
2.3.1.1	G+ IPCs	GAC1	1	G	G
2.3.3.x	DA+ interplexiform cells		1		DA
2.3.3.1	DA IPCs	DA IPC	1	γ−G-DA	DA

serotonin mapping has not yet been achieved, it would be likely that the zebrafish would express a similar pattern. We also provide evidence that the bipolar cell signature class BC6 corresponds to the Bb3 bipolar cell, a cell that contacts rods and both red and green cones in the goldfish and has a wide dendritic arbor (Ishida *et al.*, 1980a). The remaining BC5 superclass is large enough to encompass at least two more classes and it is likely that it contains both Bb1 and Bb2 bipolar cells. The cone bipolar cell population is complex and likely contains some 12 classes in goldfishes. We have not been able to sort specific classes, but the pattern of cone bipolar cell terminal labeling in the inner plexiform layer is, in fact, indistinguishable from that in the goldfish. Given the same spectral classes of cones and horizontal cells in carps and zebrafishes, we find no evidence

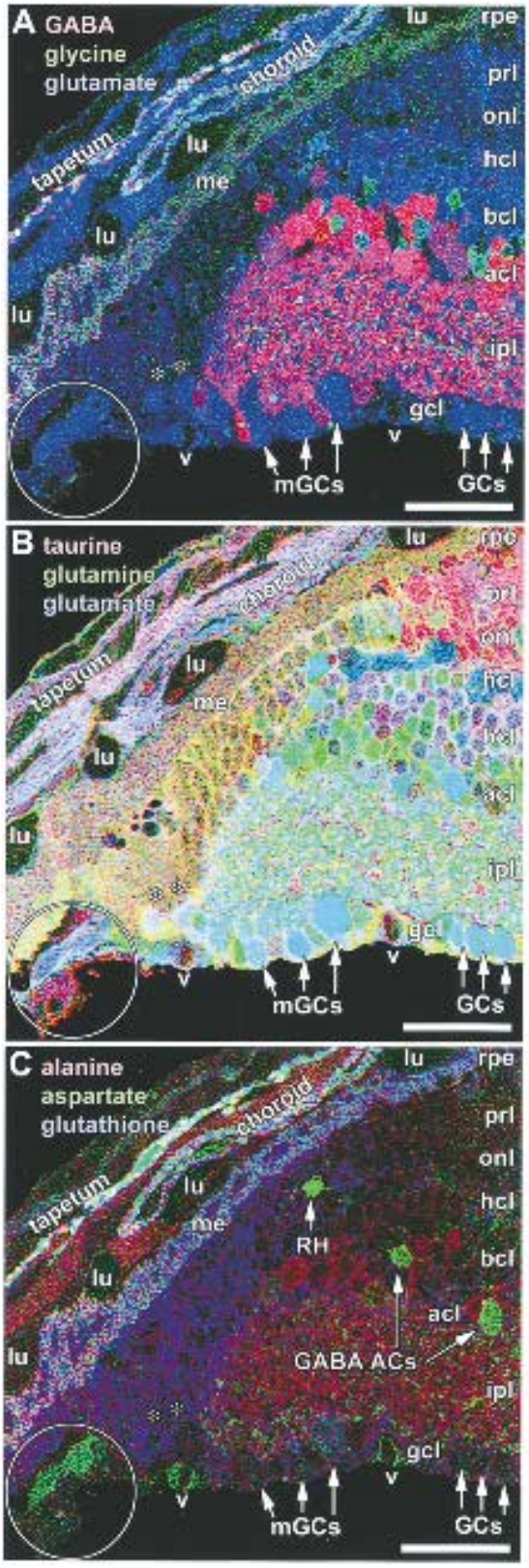

that the bipolar cell population of the zebrafish is in any way less complex. The molecular phenotype classes of bipolar cells are better differentiated in zebrafish than in carps, a phenomenon for which we have no good explanation. Class BC1 bipolar cell signatures in zebrafish are a strong departure from all other cyprinids examined so far in their weak E and modest γ signals. But for their high τ signal, one could mistake their phenotype for H1 horizontal cells. Other non-mammalians display $\gamma+$ bipolar cells (Yang & Yazulla, 1988); this is an *apparent* departure from other cyprinids. There is no rule that precludes a bipolar cell from using an inhibitory neurotransmitter, but we do know that such phenomena in the mammalian retina can be due to heterocellular coupling. The ON-center cone bipolar cells of mammals are coupled to glycinergic amacrine cells, and a signal leak is inevitable. The problem with this analogy is simply that mammalian ON-center bipolar cells have a perfectly good Eτ glutamatergic signature similar to all vertebrate bipolar cell types, including the zebrafish, but class BC1 cells in the zebrafish *do not*. Their signal more closely resembles a weak $\gamma+$ GABAergic cell. It is also likely that they represent a single natural class, as the spacing of their somas has a conformity ratio >3.

AMACRINE CELL COHORTS AND MOLECULAR PHENOTYPES

The amacrine cells of the zebrafish retina generally resemble those of the carps: separate $\gamma+$ or G+ populations, with the $\gamma+$ cells dominating the inner plexiform layer. In fact, over 90% of the neuronal space in the zebrafish inner plexiform layer is $\gamma+$, just as in goldfish. Previous reports of GABA banding in fish retinas are actually anoxia-induced and technical artefacts. The patterning of $\gamma+$ and G+ signals in the zebrafish inner plexiform layer would be indistinguishable from other cyprinids but for the distinctive band at L 50, first described by Connaughton *et al.* (1999). Since few other teleosts have yet been surveyed comprehensively, it is not difficult to tell whether this is apomorphic for the zebrafish. That aside, the sparseness of G+ terminals in the inner plexiform layer, the presence of glycinergic interplexiform cell, and the uniformity of GABA signals is strongly homologous for cyprinids in general. Breaking down the amacrine cell populations will be daunting and there is, in fact, only one quantitative assessment of amacrine cell diversity: the Golgi study of Wagner and Wagner (1988). In that work the

Fig. 38. Triplet mappings of marginal zone. A, γGE $\rightarrow$ *rgb*. B, τQE $\rightarrow$ *rgb*. C, ADJ, the presumed emerging RH cell is indicated. Scale 50 μm.

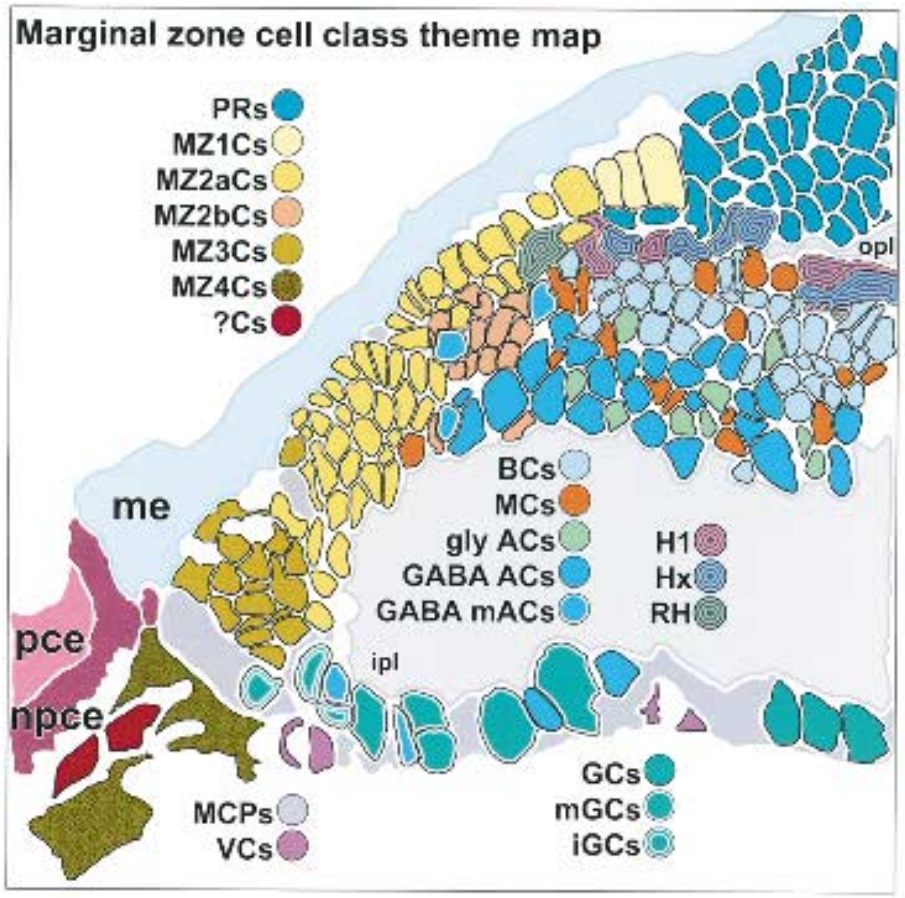

Fig. 39. A formal theme map of the marginal zone. Each cell type is coded by class membership based on isodata clustering and histogram deconvolution. Abbreviations: iGCs, immature ganglion cells; MCPs, Müller cell processes; mGCs, maturing ganglion cells; GABA mACs, maturing GABA amacrine cells; MZ1Cs, marginal zone 1 cells; MZ2aCs, marginal zone 2a cells; MZ2bCs, marginal zone 2b cells; MZ3Cs, marginal zone 3 cells; MZ4Cs, marginal zone 4 cells, PRs, photoreceptors; ?Cs, unknown cells associated with MZ4; VCs, vascular cells.

authors concluded that there were ≈70 distinct classes of amacrine cells. Given that the zebrafish retina contains some 30,000 amacrine cells/ mm^2, that would limit the density of amacrine cell classes to an average of ≈400/ mm^2 if all were equally frequent. Of course that is not likely to be the case. Goldfish displaced amacrine cells are $\gamma+$ cholinergic starburst homologues and have a density of around 1600/ mm^2 while glycinergic and dopaminergic interplexiform cells densities in the range 40–100/ mm^2. From the atlas data provided here, zebrafish displaced amacrine cells (structurally and metabolically identical to those in goldfish) have a density of ≈2500/ mm^2 and glycinergic interplexiform cells are between 75–100/ mm^2. Thus the zebrafish amacrine cells could easily comprise 70 classes, although it is clear that the zebrafish retina is more compact, with higher cell densities of all types: a logical compensation for a small eye requiring high sampling densities to track its small prey.

The strong metabolic differentiation of the zebrafish retina and improved methods permit finer discrimination of molecular phenotypes than obtained previously for goldfish and koi. Thus we would be hesitant to say that the zebrafish is qualitatively different in this regard, since signature discrimination is explicitly quantitative. Nevertheless, the variations in E, D, Q and τ signals in $\gamma+$ amacrine cells permit a strong segregation into groups that are almost certainly superclasses.

It is difficult to make direct comparisons with mammalian retinas. At least the starburst amacrine cell $\gamma+$ cholinergic cohorts are similar, but the cholinergic system in goldfish is far more complex with five cell classes: two amacrine cell classes forming each cholinergic band (radiate and starburst amacrine cells) and a bistratified cholinergic cell (Marc *et al.*, 1993). Mammalian retinas lack true serotoninergic amacrine cells and the serotonin-accumulating $\gamma+$ rod amacrine cell of the mammalian retina (Sandell & Masland, 1989;

Table 2. Non-neuronal cell types and signatures.

Tissue and cell type	*Signature*
Tapetum	
Iridophores	E
Choroid	
Pigmented epithelium	DJE
Vascular endothelium	τE
Capillary endothelium	τE
Choroidal rete	τE
RPE	
RPE	QE
Retina	
Müller cells	QJ
Astrocytes	τE
Vascular endothelium	τDE
Ciliary Zone	
PCE	QτJ
NPCE	Qτ
Transitional epithelium	EJ
Iris epithelium	Low Qτ
Marginal Zone	EJQτ mixtures
MZ1Cs	Mixtures
MZ2aCs	Mixtures
MZ2bCs	Mixtures
MZ3Cs	Mixtures
MZ4Cs	Mixtures
MZ epithelium	JτQ

Sandell *et al.*, 1989; Massey *et al.*, 1992) has no tetrapod homologue. Mammalian glycinergic rod amacrine cells (AII) are also absent from non-mammalian retinas as none of them have a pure rod bipolar cell pathway. Considering that the best amacrine cell estimates for the rabbit retina are $\approx$27 (MacNeil *et al.*, 1999), it is fair to say mammalian retinas are highly simplified; that the retinas of visual non-mammalians are highly advanced and specialized. To the extent that the zebrafish is chosen as a model for studying *vision*, one would have to accept this complexity as a cost of doing business, running the risk that some features of visual encoding, development and plasticity gleaned from the zebrafish may not be easily generalized.

GANGLION CELL COHORTS AND MOLECULAR PHENOTYPES

The signatures of the zebrafish ganglion cell layer are identical to those of other cyprinds, displaying only two intrinsic neurons: EQ ganglion cells and $\gamma+$ displaced amacrine cells. On occasion, some pyriform amacrine cells have misplaced somas (Marc *et al.*, 1993) and are rare intrusions. The only strong estimate of ganglion cell diversity in cyprinid retinas comes from Hitchcock and Easter (1986), and one can estimate $\approx$15 classes from their data. This roughly matches the diversity of bipolar cells in cyprinids and would suggest that each ganglion cell circuit requires an average of 4 unique amacrine cell classes. This is a greater complexity than any published model for receptive field organization. There is no reason to believe that the zebrafish retina is any simpler, as it seems to have the full complement of all other cyprinid neurons.

GLIAL CELL MOLECULAR PHENOTYPES

The Müller cells of the zebrafish retina have signatures similar to other vertebrates, primarily characterized by elevated glutamine and depressed glutamate contents. This is consistent with the role of Müller cell glutamine synthetase in converting transported glutamate to glutamine with high efficiency (Pow & Robinson, 1994; Pow & Crook, 1996). The zebrafish appears unexceptional in this regard. Mammals also express GAT3 GABA transporters (Johnson *et al.*, 1996), but most bony non-mammalians and all teleosts do not have any glial GABA transport (Marc, 1992). Most vertebrates also display extremely high taurine contents in their Müller cells, yielding the distinctive τQ signatures of goldfish and koi (Marc *et al.*, 1995), avians (Kalloniatis & Fletcher, 1993; Kalloniatis *et al.*, 1994; Kalloniatis & Napper, 1996), rat (Fletcher & Kalloniatis, 1996), cat (Marc *et al.*, 1998b), rabbit (Marc, 1999a), and macaque (Kalloniatis *et al.*, 1996). However, mouse Müller cells also show a modest taurine signal (Marc, unpublished). This may be due to their small size, but this is speculation.

Although not fully analyzed here, zebrafish obviously have further glial cell types in their optic fiber layers, optic nerve head and its surrounding sheath. The high τ signal of the optic fiber layer is likely an astrocyte signal, but the Müller cells clearly traverse this zone and form a lower τ band at the vitreal margin. Thus it appears that Müller cells are the sole determinants of the inner limiting membrane in zebrafish, and that there is no astrocyte involvement, as there often appears to be in mammals.

EPITHELIAL/ ENDOTHELIAL COHORTS AND MOLECULAR PHENOTYPES

The choroid, tapetum, RPE, ciliary zone and various vascular elements comprise a large mixture of non-neural cells essential to ocular function. One feature of virtually all of these cells is their relatively high glutamate signals. Some of them, such as the NPCE epithelium, choroidal pigmented epithelium, and especially the radial vitreal vessel endothelium, contain glutamate signals that rival those of neurons. Many somatic transport epithelia and immune cells have millimolar glutamate contents. It appears that the basic glutamate content of such cells is archetypal; that the high glutamate contents of neurons are derivative and not novel. The high glutamate and taurine contents of the

zebrafish vascular endothelia are common to the retinal vessels of all vertebrates so far examined. The fenestrated endothelia of the choroid in all vertebrates also have much lower standing amino acids contents, so there is a molecular phenotype variation that tracks endothelial type. The signatures of the zebrafish PCE and NPCE almost exactly mirror those of the mammalian retina, with significant basal levels of glutamate, glutamine, and taurine (Marc, unpublished signatures of the ciliary body). And the RPE is similar as well, except for the extremely high glutathione and glutamine levels of the zebrafish RPE. The former may be related to the high oxygen tensions created in the outer retina by the teleost choroidal rete, serving to quench the likely excessive formation of reactive oxygen species.

THE OPTIC NERVE

The optic nerves of teleosts are well-known for their unique architecture: a loose, fasciculated bundle that in many cases approximates a folded ribbon with central axons at the thicker margin of the ribbon cross-section and peripheral axons at the thinner margin. Little is known of the homoeostatic events underlying ribbon maintenance, but molecular phenotyping suggests a shift in the types of glia that comprise the stroma and sheath of the nerve, as the molecular signatures of the retinal optic fiber layer fade out in the optic nerve head and a new spectrum arises in the nerve proper. Teleosts continually add ganglion cells and axons at the retinal margin throughout life, and these new axons find their paths to the central nervous system at the thin margin of the ribbon. Molecular phenotyping consistently shows a small cap of glutathione-rich elements with a charactertistic glial or epithelial signature, quite unlike those of glutamatergic axons. Yet this structure is similar in size and location to the non-myelinated fiber zone described by Easter *et al.*(1981)for the adult goldfish optic nerve. It is possible that the nonmyelinated axons express this unusual signature, but this would require them to be different from their somatic sources.

THE MARGINAL ZONE

Also known as the germinal zone, the marginal zone is recognized as a source of new retinal neurons at the retinal margin (Johns, 1977; Marcus *et al.*, 1999). The basic signatures of marginal zone cells (MZCs) are not very dramatic, with modest glutamine and taurine signals, and low levels of most other metabolites. This suggests that MZCs are not very metabolically active. They are small, far from the choroidal rete and have scant cytoplasm, with little room for mitochondria. A cross-section of $\approx$50–60 cells abuts the retina proper. Incipient retinal neurons clearly begin to develop mature signatures while in the marginal zone and in roughly their correct locations: the outer nuclear layer, the inner nuclear layer and the ganglion cell layer. A small strand of type MZ2aCs arises from the proximal part of the small core of the marginal zone, and those cells immediately adjacent to the ganglion cell layer proper are already developing elevated glutamate signals, although their taurine signals remain high, similar to other MZCs. As ganglion cells move into the retina proper, their taurine and glutathione levels drop, and by the time they are some 50–100 μM from the margin, they develop normal $\tau-$ J$-$ and high EQ signatures of mature ganglion cells. One plausible source of τ and J signals in immature and maturing ganglion cells is through heterologous coupling with their neighbors or even retinal glia while close to the marginal zone. The marginal zone is highly structured: distal cells apposed to the marginal epithelium appear to be incipient photoreceptors (MZ1Cs); those just beneath this layer (MZ2aCs) give rise to horizontal cells, the core generates bipolar and amacrine cells (MZ2bCs), while the thin proximal strand indistinguishable from MZ2aCs generates ganglion and displaced amacrine cells. New neurons do not produce arbors until they enter the retinal proper and then never erroneously invade the marginal zone. If there are any true embryonic stem cells that have not been precommitted, it is difficult to locate them. The bottom of the marginal zone shares a signature with the NPCE and is likely the source for expansion of the ciliary zone in growth.

FINAL NOTES ON THE GENERAL METABOLISM OF NEURONS

The basis set of small molecules was chosen in part because of prior successes in differentiating cells, and in part because of the central roles each target species plays in a variety of pathways. No one species is involved in just one conversion and some, such as glutamine and glutamate, are linked in multiple cycles and epicycles as well as some 5–10 straight conversions. Thus is it not surprising that the molecular phenotypes of cells are so diverse. If anything is clear from molecular signatures, it is that no single *simple* steady-state mixture uniquely defines neuronal neurotransmitter groups. There are wide variations in glutamate content across accepted glutamatergic neurons. In general, glutamatergic photoreceptor cells in all vertebrates tend to maintain roughly 5–10$\times$ less cytosolic glutamate than bipolar and ganglion cells. And the correlative signatures of glutamatergic neurons is also diversified across types and homogenous across species: photoreceptors are low EQ, high τ; bipolar cells are high Eτ, variable Q; ganglion cells are high EQ, and τ negative. This is true of fishes, turtles, pigeons, monkeys, rabbits and mice. The high EQ signature seems to persist into the CNS (Schmolesky, Marc & Leventhal, unpublished mammalian LGN and cortex data), there might be a basic association between long axons and the ability to

produce EQ signals. Short, non-spiking neurons might have less need for large Q pools but a higher local osmoregulatory challenge, thus maintaining higher τ levels. Of course there are other osmoregulatory species that we cannot detect, but the pattern remains useful across many vertebrates so far.

In general, many $\gamma+$ amacrine cells maintain glutamate levels lower than those of bipolar and ganglion cells, but this is a quantitative and not a qualitative distinction. $\gamma+$ classes AC2 and AC3 contain glutamate levels equal to or higher many bipolar and ganglion cells. Thus any ultrastructural analysis of the inner plexiform layer neuropil using glutamate as a sole signal is doomed. Multivariate signatures are essential. The source of glycine in presumed glycinergic amacrine cells has long been a mystery. The best known eukaryote pathway is through glycine hydroxymethyl transferse with serine as a substrate (Michal, 1999) but neither elevated content of this protein or the precursor serine has been achieved by immunocytochemistry. One alternative model based on constitutive accumulation aided by the glycine transporter is attractive (Pow, 1998) though not without alternatives. It is now evident that mammals and many other vertebrates can express alanine glyoxylate transaminase (Holmes & Assimos, 1998; Lee *et al.*, 1999; Li *et al.*, 1999), with glycine and pyruvate as products. While this enzyme has not been mapped in the retina, the preferential association of alanine and glycine signals is provocative.

The discovery of extensive apparent GABA → glycine coupling in the light-adapted retina was disconcerting as we had not previously attended to this issue in amacrine cells in general. A weak colocalization of GABA in a strongly G+ amacrine cell had been described for goldfish and it is very likely that the G+ cells arborizing at level 50 in the zebrafish are homologues of these cells, in spite of the apparent difference in arborization density. If these cells are coupled, then the signals ought to be reciprocal. The problem is that the leak (if that is the explanation) appears to be roughly 10% efficient: 5–10 mM in a $\gamma+$ cell produces about 0.5–1 mM in a G+ cell. Since most G+ amacrine cell glycine signals only reach about 2–3 mM, the resultant coupling signal would be very close to the basal glycine signal of most cells and probably undetectable. Even so, this finding unexpectedly prompts reevaluation of the goldfish amacrine cell populations as a function of adaptation. Amacrine-amacrine coupling has been long known in teleosts (Naka & Christensen, 1981; Marc *et al.*, 1988a; Miyachi *et al.*, 1999), and gap junctions are widespread in the goldfish inner plexiform layer (Marc *et al.*, 1988a). None of these prior data suggested any heterotypic coupling, although sensitive multi-cell recordings in catfish led to a model where extensive heterotypic coupling was proposed (Sakai & Naka, 1988). Finally, the rare BC1 $\gamma+$ bipolar cell might be deemed the one apomorphic feature of the zebrafish but for the fact that it would be easily missed amongst the hundreds of $\gamma+$ horizontal cell axon terminals in the goldfish inner plexiform layer. The zebrafish inner nuclear layer is much better laminated than any other cyprinid and the horizontal cell axon terminals are miniscule. A careful τ mask in the goldfish might reveal these $\gamma+$ bipolar cells. In the end, the only feature that seems to distinguish the zebrafish retina from other cyprinids is its more precise laminar and spatial patterning. This argues that most of the detailed anatomy, neurochemistry and physiology performed on other cyprinids (and teleosts in general) might be safely assumed.

Note

1. Disclosure: REM is a principal of Signature Immunologics Inc.

References

AMMERMULLER, J. & WEILER, R. (1981) The ramification pattern of amacrine cells within the inner plexiform layer of the carp retina. *Cell & Tissue Research* **220**, 699–723.

BALL, G. & HALL, D. (1967) Clustering technique for summarizing multivariate data. *Behavioral Science* **12**, 153–155.

BRANDON, C. (1985) Retinal GABA neurons: Localization in vertebrate species using an antiserum to rabbit brain glutamate decarboxylase. *Brain Research* **344**, 286–295.

CAMERON, D. A. (2000) Cellular proliferation and neurogenesis in the injured retina of adult zebrafish. *Visual Neuroscience* **17**, 789–797.

CAMERON, D. A. & CARNEY, L. H. (2000) Cell mosaic patterns in the native and regenerated inner retina of zebrafish: Implications for retinal assembly. *Journal of Comparative Neurology* **416**, 356–367.

CAMERON, D. A. & POWERS, M. K. (2000) Morphology and visual pigment content of photoreceptors from injured goldfish retina. *Visual Neuroscience* **17**, 623–630.

CARROLL, R. (1988) *Vertebrate Paleontology and Evolution*. New York: W. H. Freeman and Company.

CONNAUGHTON, V. P., BEHAR, T. N., LIU, W. L. & MASSEY, S. C. (1999) Immunocytochemical localization of excitatory and inhibitory neurotransmitters in the zebrafish retina. *Visual Neuroscience* **16**, 483–490.

COOK, J. E. (1996) Spatial properties of retinal mosaics: An empirical evaluation of some existing measures. *Visual Neuroscience* **13**, 15–30.

DJAMGOZ, M. B. A., WAGNER, H. J. & WITKOVSKY, P. (1995) Photoreceptor-horizontal cell connectivity, synaptic transmission and neuromodulation. In *Neurobiology and Clinical Aspects of the Outer Retina* (edited by Djamgoz, M., Archer, S. & Vallerga, S.) pp. 155–193. London: Chapman and Hall.

EASTER, S. S., RUSOFF, A. C. & KISH, P. E. (1981) The growth and organization of the optic nerve and tract in juvenile and adult goldfish. *Journal of Neuroscience* **1**, 793–811.

FAMIGLIETTI, E. V. JR., KANEKO, A. & TACHIBANA, M. (1975) Neuronal architecture of on and off pathways

to ganglion cells in carp retina. *Science* (Washington DC) **198**, 1267–1269.

FLETCHER, E. L. & KALLONIATIS, M. (1996) Neurochemical architecture of the normal and degenerating rat retina. *Journal of Comparative Neurology* **376**, 343–360.

FONNER, D. B., HOFFERT, J. R. & FROMM, P. O. (1973) The importance of the counter current oxygen multiplier mechanism in maintaining retinal function in the teleost. *Comparative Biochemistry & Physiology A—Comparative Physiology* **46**, 559–567.

HITCHCOCK, P. F. & EASTER, S. S. (1986) Retinal ganglion cells in goldfish: A qualitative classification into four morphological types, and a quantitative study of the development of one of them. *Journal of Neuroscience* **6**, 1037–1050.

HOLMES, R. P. & ASSIMOS, D. G. (1998) Glyoxylate synthesis, and its modulation and influence on oxalate synthesis. *Journal of Urology* **160**, 1617–1624.

INSELBERG, A. & DIMSDALE, B. (1990) Parallel coordinates: A tool for visualizing multidimensional geometry. *Proceedings of the First IEEE Conference on Visualization* **1**, 361–375.

ISHIDA, A., STELL, W. & LIGHTFOOT, D. (1980a) Rod and cone inputs to bipolar cells in goldfish retina. *Journal of Comparative Neurology* **191**, 315–335.

ISHIDA, A. T., STELL, W. K. & LIGHTFOOT, D. O. (1980b) Rod and cone inputs to bipolar cells in goldfish retina. *Journal of Comparative Neurology* **191**, 315–335.

JOHNS, P. R. (1977) Growth of the adult goldfish eye. III. Source of the new retinal cells. *Journal of Comparative Neurology* **176**, 343–357.

JOHNSON, J., CHEN, T. K., RICKMAN, D. W., EVANS, C. & BRECHA, N. C. (1996) Multiple gamma-Aminobutyric acid plasma membrane transporters (GAT-1, GAT-2, GAT-3) in the rat retina. *Journal of Comparative Neurology* **375**, 212–224.

JONES, B. W., HOWARD, J., BEG, A., WATT, C. B. & MARC, R. E. (1999) Ionotropic glutamatergic drive histories of amacrine cell layer neurons reported by 1-amino-4-guanidobutane (AGB) *in vivo*. *Investigative Ophthalmology and Visual Science* **40**, S440.

KALLONIATIS, M. & FLETCHER, E. L. (1993) Immunocytochemical localization of the amino acid neurotransmitters in the chicken retina. *Journal of Comparative Neurology* **336**, 174–193.

KALLONIATIS, M. & MARC, R. E. (1990) Interplexiform cells of the goldfish retina. *Journal of Comparative Neurology* **297**, 340–358.

KALLONIATIS, M., MARC, R. E. & MURRY, R. F. (1996) Amino acid signatures in the primate retina. [erratum appears in *J Neurosci* 1997 Jan 1;**17**(1), 500–503]. *Journal of Neuroscience* **16**, 6807–6829.

KALLONIATIS, M. & NAPPER, G. A. (1996) Glutamate metabolic pathways in displaced ganglion cells of the chicken retina. *Journal of Comparative Neurology* **367**, 518–536.

KALLONIATIS, M. & TOMISICH, G. (1999) Amino acid neurochemistry of the vertebrate retina. *Progress in Retinal & Eye Research* **18**, 811–866.

KALLONIATIS, M., TOMISICH, G. & MARC, R. E. (1994) Neurochemical signatures revealed by glutamine labeling in the chicken retina. *Visual Neuroscience* **11**, 793–804.

KAMERMANS, M., FAHRENFORT. I., SCHULTZ, K., JANSSEN-BIENHOLD, U., SJOERDSMA, T. & WEILER, R. (2001) Hemichannel-mediated inhibition in the outer retina. *Science* **292**, 1178–1180.

KAMERMANS, M. & SPEKREIJSE, H. (1999) The feedback pathway from horizontal cells to cones. A mini review with a look ahead. *Vision Research* **39**, 2449–2468.

LAM, D. M., SU, Y. Y., SWAIN, L., MARC, R. E., BRANDON, C. & WU, J. Y. (1979) Immunocytochemical localisation of L-glutamic acid decarboxylase in the goldfish retina. *Nature* **278**, 565–567.

LEE, I. S., NISHIKIMI, M., INOUE, M., MURAGAKI, Y. & OOSHIMA, A. (1999) Specific expression of alanine-glyoxylate aminotransferase 2 in the epithelial cells of Henle's loop. *Nephron* **83**, 184–185.

LI, X. M., SALIDO, E. C. & SHAPIRO, L. J. (1999) The mouse alanine: Glyoxylate aminotransferase gene (Agxt1): Cloning, expression, and mapping to chromosome 1. *Somatic Cell & Molecular Genetics* **25**, 67–77.

MACNEIL, M. A., HEUSSY, J. K., DACHEUX, R. F., RAVIOLA, E. & MASLAND, R. H. (1999) The shapes and numbers of amacrine cells: Matching of photofilled with Golgi-stained cells in the rabbit retina and comparison with other mammalian species. *Journal of Comparative Neurology* **413**, 305–326.

MARC, R., LI, H.-B., KALLONIATIS, M. & ARNOLD, J. (1993) Cholinergic subsets of GABAergic amacrine cells in the goldfish retina. *Investigative Ophthalmology and Visual Science* **34**, S1061.

MARC, R. E. (1982) Chromatic organization of the retina. In *Cellular Aspects of the Eye* (edited by McDevitt, D.) pp. 435–473. NY: Academic Press.

MARC, R. E. (1986) Neurochemical stratification in the inner plexiform layer of the vertebrate retina. *Vision Research* **26**, 223–238.

MARC, R. E. (1992) Structural organization of GABAergic circuitry in ectotherm retinas. *Progress in Brain Research* **90**, 61–92.

MARC, R. E. (1999a) Mapping glutamatergic drive in the vertebrate retina with a channel-permeant organic cation. *Journal of Comparative Neurology* **407**, 47–64.

MARC, R. E. (1999b) The structure of vertebrate retinas. In *The Retinal Basis of Vision* (edited by Toyoda, J.-I., Murkami, M., Kaneko, A. & Saito, T.) pp. 3–19. Amsterdam: Elsevier.

MARC, R. E. & JONES, B. W. (2002) Molecular phenotyping of retinal ganglion cells. *Journal of Neuroscience* **22**, 413–427.

MARC, R. E. & LAM, D. M. K. (1981) Glycinergic pathways in the goldfish retina. *Journal of Neuroscience* **1**, 152–165.

MARC, R. E. & LIU, W. L. (1984) Horizontal cell synapses onto glycine-accumulating interplexiform cells. *Nature* **312**, 266–269.

MARC, R. E. & LIU, W. (2000) Fundamental GABAergic amacrine cell circuitries in the retina: Nested feedback, concatenated inhibition, and axosomatic synapses. *Journal of Comparative Neurology* **425**, 560–582.

MARC, R. E., LIU, W. L., KALLONIATIS, M., RAIGUEL, S. F. & VAN HAESENDONCK, E. (1990) Patterns of glutamate immunoreactivity in the goldfish retina. *Journal of Neuroscience* **10**, 4006–4034.

MARC, R. E., LIU, W. L. & MULLER, J. F. (1988a) Gap junctions in the inner plexiform layer of the goldfish retina. *Vision Research* **28**, 9–24.

MARC, R. E., LIU, W. L., SCHOLZ, K. & MULLER, J. F. (1988b) Serotonergic and serotonin-accumulating neurons in the goldfish retina. *Journal of Neuroscience* **8**, 3427–3450.

MARC, R. E., MURRY, R. F. & BASINGER, S. F. (1995) Pattern recognition of amino acid signatures in retinal neurons. *Journal of Neuroscience* **15**, 5106–5129.

MARC, R. E., MURRY, R. F., FISHER, S. K., LINBERG, K. A. & LEWIS, G. P. (1998a) Amino acid signatures in the detached cat retina. *Investigative Ophthalmology & Visual Science* **39**, 1694–1702.

MARC, R. E., MURRY, R. F., FISHER, S. K., LINBERG, K. A., LEWIS, G. P. & KALLONIATIS, M. (1998b) Amino acid signatures in the normal cat retina. *Investigative Ophthalmology & Visual Science* **39**, 1685–1693.

MARC, R. E., STELL, W. K., BOK, D. & LAM, D. M. (1978) GABAergic pathways in the goldfish retina. *Journal of Comparative Neurology* **182**, 221–244.

MARC, R. E. & SPERLING, H. G. (1976) Color receptor identities of goldfish cones. *Science* **191**, 487–489.

MARC, R. E. & SPERLING, H. G. (1977) The chromatic organization of the goldfish cone mosaic. *Vision Research* **16**, 1211–1224.

MARCUS, R. C., DELANEY, C. L., & EASTER, S. S., JR. (1999) Neurogenesis in the visual system of embryonic and adult zebrafish (Danio rerio). *Visual Neuroscience* **16**, 417–424.

MARSHAK, D. W. & DOWLING, J. E. (1987) Synapses of cone horizontal cell axons in goldfish retina. *Journal of Comparative Neurology* **256**, 430–443.

MARSHAK, D. W., YAMADA, T. & STELL, W. K. (1982) Synaptic contacts of somatostatin immuno reactive amacrine cells in goldfish retina. *Journal of Comparative Neurology* **225**, 44–52.

MASSEY, S. C., MILLS, S. L. & MARC, R. E. (1992) All indoleamine-accumulating cells in the rabbit retina contain GABA. *Journal of Comparative Neurology* **322**, 275–291.

MICHAL, G. (1999) Amino acids and derivatives. In *Biochemical Pathways* (edited by Michal, G.) pp. 46–67. NY: Wiley & Sons.

MIYACHI, E., HIDAKA, S. & MURKAMI, M. (1999) Electrical couplings of retinal neurons. In (edited by Toyoda, J.-I., Murakami, M., Kaneko, A. & Saito, T.) pp. 171–184. Amsterdam: Elsevier.

MOECKEL, G. W., LAI, L. W., GUDER, W. G., KWON, H. M. & LIEN, Y. H. (1997) Kinetics and osmoregulation of Na^+- and Cl^--dependent betaine transporter in rat renal medulla. *American Journal of Physiology* **272**, F100–106.

MORIMURA, H., SHIMADA, S., OTORI, Y., SAISHIN, Y., YAMAUCHI, A., MINAMI, Y., INOUE, K., ISHIMOTO, I., TANO, Y. & TOHYAMA, M. (1997) The differential osmoregulation and localization of taurine transporter mRNA and Na^+/ myo-inositol cotransporter mRNA in rat eyes. *Brain Research Molecular Brain Research* **44**, 245–252.

MOSINGER, J. L. & YAZULLA, S. (1985) Colocalization of GAD-like immunoreactivity and ^{3}H-GABA uptake in amacrine cells of rabbit retina. *Journal of Comparative Neurology* **240**, 396–406.

MOSINGER, J. L., YAZULLA, S. & STUDHOLME, K. M. (1986) GABA-like immunoreactivity in the vertebrate retina: A species comparison. *Experimental Eye Research* **42**, 631–644.

NAKA, K. I. & CHRISTENSEN, B. N. (1981) Direct electrical connections between transient amacrine cells in the catfish retina. *Science* **214**, 462–464.

POW, D. V. (1998) Transport is the primary determinant of glycine content in retinal neurons. *Journal of Neurochemistry* **70**, 2628–2636.

POW, D. V. & CROOK, D. K. (1996) Direct immunocytochemical evidence for the transfer of glutamine from glial cells to neurons: Use of specific antibodies directed against the d-stereoisomers of glutamate and glutamine. *Neuroscience* **70**, 295–302.

POW, D. V. & ROBINSON, S. R. (1994) Glutamate in some retinal neurons is derived solely from glia. *Neuroscience* **60**, 355–366.

RAYMOND, P. A. (1990) Horizontal cell axon terminals in growing goldfish. *Experimental Eye Research* **51**, 675–683.

RAYMOND, P. A., BARTHEL, L. K., ROUNSIFER, M. E., SULLIVAN, S. A. & KNIGHT, J. K. (1993) Expression of rod and cone visual pigments in goldfish and zebrafish: A rhodopsin-like gene is expressed in cones. *Neuron* **10**, 1161–1174.

ROBERTS, M. F. (2000) Osmoadaptation and osmoregulation in archaea. *Frontiers in Bioscience* **5**, D796–D812.

ROBINSON, J., SCHMITT, E. A., HAROSI, F. I., REECE, R. J. & DOWLING, J. E. (1993) Zebrafish ultraviolet visual pigment: Absorption spectrum, sequence, and localization. *Proceedings of the National Academy of Sciences of the United States of America* **90**, 6009–6012.

SAKAI, H. M. & NAKA, K. (1988) Dissection of the neuron network in the catfish inner retina. II. Interactions between ganglion cells. *Journal of Neurophysiology* **60**, 1568–1583.

SANDELL, J. H. & MASLAND, R. H. (1989) Indoleamine accumulation by retinal neurons exposed to blood. *Histochemistry* **92**, 57–60.

SANDELL, J. H., MASLAND, R. H., RAVIOLA, E. & DACHEUX, R. F. (1989) Connections of indoleamine-accumulating cells in the rabbit retina. *Journal of Comparative Neurology* **283**, 303–313.

SCHAFFER, S., TAKAHASHI, K. & AZUMA, J. (2000) Role of osmoregulation in the actions of taurine. *Amino Acids* **19**, 527–546.

SCHOLES, J. H. (1975) Colour receptors, and their synaptic connexions, in the retina of a cyprinid fish. *Philosophical Transactions of the Royal Society of London—Series B: Biological Sciences* **270**, 61–118.

SCHOLES, J. & MORRIS, J. (1973) Receptor—bipolar connectivity patterns in fish retina. *Nature* **241**, 52–54.

SHERRY, D. M. & YAZULLA, S. (1992) Goldfish bipolar cells and axon terminal patterns: A Golgi study. *Journal of Comparative Neurology*.

STELL, W. K. (1965) Correlation of retinal cytoarchitecture and ultrastructure in Golgi preparations. *Anatomical Record* **153**, 389–397.

STELL, W. K. (1967) The structure and relationships of horizontal cells and photoreceptor-bipolar synaptic complexes in goldfish retina. *American Journal of Anatomy* **121**, 401–423.

STELL, W. K. (1975) Horizontal cell axons and axon terminals in goldfish retina. *Journal of Comparative Neurology* **159**, 503–520.

STELL, W. K. & HAROSI, F. I. (1975) Cone structure and visual pigment content in the retina of the goldfish. *Vision Research* **16**, 647–657.

STELL, W. K. & LIGHTFOOT, D. O. (1975) Color-specific interconnections of cones and horizontal cells in the retina of the goldfish. *Journal of Comparative Neurology* **159**, 473–502.

STENKAMP, D. L., POWERS, M. K., CARNEY, L. H. & CAMERON, D. A. (2001) Evidence for two distinct mechanisms of neurogenesis and cellular pattern formation in regenerated goldfish retinas. *Journal of Comparative Neurology* **431**, 363–381.

STUDHOLME, K. M. & YAZULLA, S. (1988) Localization of GABA and glycine in goldfish retina by electron microscopic postembedding immunocytochemistry: Improved visualization of synaptic structures with LR white resin. *Journal of Neurocytology* **17**, 859–870.

TUMOSA, N., ECKENSTEIN, F. & STELL, W. K. (1984) Immunocytochemical localization of putative cholinergic neurons in the goldfish retina. *Neuroscience Letters* **48**, 255–259.

TUMOSA, N. & STELL, W. K. (1986) Choline acetyltransferase immunoreactivity suggests that ganglion cells in the goldfish retina are not cholinergic. *Journal of Comparative Neurology* **244**, 267–275.

VAN HAESENDONCK, E., MARC, R. E. & MISSOTTEN, L. (1993) New aspects of dopaminergic interplexiform cell organization in the goldfish retina. *Journal of Comparative Neurology* **333**, 503–518.

VERWEIJ, J., KAMERMANS, M., NEGISHI, K. & SPEKREIJSE, H. (1998) GABA sensitivity of spectrally classified horizontal cells in goldfish retina. *Visual Neuroscience* **15**, 77–86.

WAGNER, H. J. & WAGNER, E. (1988) Amacrine cells in the retina of a teleost fish, the roach (Rutilus rutilus): A Golgi study on differentiation and layering. *Philosophical Transactions of the Royal Society of London—Series B: Biological Sciences* **321**, 263–324.

WATT, C. B., KALLONIATIS, M., JONES, B. W. & MARC, R. E. (2000) Studies examining the neurotransmitter properties of horizontal cell populations in the goldfish retina. *Investigative Ophthalmology and Visual Science* **41**, S943.

YANG, C. Y. & YAZULLA, S. (1988) Localization of putative GABAergic neurons in the larval tiger salamander retina by immunocytochemical and autoradiographic methods. *Journal of Comparative Neurology* **277**, 96–108.

YAZULLA, S. (1981) Gamma aminobutyric-acid-ergic synapses in the goldfish carassius-auratus retina an auto radiographic study of tritium labeled muscimol and tritium labeled gamma aminobutyric-acid binding. *Journal of Comparative Neurology* **200**, 83–94.

YAZULLA, S. (1991) The mismatch problem for gabaergic amacrine cells in goldfish retina resolution and other issues. *Neurochemical Research*.

YAZULLA, S., MOSINGER, J. & ZUCKER, C. (1984) Two types of pyriform Ab amacrine cells in the goldfish retina: An EM analysis of [^{3}H]GABA uptake and somatostatin-like immunoreactivity. *Brain Research* **321**, 352–356.

YAZULLA, S. & STUDHOLME, K. M. (1991) Glycinergic interplexiform cells make synaptic contact with amacrine cell bodies in goldfish retina. *Journal of Comparative Neurology* **310**, 1–10.

YAZULLA, S., STUDHOLME, K. & WU, J. Y. (1986) Comparative distribution of 3H-GABA uptake and GAD immunoreactivity in goldfish retinal amacrine cells: A double-label analysis. *Journal of Comparative Neurology* **244**, 149–162.

YAZULLA, S., STUDHOLME, K. M. & WU, J. Y. (1987) GABAergic input to the synaptic terminals of mb1 bipolar cells in the goldfish retina. *Brain Research* **411**, 400–405.

YAZULLA, S., STUDHOLME, K. M. & ZUCKER, C. L. (1985) Synaptic organization of substance P-like immunoreactive amacrine cells in goldfish retina. *Journal of Comparative Neurology* **231**, 232–238.

YAZULLA, S. & ZUCKER, C. L. (1988) Synaptic organization of dopaminergic interplexiform cells in the goldfish retina. *Visual Neuroscience* **1**, 13–29.